PALEOCLIMATE RECONSTRUCTION IN NORTHWEST SCOTLAND AND SOUTHWEST FLORIDA DURING THE LATE HOLOCENE

Ting Wang

A dissertation submitted to the faculty of the University of North Carolina at Chapel Hill in partial fulfillment of the requirements for the degree of Doctor of Philosophy in the Department of Geological Sciences.

Chapel Hill
2011

Approved by:

Dr. Donna M. Surge

Dr. Joseph G. Carter

Dr. Jose A. Rial

Dr. Justin B. Ries

Dr. Karen J. Walker

ABSTRACT

TING WANG: Paleoclimate Reconstruction in Northwest Scotland and Southwest Florida
during the Late Holocene
(Under the direction of Dr. Donna M. Surge)

The study reconstructed seasonal climate change in mid-latitude northwest Scotland

during the climate episodes Neoglacial (~3300-2500 BP) and Roman Warm Period (RWP;

~2500-1600 BP) and in subtropical southwest Florida during the latter part of RWP (1-550

AD) based on archaeological shell accumulations in two study areas. In northwest Scotland,

seasonal sea surface temperature (SST) during the Neoglacial and RWP was estimated from

high-resolution oxygen isotope ratios ($\delta^{18}O$) of radiocarbon-dated limpet (*Patella vulgata*)

shells accumulated in a cave dwelling on the Isle of Mull. The SST results revealed a cooling

transition from the Neoglacial to RWP, which is supported by earlier studies of pine pollen in

Scotland and European glacial events and also coincident with the abrupt climate

deterioration at 2800-2700 BP. The cooling transition might have been driven by decreased

solar radiation and weakened North Atlantic Oscillation (NAO) conditions. In southwest

Florida, seasonal-scale climate conditions for the latter part of RWP were reconstructed by

using high-resolution $\delta^{18}O$ of archaeological shells (*Mercenaria campechiensis*) and otoliths

(*Ariopsis felis*). The reconstructions agree with archaeological observations and are partially

coherent with the history of sea-level change. Moreover, the results suggest a marked drying

and cooling trend across the RWP to Vandal Minimum (VM; ~500-800 AD) transition, which is consistent with falling sea level and reduced solar radiation. Reduced solar radiation might have triggered a change in atmospheric circulation patterns that precipitated the observed climate transition. Although NAO and other atmospheric circulation patterns have been proposed as the internal climate mechanism responsible for the climate fluctuations in the late Holocene, other studies suggest that stochastic processes are possibly associated with the internal climate mechanism. Therefore, I also examined the extent to which the internal climate mechanism in the late Holocene is stochastic. Our results indicate that the stochastic extent of climate change over the past millennium generally decreased during the intervals of climate transition.

ACKNOWLEDGEMENTS

Last, but not least, I would like to thank my beloved mother, father, and brother in China, and especially my husband for your support and encouragement. I'm also grateful to my friends at Chapel Hill and my host family Ms. Marjorie White for your precious friendship.

TABLE OF CONTENTS

LIST OF TABLES

Table

LIST OF FIGURES

Figure

LIST OF ABBREVIATIONS AND SYMBOLS

AD   Anno Domini

A. felis   *Ariopsis felis*

AMO   Atlantic Multidecadal Oscillation

AMS   accelerator mass spectrometry

AO   Arctic Oscillation

BC   Before Christ

BP   before present

CALIB   calibration program for radiocarbon age

^{14}C radiocarbon isotope 14

CIIA   cultural period of Caloosahatchee IIA

CI   cultural period of Caloosahatchee I

CI-A   Caloosahatchee I-*Ariopsis felis*

CIIA-A   Caloosahatchee IIA-*Ariopsis felis*

CIIA-M   Caloosahatchee IIA-*Mercenaria campechiensis*

CI-M   Caloosahatchee I-*Mercenaria campechiensis*

cm   centimeter

CR   Citrus Ridge

^{o}C degrees Celsius

$\delta^{13}C$ carbon isotope ratio

$\delta^{18}O$ oxygen isotope ratio

$\Delta^{14}C$ carbon isotope 14 fractionation factor

ENSO   El Nino-Southern Oscillation

et al.	and others
FLMNH	Florida Museum of Natural History
GISS GCM	Goddard Institute for Space Studies general circulation model
GISP2	Greenland Ice Sheet Project 2
i.e.,	that is
ITCZ	Intertropical Convergence Zone
LIA	Little Ice Age
LM	Low Mound
Lv	Level
M. camphechiensis	*Mercenaria campechiensis*
M. mercenaria	*Mercenaria mercenaria*
μg	microgram, 10^{-6} gram
mm	millimeter
MWP	Medieval Warm Period
NAO	North Atlantic Oscillation
NBS	National Bureau of Standard
NH	Northern Hemisphere
NOAA	National Oceanic and Atmospheric Administration
NOSAMS	National Ocean Sciences Accelerator Mass Spectrometry
NWP	Northwest Pasture
OM	Old Mound
1σ	one sigma range
^{18}O	oxygen isotope 18

‰	per mil or parts per thousand
±	plus or minus
psu	practical salinity units
P. vulgate	*Patella vulgata*
RESTS	randomness evaluation for stochastic time series
RWP	Roman Warm Period
SCR	Surf Clam Ridge
SP	South Pasture
SPG	sub-polar gyres
SST	sea surface temperature
St	Stratum
STG	sub-tropical gyres
TSI	total solar irradiance
VM	Vandal Minimum
VPDB	Vienna Pee Dee Belemnite
VSMOW	Vienna Standard Mean Ocean Water

PREFACE

Climate in the late Holocene (0-3000 BP) was more variable and dynamic than previously thought. Several climate change episodes have been detected, such as the Subboreal/Subatlantic transition (2800-2700 cal. BP), Roman Warm Period (RWP; ~2500-1600 cal. BP), Vandal Minimum (VM; ~400-800 AD), Medieval Warm Period (MWP; ~1200-1400 AD) and Little Ice Age (LIA; ~1500-1700 AD). Paleoclimate reconstructions during these climate episodes in the sensitive North Atlantic sector are pivotal for understanding natural variation in the climate system prior to anthropogenic influence. However, the majority of Holocene climate proxies in the North Atlantic sector provide decadal or annual resolution. Few studies provide the high resolution necessary to reconstruct seasonal-scale variability, which can provide more accurate reconstruction necessary to gain insights into climate mechanism. Therefore, there is an increasing demand for seasonal-scale resolution.

High-resolution time series of oxygen isotope ratios ($\delta^{18}O$) preserved in mollusc shells or fish otoliths (ear bone) have been widely used in seasonal-scale paleoclimate studies and are accepted as reliable and accurate climate proxies (Jones and Allmon, 1995; Schöne et al., 2005; Surge and Walker, 2005, 2006; Goewert and Surge, 2008, and many others). Moreover, paleoclimate reconstructions that use archaeological shells or otoliths also contain information of human behavior in the late Holocene, and hence can contribute to our

understanding of human-climate relationships (Surge and Walker, 2005; Walker and Surge, 2006; Hallmann et al., 2009; Hufthammer et al., 2010; Jones et al., 2010; Patterson et al., 2010; Helama and Hood, 2011; Wang et al., 2011). The archaeological middens found along the northwest coast of Scotland and the southwest coast of Florida contain abundant shells, providing a rich source of seasonal climate records and information on human subsistence strategies. Chapter 1 reconstructs seasonal sea surface temperature (SST) variability during the Neoglacial (3300-2500 BP) and the RWP using $\delta^{18}O$ values of archaeological limpet (*Patella vulgata*) shells from Croig Cave, an archaeological site in northwest Scotland. Chapter 2 reconstructs the variability of summer precipitation and winter temperature during the latter part of RWP (1-500 AD) using $\delta^{18}O$ values of archaeological shell-otolith pairs (*Mercenaria campechiensis* and *Ariopsis felis*) from southwest Florida.

Although solar radiation change has generally been accepted as the external trigger for climate change in the late Holocene, there is no consensus on the internal mechanism for the changes. Stochastic climate models have been widely used to help understand the fundamental dynamics of climate systems (Majda et al., 1999; Dobrovalski, 2000; Ditlevsen, 2001; Király and Jánosi, 2002; Roe and Steig, 2004, and many others). Chapter 3 uses a conceptual stochastic climate model to examine the extent to which the climate change in the late Holocene is stochastic, to enhance our insight into internal climate dynamics during the late Holocene.

References

Ditlevsen PD. 2001. Stochastic climate dynamics observed in an ice-core record. *Proceedings ISSAOS 2001*, l'Aquilla.

Dobrovolski SG. 2000. *Stochastic climate theory: models and applications*. Springer-Verlag Berlin: Heidelberg New York.

Goewert AE, Surge D. 2008. Seasonality and growth patterns using isotope sclerochronology in shells of the Pliocene scallop *Chesapecten madisonius*. *Geo-Marine Letters* **28**: 327-338.

Hallmann N, Burchell M, Schöne BR, Irvine GV, Maxwell D. 2009. High-resolution sclerochronological analysis of the bivalve mollusk *Saxidomus gigantea* from Alaska and British Columbia: Techniques for revealing environmental archives and archaeological seasonality. *Journal of Archaeological Science* **36**: 2353-2364.

Helama S, Hood BC. 2011. Stone Age midden deposition assessed by bivalve sclerochronology and radiocarbon wiggle-matching of *Arctica islandica* shell increments. *Journal of Archaeological Science* **38(2)**: 452-460.

Hufthammer AK, Høie H, Folkvord A, Geffen AJ, Andersson C, et al. 2010. Seasonality of human site occupation based on stable oxygen isotope ratios of cod otoliths. *Journal of Archaeological Science* **37**: 78-83.

Jones KB, Hodgins GWL, Etayo-Cadavid MF, Andrus CFT, Sandweiss DH. 2010. Centuries of marine radiocarbon reservoir age variation within archaeological *Mesodesma donacium* shells from southern Peru. *Radiocarbon* **52(3)**: 1207-1214.

Jones D., Allmon WD. 1995. Records of upwelling, seasonality and growth in stable-isotope profiles of Pliocene mollusk shells from Florida. *LETHAIA* **28**: 61-74.

Király A, Jánosi IM. 2002. Stochastic modeling of daily temperature fluctuations. *Physical Review* **65**: 051102, doi: 10.1103/PhysRevE.65.051102.

Majda AJ, Timofeyev I, Eijnden EV. 1999. Models for stochastic climate prediction. *PNAS* **96**: 14687-14691, doi: 10.1073/pnas.96.26.14687.

Patterson WP, Dietrich KA, Holmden C, Andrews JT. 2010. Two millennia of North Atlantic seasonality and implications for Norse colonies. *Proceedings of the National Academy of Sciences* **107 (12)**: 5306-5310.

Roe GH, Steig EJ. 2004. On the characterization of millennial-scale climate variability. *J. Climate* **17**: 1929-1944.

Schöne BR, Fiebig J, Pfeiffer M, Gleβ R, Hickson J, Johnson ALA, Dreyer W, Oschmann W. 2005. Climate records from a bivalved Methuselah (*Arctica islandica*, Mollusca; Iceland). *Palaeography, Palaeoclimatology, Palaeoecology* **228**: 130-148.

Surge D, Walker K J. 2005. Oxygen isotope composition of modern and archaeological otoliths from the estuarine hardhead catfish (*Ariopsis felis*) and their potential to record low-latitude climate change. *Palaeogeography, Palaeoclimatology, Palaeoecology* **228**: 179-191.

Surge D, Walker KJ. 2006. Geochemical variation in microstructural shell layers of the southern quahog (*Mercenaria campechiensis*): Implications for reconstructing seasonality. *Palaeogeography, Palaeoclimatology, Palaeoecology* **237**: 182-190.

Walker KJ, Surge D. 2006. Developing oxygen isotope proxies from archaeological sources for the study of Late Holocene human–climate interactions in coastal southwest Florida. *Quaternary International* **150**: 3-11.

Wang T, Surge D, Walker KJ. (2011). Isotopic evidence for climate change during the Vandal Minimum from *Ariopsis felis* otoliths and *Mercenaria campechiensis* shells, southwest Florida, USA. *Holocene* **21(7)**: 1081-1091. doi:10.1177/0959683611400458.

CHAPTER I

SEASONAL TEMPERATURE VARIABILITY OF THE NEOGLACIAL AND ROMAN WARM PERIOD RECONSTRUCTED FROM OXYGEN ISOTOPE RATIOS OF LIMPET SHELLS (PATELLA VULGATA), NORTHWEST SCOTLAND

Abstract

Seasonal SST variability for the Neoglacial (3300-2500 BP) and Roman Warm Period (RWP; 2500-1600 BP), which correspond to the Bronze and Iron Ages, respectively was estimated using oxygen isotope ratios obtained from high-resolution samples micromilled from radiocarbon-dated, archaeological limpet (*Patella vulgata*) shells. The coldest winter months recorded in Neoglacial shells averaged 6.6±0.3ºC, and the warmest summer months averaged 14.7±0.4ºC. One Neoglacial shell captured a year without a summer, which may have resulted from a dust veil from a volcanic eruption in the Katla volcanic system in Iceland. RWP shells record average winter and summer monthly temperatures of 6.3±0.1$^{\text{o}}$C and 13.3±0.3ºC, respectively. These results capture a cooling transition from the Neoglacial to RWP, which is further supported by earlier studies of pine pollen in Scotland and European glacial events. The cooling transition observed at the boundary between the Neoglacial and RWP also agrees with the abrupt climate deterioration at 2800-2700 BP (also referred to as the Subboreal/Subatlantic transition) and therefore may have been driven by decreased solar radiation and weakened NAO conditions.

1. Introduction

Pre-industrial climate reconstructions during the mid to late Holocene provide the necessary information for understanding natural variation in the climate system prior to anthropogenic changes in the atmosphere, hydrosphere, and land use. Moreover, paleoclimate reconstructions that use archaeological sources contribute to our understanding of human-climate relationships (Surge and Walker, 2005; Walker and Surge, 2006; Hallmann et al., 2009; Hufthammer et al., 2010; Jones et al., 2010; Patterson et al., 2010; Helama and Hood, 2011; Wang et al., 2011), particularly in regions that are sensitive to climate change, such as mid-latitude coastal areas of the North Atlantic. These paleoclimate records can be compared to proxies of possible climate forcings (e.g., solar activity, the North Atlantic Oscillation, Atlantic Meridional Overturning Circulation) and to predictions made by regional climate models (Shindell et al., 2001; Renssen et al., 2006; Swindles et al., 2007; Mann et al., 2009, and many others). Linking paleoclimate records with proxies of climate forcings is particularly important for the North Atlantic sector because the North Atlantic plays a critical role in heat transport and climate change at regional and global scales.

The majority of Holocene climate proxies provide decadal, annual, or single season (mostly summer and the growing season) resolution. Few studies provide the high resolution necessary to reconstruct seasonal-scale variability. Regional climate models demonstrate the

need for such high-resolution, seasonality studies. Numerical (idealized multi-level primitive equation) and sensitivity (ECBilt-Clio) model experiments show that small changes in the coupled atmospheric-oceanographic climate system influence regional mid-latitude seasonality in the North Atlantic sector (Lee and Kim, 2003; van der Schrier et al., 2007). Therefore, climate archives capable of capturing seasonal-scale resolution can provide the data necessary to gain insights into the mechanisms controling seasonal variability at mid latitudes in the North Atlantic.

High-resolution time series of oxygen isotope ratios ($\delta^{18}O$) in mollusc shells have been widely used in paleoclimate and paleoecological studies (Jones and Allmon, 1995; Schöne et al., 2005; Surge and Walker, 2005, 2006; Goewert and Surge, 2008, and many others). Their fast growth makes them ideal candidates to capture seasonal variability. Archaeological middens found along the northwest coast of Scotland contain abundant limpet (*Patella vulgata*) shells, providing a rich source of seasonal climate records and information on human subsistence strategies. Isotopic studies of *Patella* shells have shown that these shells are useful for reconstructing sea surface temperature (SST) and inferring climate change (Shackelton, 1973; Cohen and Tyson, 1995; Fenger, et al. 2007;). Other advantages of using *P. vulgata* shells from this area include environmental conditions and shell mineralogy. Shells from the study area occupy a marine environment where the salinity and $\delta^{18}O_{WATER}$ values are quite stable (Crisp, 1965; Branch, 1981; Inall et al., 2009). Their shells are composed primarily of calcite, which makes them less susceptible to diagenetic alteration (Fenger et al., 2007).

In this study, we reconstructed the seasonal SST variability during the Neoglacial (3300-2500 BP) and the RWP (RWP; 2500-1600 BP) using oxygen isotope ratios of ten archaeological *P. vulgata* shells from Croig Cave, an archaeological site on the Isle of Mull in the Hebrides Islands west of mainland Scotland. We also compared our reconstructed temperatures with previous climate reconstructions to discuss the potential forcing factors responsible for the two climate change episodes. Based on results of climate modeling experiments (Lee and Kim, 2003; van der Schrier et al., 2007), our approach allowed us to test the hypothesis that seasonal temperature should also change when climate forcing drives climate change from one episode to the other one.

1.1. *Ecology of Patella vulgata*

The common European limpet, *P. vulgata,* is a gastropod that inhabits rocky shorelines in the high intertidal and shallow subtidal zones. This species grazes on diatoms, algae, algal spores, and small plants from the substratum. It rarely shows migratory movements much beyond its home base and is able to record environmental conditions at a fixed location. *P. vulgata* occurs in the cold- and warm-temperate biogeographic provinces from Norway to northern Spain and is particularly widespread around the British Isles (Blackmore, 1969). Water temperature and salinity tolerances of *P. vulgata* range from −8.7 to 42.8°C and 20 to 35 psu (practical salinity units) (Crisp, 1965; Branch, 1981), although shell growth rate slows down at extreme temperatures. Although they can inhabit a range of salinities, our specimens came from fully marine environments where surface salinity measured from a seabird SBE37 moored at the surface ranges from 34.0-34.6 psu (Inall et al., 2009).

P. vulgata has a conical, cap-shaped shell (~2-4 cm in length on average), which the apex of the shell located at the center or slightly anterior. The shell exterior exhibits gray to white color similar to the substratum, and the coarse surface is sculptured with radiating ribs and concentric growth rings. The shell interior is smooth and exhibits a prominent muscle scar. The shell cross-section reveals its major sclerochronological features, such as annual growth lines and growth increments. When the cross-section is processed with Mutvei's solution (Schöne, et al., 2005), the sclerochronological features are enhanced and more detailed microstructures can be observed, such as semidiurnal, lunar daily, fortnightly growth lines and increments (Fenger et al., 2007). The growth rate of *P. vulgata* shells is not constant throughout the year and varies from 0.005mm/month to 2.6mm/month (Blackmore, 1969; Ekaratne and Crisp, 1984). Growth rate is primarily controlled by temperature. In mid to high latitudes, such as the United Kingdom, shells form a prominent growth line in the coldest winter month. In contrast, shells in low latitudes, such as the Mediterranean, slow their growth rate during the summer (Schifano and Censi, 1986). Although temperature plays the dominant role on growth rate and the formation of annual growth lines (Blackmore, 1969), reproduction can also influence growth rate (Ekaratne and Crisp, 1984).

1.2. *Oceanography of study area*

Coastal northwest Scotland is located in the cold-temperate biogeographic province. The climate is typically maritime and, therefore, relatively mild and wet compared to other regions at the same latitude (Baxter et al., 2008). Climate is strongly influenced by the prevailing southwesterly winds that deliver heat from the North Atlantic Current. The

strength of the prevailing winds is largely governed by the North Atlantic Oscillation (NAO).

During positive NAO phases, a large sea-level pressure gradient between the subtropical

Azores High and the subpolar Icelandic Low will generate strong mid-latitude westerly

winds and bring warm and saturated air masses northward to this region (Hurrell, 1995). The

close relationship between the climate and NAO pattern has been indicated by the residual

winter flows through Tiree Passage (56°37.7'N, 6°23.8'W, Fig. 1.1). Inall et al. (2009)

measured the residual winter flow through Tiree Passage from 1980 to 2006 and found that

winter flow has significant correlation with the NAO index.

The coastal waters in our study area are dominantly marine with a narrow (±0.3 psu)

salinity range around 34.3 psu (Inall et al., 2009). The coastal waters are primarily composed

of two sources: the Scottish Coastal Current from the Irish and Clyde Seas and the North

Atlantic Current from Atlantic origin. Inall et al. (2009) reported that ~50% of the

temperature variance is attributed to the temperature variations of Irish and Clyde Sea waters,

and ~17% of the variance to that of the North Atlantic Current.

2. Materials and methods

2.1. *Archaeological site, shell selection and radiocarbon dating*

Croig Cave is a small rock shelter among a number of caves on the Isle of Mull, west

of mainland Scotland (Fig. 1.1). The cave has thick shell midden deposits that contain a

nearly continuous accumulation of shells ranging from 800 BC-500 AD, and possibly older

based on radiocarbon dating of shells and charcoals collected throughout the stratigraphic

sequence. This range represents a long chronology of human use from the late Bronze to Iron

Ages and spans the Neoglacial through Little Ice Age climate episodes. The midden deposits of Croig Cave were first excavated in 2006 and were further explored in 2007.

Bulk samples were collected from discrete stratigraphic horizons, and shells were hand picked from bulk samples for radiocarbon dating. Shells were selected based on growth rate, preservation (diagenetic assessment), and pristine taphonomic grade. Only specimens with >1mm of growth per year were used to avoid truncated records (i.e., diminished amplitudes in the $\delta^{18}O$ time series) due to slow ontogenetic growth (e.g., Fig. 5 in Fenger et al., 2007). Assessment of diagenetic alteration requires preservation of original mineralogy. We selected shells with original calcitic microstructure (concentric cross-foliated and radial cross-foliated layers) indicating fidelity of the stable isotopic ratios. Shells containing remnants of encrusting or boring organisms were not selected to avoid secondary calcite contamination (taphonomic assessment).

The selected shells were dated by accelerator mass spectrometry (AMS) at Beta Analytic Inc. in the United Kingdom. Radiocarbon dates of the archaeological shells were calibrated using MARINE04 of CALIB 6.0 (Hughen et al., 2004) and corrected for the global ocean reservoir effect (408 years), local reservoir effect (−68±6 years; Harkness, 1983), and ^{13}C fractionation (Stuiver et al., 2005) (Table 1.1). We identified 5 shells (110-30-1, 109-23-1, 110-32-1, 109-33-1, 112-20-2) from the Neoglacial climate episode and 5 shells (103a-37-1, 103a-39-1, 111-31-1, 103a-38-1, 102b-43-1) from the RWP (Table 1.1).

2.2. *Geochemical analysis*

Selected shells were coated with a quick-dry metal epoxy resin (J-B KWIK WELD) on the outer and inner surface to prevent the shells from breaking during cutting. The shells were sectioned from the anterior to posterior margins along the axis of maximum growth and mounted on microscope slides. The slides were attached to a Buehler Isomet low speed saw and cut into ~1 mm thick cross-sections. Cross-sections were polished down to 1µm diamond suspension grit until the internal growth lines and increments were visible. We identified prominent annual growth lines to guide our microsampling strategy by using an Olympus stereomicroscope with a 12.5 megapixel DP71 digital camera. The light control of the stereomicroscope allows viewing with reflected (Fig. 1.2A) and transmitted light (Fig. 1.2B). Transmitted light enhanced the prominence of winter growth lines enabling identification of these annual features to guide microsampling (Fig. 1.2B).

Limpet shells were microsampled at 20-26 samples per year from the margin toward the apex to achieve submonthly resolution. Microsampling was conducted on a Merchantek micromill with a carbide dental scriber (Brasseler). Oxygen isotope ratios of carbonate powder were measured using an automated carbonate preparation device (Kiel-III) coupled to a gas-ratio mass spectrometer (Finnigan MAT 252) housed in the Environmental Isotope Laboratory at the University of Arizona. The precision of the measurements was better than ±0.1‰ VPDB (Vienna Pee Dee Belemnite) for $\delta^{18}O$ (1σ).

2.3. *Estimated temperature*

High-resolution temperature records were estimated from the measured $\delta^{18}O$ values according to the previous calibration of Fenger et al. (2007). Pursuant to their calibration,

1.01‰ was subtracted from each $\delta^{18}O$ value to account for the predictable vital effect in *P. vulgata*. Calculated temperatures from the subtracted values were based on the equilibrium fractionation equation for calcite and water (Friedman and O'Neil, 1977) modified from Tarutani et al (1969):

$$1000\ln\alpha = 2.78 \times 10^6/T^2 - 2.89$$

where α is the fractionation factor between calcite and water, and T is temperature in Kelvin. The relationship between α and δ is as follows:

$$\alpha = (\delta^{18}O_{CALCITE} + 1000) / (\delta^{18}O_{WATER} + 1000)$$

where δ is expressed relative to the standard VSMOW (Vienna-Standard Mean Ocean Water). $\delta^{18}O_{CALCITE}$ values of limpet shells were converted from the VPDB scale to the VSMOW scale before applying the above equations using the following relationship reported by Coplen et al. (1983) and Gonfiantini et al. (1995)

$$\delta^{18}O_{VPDB} = (\delta^{18}O_{VSMOW} - 30.91)/1.03091$$

Although *P. vulgata* grows under normal marine conditions, the oxygen isotope composition of marine seawater is closely related to the mixing of local freshwater run-off (e.g. rainfall) with oceanic water, and consequently varies more or less among different locations. We applied a $\delta^{18}O_{WATER}$ value of +0.1‰±0.04‰ (VSMOW) in the temperature calculation

because the annual mean seawater oxygen isotope ratio in the study area is similar to that of Fenger et al. (2007)'s location according to the global gridded data set of LeGrande and Schmidt (2006). This value is reasonable because it is close to the estimation from the salinity:$\delta^{18}O_{WATER}$ relationship (mixing line) in nearby Loch Sunart (Austin and Inall, 2002; Fig. 1.1). The $\delta^{18}O_{WATER}$ mixing line for Loch Sunart indicated that at 34 psu, the $\delta^{18}O_{WATER}$ value is approximately 0.12‰, in agreement with our assumed value from LeGrande and Schmidt (2006). Estimated temperature from the measured $\delta^{18}O_{SHELL}$ values and the assumed +0.1‰±0.04‰ (VSMOW) of $\delta^{18}O_{WATER}$ has an overall error of ±0.6ºC.

3. Results

3.1. *Neoglacial*

All Neoglacial shells (110-30-1, 109-23-1, 110-32-1, 109-33-1, 112-20-2) have a temporal variation of $\delta^{18}O$ values following a quasi-sinusoidal trend (Fig. 1.3). The prominent growth lines occur at or near peaks in the $\delta^{18}O$ time series. Distances between growth lines measured around 2mm except specimen 109-33-1 which measured around 4mm (Fig. 1.3 and 1.4, Table 1.2). Estimated warmest summer temperatures range from 12.6ºC to 15.7ºC (Fig. 1.4, Table 1.2). Estimated coldest winter temperatures of the two chronologically youngest shells (110-30-1, 109-23-1) recorded the coldest winter temperature around 7.0ºC, whereas the three more recent shells (110-32-1, 109-33-1, 112-20-2) recorded cooler temperatures during the coldest winter months (Fig. 1.4, Table 1.2).

3.2. *Roman Warm Period*

The $\delta^{18}O$ values of the RWP limpets vary sinusoidally with prominent growth lines occurring at or near the most positive $\delta^{18}O$ values (Fig. 1.5). Distances between growth lines ranged from 1.04 to 2.56 mm, although most of them are close to 2mm except specimen 103a-38-1 (Figs. 1.5 and 1.6, Table 1.3). Estimated warmest summer temperatures range from 11.6^{o}C to 14.9^{o}C (Fig. 1.6, Table 1.3). Coldest winter temperatures in all shells showed a consistent trend with the exception of specimen 103a-38-1 which recorded ~2°C warmer winter temperature (Fig. 1.6, Table 1.3).

4. Discussion

4.1. *Neoglacial*

The Neoglacial climate interval is conventionally defined as the advancing of continental glaciers following the retreat of the Wisconsin glaciation during the early Holocene thermal maximum (Porter and Denton, 1967). Because the boundaries between the Neoglaciation and the early Holocene thermal maximum are not isochronous across regions, there is no universal beginning of Neoglacial conditions, although the interval is generally dated to 3300-2500 BP. For southern Norway, Europe, Matthews and Dresser (2008) reported 13 major century- to millennial-scale European Neoglacial events by correlating events recognized from the Alps and southern Norway extending throughout Europe. The forcing factors for the European Neoglacial events are complex, and low solar irradiance can explain only part of the Neoglacial events. Other potential forcing factors include volcanic eruptions and freshwater outbursts.

In our study, the temporal variation of $\delta^{18}O$ values in Neoglacial shells (110-30-1, 109-23-1, 110-32-1, 109-33-1, 112-20-2) recorded seasonal temperature changes during the Neoglacial (Fig. 1.3). The most positive $\delta^{18}O$ values represent winter, whereas the lowest $\delta^{18}O$ values represent summer. Prominent annual growth lines formed during cold winter months (Figs. 1.3 and 1.4), which is consistent with the modern calibration study of Fenger et al. (2007). We also observed fewer numbers of $\delta^{18}O$ data points in cold seasons relative to warm seasons, reflecting slower growth during winter and fast growth during the warm months. Both these observations are in agreement with previous studies that *P. vulgata* from the cold-temperate biogeographic province slows its growth during the winter (Blackmore, 1969; Jenkins and Hartnoll, 2001).

The temporal variation of $\delta^{18}O$ values also showed differences among individuals. Specimen 112-20-2 exhibited the smoothest sinusoidal curve. Specimens 109-23-1, 110-30-1 and 110-32-1 are generally smooth with several fluctuations interrupting the sinusoidal curve. Specimen 109-33-1 has the most fluctuations and therefore least smooth. These high-frequency fluctuations likely reflect frequent changes in SST rather than changes in $\delta^{18}O_{WATER}$ because the study area is not affected by influxes of freshwater and is dominated by well-mixed shelf water (Connor et al, 2006). Perhaps these fluctuations represent times of increased storminess.

One shell (specimen 112-20-2) recorded a year (~4.58-7.09 mm from margin) lacking the typical seasonal variation (Fig. 1.4). Normally, the $\delta^{18}O$ values between two neighboring winter growth lines should follow the sinusoidal trend which includes the coldest winter and

the warmest summer. However, the third annual growth increment from the margin of specimen 112-20-2 exhibited only a slight change in temperature. We interpret this observation as a year without a summer. Such an event has been documented in 536 AD, within the Vandal Minimum climate episode. Historical documents report a widespread dust veil event that caused dimming and cooling across much of the Northern Hemisphere (Stothers and Rampino, 1983; Rampino et al., 1988). In some regions, dry fog or aerosols were so persistent that the fine dust existed in the atmosphere for as long as 18 months. Due to the extended residence time of the dry fog or aerosols, the solar radiation was reduced to one tenth of normal and the year 536 AD was a year without summer (Gunn, 2000). In addition to the historical records, Larsen et al. (2008) reported evidence from Greenland and Antarctic ice cores suggesting that the dust veil causing the year without a summer in 536 AD resulted from a large explosive eruption from an equatorial volcano. This episode in 536 AD likely surpassed the severity of the cold period following the Tambora eruption in 1815. We hypothesize a similar cause for the year without a summer in specimen 112-20-2. The age range of specimen 112-20-2 is 2950-2760 cal. BP and is close to the time of GB4-150 tephra (2750-2708 cal. BP) identified from a peat deposit in Northern Ireland (Swindles et al., 2007). The GB4-150 tephra preserved in the Irish peat is believed to correspond to a large volcanic eruption in the Katla volcanic system in Iceland identified by Larsen et al. (2001) and Swindles et al. (2007).

Neoglacial shells were also compared to monthly records of modern sea surface temperature (SST) near the study area for years 1961 to 1990 (Fig. 1.4). The average modern SST for the warmest month is 14.12±0.54ºC and for the coldest month is 7.40±0.35ºC based

on the temperature record from the National Oceanic and Atmospheric Administration (NOAA) Extended Reconstructed SST V2 database (http://www.cdd.noaa.gov). The comparison between the estimated temperatures from the Neoglacial shells and modern SST record indicated that the coldest winter temperatures during the Neoglacial were similar to the late 20th century in the beginning of Neoglacial as recorded by the specimens 110-30-1 and 109-23-1(Fig. 1.4, Table 1.2). Following this earlier interval, the coldest winter temperatures became ~1°C colder than the late 20th century (Fig. 1.4, Table 1.2). In the early part of our Neoglacial record, the warmest summer temperatures were ~1°C warmer than the late 20th century, subsequently became slightly colder (at the time of specimen 109-23-1), and then became warmer again (at the time of 110-32-1 and 109-33-1). The latest part of our Neoglacial summer temperature record was similar to the late 20th century (Fig. 1.4, Table 1.2). The observed temperature fluctuations are in agreement with temporal fluctuations of the pollen record from south of the Alps during the Neoglacial (Tinner et al., 2003). Aside from the temperature fluctuations, the average winter temperature for the overall Neoglacial period was 6.6±0.3ºC based on the estimated winter temperatures of all our specimens, and the average summer temperature was 14.7±0.4ºC (Table 1.2). Our results indicated that the Neoglacial winters were slightly colder than the late 20th century winters and Neoglacial summers were slightly warmer than the late 20th century summers.

4.2. *Roman Warm Period*

The RWP, also called the Roman Climate Optimum, is defined as the climate episode during Roman times. The time span for RWP is generally 2500-1600 BP, although it varies in different regions: 2400-1600 BP in the North Sea (Hass, 1996), 2500-2100 BP in the

Qinghai-Tibet Plateau (Ji et al., 2005), 2700-1600 BP in southwest Greenland (Seidenkrantz et al., 2007) and 2600-1600 BP in southern Spain (Martín-Puertas et al., 2009). The character of this climate change is not always warm; for instance, the record from Martín-Puertas et al. (2009) suggests wet and humid climate during this time.

The sinusoidal time series of $\delta^{18}O$ values recorded in the RWP shells reflect seasonal temperature fluctuation (Fig. 1.5). Like the Neoglacial shells, the prominent annual growth lines all coincide with winter months (Figs. 1.5 and 1.6). The annual growth rate of the specimens is ~2mm except specimen 103a-38-1 (Figs. 1.5 and 1.6, Table 1.3). Further investigation revealed that the RWP specimen 103a-38-1 recorded winter temperature that was significantly different from the other four RWP shells (Table 1.3). There are two possibilities for this difference. One possibility is that the temperature during the growth period of shell 103a-38-1 was indeed significantly warmer than the other RWP shells. However, this possibility has low confidence because we would expect the summer temperature recorded in shell 103a-38-1 to be distinctive from the other RWP shells. Our preferred explanation is the time-averaging effect resulting from slow growth rate during winter. A similar time-averaging effect was also observed modern *P. vulgata* shells and produced the truncated range in $\delta^{18}O$ values and hence estimated temperatures (Fenger et al., 2007). Therefore, we consider the winter record of shell 103a-38-1 to be biased by time averaging due to slow winter growth rates, and we exclude its winter temperatures from further interpretations.

We also compared the estimated RWP temperatures to the modern SST record from 1961 to 1990 near the study area. For the winter months, the RWP shells (not including excluded specimen 103a-38-1) were consistent in the coldest winter temperatures at ~6°C and therefore all recorded winter temperatures that were colder than the late 20th century. For the summer months, the RWP was initially ~2°C colder than the late 20th century as recorded by the specimen 103a-37-1 (Table 1.3). Summer temperature subsequently increased to 13°C at the time of 103a-39-1 and 111-31-1, but was still 1°C colder relative to the late 20th century. At the time of 103a-38-1, the summer temperature was similar to the late 20th century and then dropped back to 13°C at the time of 102b-43-1. By averaging the temperatures of all the specimens, we concluded that the RWP winters (6.3±0.1°C) were ~1°C colder than late 20th century winters and the RWP summers (13.3±0.3°C) were slightly colder than late 20th century summers.

4.3. *Comparison of Neoglacial and Roman Warm Period*

As previously discussed, the five Neoglacial shells recorded average winter temperature of 6.6±0.3°C and average summer temperature of 14.7±0.4°C, whereas the RWP shells recorded average winter temperature of 6.3±0.1°C and average summer temperature of 13.3±0.3°C. Therefore, the RWP winters were similar to or slightly colder than the Neoglacial winters, and the RWP summers were ~1°C colder than the Neoglacial summers, which is statistically significant according to the results of one-way analysis of variance (F= 3.46, α=0.10, with 1 and 8 degrees of freedom). Consequently, the seasonal range of the RWP is approximately 1°C smaller than that of the Neoglacial (Tables 1.2 and 1.3).

Our findings that the RWP was colder than the Neoglacial are consistent with previous studies. The Neoglacial shells primarily recorded the temperature during 3500-3100 cal. BP, and most of the RWP shells recorded the temperature in 2300-1900 cal. BP (Table 1.1, Fig. 1.7). According to the pine history in Scotland (Bridge et al., 1990) and the European glacier record (Matthews and Dresser, 2008), the climate between 3500-3100 cal. BP was relatively warm compared to other times during the Neoglacial period, and the climate between 2300-1900 cal. BP was relatively cold compared to the rest of the RWP. The macrofossil record of Scots pine (*Pinus sylvestris*) from Scotland indicates that the percentage of pine pollen was high at 3520-3030 ^{14}C yr BP but decreased to a minimum at 2500-1800 ^{14}C yr BP (Bridge et al., 1990). Because pine growth requires dry, warm climate, this suggests that the RWP was colder and wetter than the Neoglacial interval; i.e., had higher effective precipitation (low temperature may reduce rates of evapotranspiration and increase wetness). Moreover, the pollen record in northeast Scotland spanning the Bronze and Iron Ages also indicates a significant increase in effective precipitation at ca. 2900 cal. BP which led to more wet mire surfaces (Tipping et al., 2008). The chronology of European Neoglacial events also showed major glacial advances around 2200-1900 cal. BP and no glacial advances between 3500-3100 cal. BP (Matthews and Dresser, 2008).

Increasing water input from the Scottish Coastal Current may have been directly responsible for the decreasing SST. The Scottish Coastal Current originates from the Irish and Clyde Seas and, hence, is colder and fresher (~1% dilution due to the brackish water from the fjords) relative to the North Atlantic Current. This hypothesis is supported by the modern instrumental records near Tiree Passage, which indicate that cooler episodes were

generally coincident with lower coastal salinities and westward migration of isohalines (Inall et al., 2009). The westward displacement of Scottish Coastal Current and isohalines is further determined by the strength of sub-polar gyres (SPG) and sub-tropical gyres (STG). A strong SPG results in a more east-west orientated gyre and, hence, colder and fresher water mass in the coast, whereas a strong STG results in a more south-north orientated gyre and modifies the coastal water mass towards warmer and saltier. In addition, Holliday (2003) investigated the air-sea interaction and circulation in the northeast Atlantic and suggested that the gyre circulation of SPG and STG are significantly influenced by the state of the NAO. Therefore, the cooling transition detected in our study may result from the change of NAO via modulating the strength of SPG and STG circulation.

4.4. *Subboreal/Subatlantic transition*

The Neoglacial-RWP climate transition detected in our study is in agreement with the Subboreal/Subatlantic transition (2800-2700 cal. BP). This climate transition is also known as the 850 cal. BC "event" and has been identified by pollen zones, and the Bronze Age/Iron Age transition based on episodes in human history. The various names for this climate shift result from its widespread impact on global climate and vegetation distribution, and hence, on prehistoric agriculture and human society.

Similar to the Little Ice Age climate episode, this abrupt climatic deterioration has been identified in many regions in both hemispheres, and is considered to be geographically widespread. Most proxy evidence for this climate event comes from the North Atlantic Ocean (Bianchi and McCave, 1999; Bond et al., 2001; Oppo et al., 2003; Hall et al., 2004),

from continental Europe (Kilian et al., 1995; van Geel et al., 1998; Speranza et al., 2000, 2002; Blaauw et al., 2004; Swindles, et al., 2007), and from eastern North America (Brown et al., 2000; Booth et al., 2003). There is also some proxy evidence from the Andean region of South America (Heusser, 1995; van Geel et al., 2000), south-central Siberia (van Geel et al., 2004), and northwest Africa (Van Geel et al., 1998; Elenga et al., 2004). In the North Atlantic, colder surface waters and accompanying prominent increases in drift ice around 2800 cal. BP were detected from the proxy records in deep-sea sediment cores (Bond et al., 2001). Synchronous with the change of overlying surface waters, deep meridional overturning circulation was reduced in the North Atlantic (Bianchi and McCave, 1999; Oppo et al., 2003; Hall et al., 2004). In continental Europe, this climate event shows more or less regional variation, although it is normally characterized by a decline of temperature or a wetter climate shift. Sudden increase in wet conditions started at ca. 2800 cal. BP in the eastern part of Netherlands based on high resolution AMS dating and micro/macro-fossil compositions of Holocene bog deposits (Kilian et al., 1995; Blaauw et al., 2004). A shift to wetter and cooler climate occurred at ca. 2800 cal. BP according to proxy records in the peat sequence of the Giant Mountains (Czech Republic) (Speranza et al., 2000, 2002). The multiproxy records from the peatlands of northern Ireland reveal a major climate shift to wetter/colder climate conditions at ca. 2700 cal. BP (Swindles, et al., 2007). The resolution for these proxy records is generally at the decadal scale.

Because this climate deterioration occurred during the period of reduced solar activity between 2800 and 2710 cal. BP (850 and 760 cal BC), the so-called "Homeric minimum" (Landscheidt, 1987), van Geel et al. (1998, 2000) proposed that the abrupt decrease of solar

irradiance probably triggered this climate shift. This hypothesis is supported by the solar activity record derived from the $\Delta^{14}C$ record of multiple peat deposits in northwest Europe (Mauquoy et al., 2004). Renssen et al. (2006) further explored the impact of reduced solar activity on centennial-scale cooling events in the Holocene by using the coupled global atmosphere-ocean-vegetation model ECBilt-CLIO-VECODE. In the simulation, the global annual atmospheric surface temperature anomaly closely followed variations in total solar irradiance (TSI) during the cooling phase of 2800-2700 cal. BP, implying that temperature change was triggered by reduced solar activity. In addition, the simulation showed a spatial pattern in the temperature change. For instance, the strongest cooling (up to 0.5ºC) was observed at Northern Hemisphere mid-latitude continents, which is in agreement with most proxy evidence. After 2700 cal. BP, the value of the TSI anomaly started to increase, but the global atmospheric surface temperature anomaly still remained low. The extended cooling of surface temperature was explained by positive oceanic feedbacks. Simulated precipitation at Northern Hemisphere mid-latitudes did not show significant change on continents, which is inconsistent with the general shift to wetter conditions found in proxy data from continental Europe.

In summary, simulations suggest that the centennial cooling event around 2800-2700 cal. BP is a combined consequence of reduced solar activity and positive oceanic feedback. In our study area, positive oceanic feedback should be largely governed by the NAO based on the modern instrumental records (Inall et al., 2009). Global circulation models conducted by Shindell et al. (2001) also suggest that the decrease of solar irradiance will trigger a low NAO index and cause regional cooling over the continents of the Northern Hemisphere.

Moreover, Mann et al. (2009) and Trouet et al. (2009) implicated weak NAO conditions as a driver of climate during the Little Ice Age, which may also explain the cooling trend observed in our study. However, we are not able to exclude other possibilities in explaining the cooling transition from the Neoglacial to the RWP.

5. Conclusions

Our study provides the first reconstruction of SST variability at seasonal time scales in the North Atlantic along northwestern coastal Scotland across the Neoglacial-RWP transition. Neoglacial shells recorded slightly colder winters and slightly warmer summers during their growth period. RWP shells generally have slightly colder summers and ~1°C colder winters than present during their growth period. Our findings document a slight winter cooling and a significant summer cooling of ~1℃ from the Neoglacial to the RWP. This cooling transition is supported by other paleoclimate proxies in Scotland and Europe. This transition is likely associated with the Subboreal/Subatlantic transition and may have been triggered by reduced solar radiation at 2800-2700 cal. BP with weakened NAO conditions. One shell from the Neoglacial period captured a year without a summer, which may have resulted from an explosive volcanic eruption in the Katla volcanic system in Iceland.

References

Austin WEN, Inall ME. 2002. Deep-water renewal in a Scottish fjord: temperature, salinity and oxygen isotopes. *Polar Research* **21**: 251-257.

Baxter JM, Boyd IL, Cox M, Cunningham L, Holmes P, Moffat CF. 2008. *Scotland's seas: towards understanding their state*. Fisheries Research Services, Aberdeen.

Bianchi GG, McCave IN. 1999. Holocene periodicity in North Atlantic climate and deep-ocean flow south of Iceland. *Nature* **397**: 515–517.

Blaauw M, van Geel B, van der Plicht J. 2004. Solar forcing of climatic change during the mid-Holocene: indications from raised bogs in the Netherlands. *Holocene* **14**: 1-35.

Blackmore DT. 1969. Studies of *Patella vulgata* L.I. Growth, reproduction, and zonal distribution. *Journal of Experimental Marine Biology and Ecology* **3**: 200–213.

Bond G, Kromer B, Beer J, Munscheler R, Evans MN, Showers W, Hoffmann S, Lotti R, Hajdas I, Bonani G. 2001. Persistent solar influence on North Atlantic climate during the Holocene. *Science* **294**: 2130–2136.

Booth RK, Jackson ST. 2003. A high-resolution record of late-Holocene moisture availability from a Michigan raised bog, USA. *Holocene* **13**: 863–876.

Branch GM. 1981. The biology of limpets: Physical factors, energy flow, and ecological interactions. *Oceanography and Marine Biology: an annual review* **19**: 235-380.

Bridge MC, Haggart BA, Lowe JJ. 1990. The history and palaeoclimatic significance of subfossil remains of *Pinus sylvestris* in blanket peats from Scotland. *Journal of Ecology* **78**: 77-99.

Brown SL, Bierman PR, Lini A, Southon J. 2000. 10000 yr record of extreme hydrological events. *Geology* **28**: 335–338.

Cohen AL, Tyson PD. 1995. Sea-surface temperature fluctuations during the Holocene off the south coast of Africa: Implications for terrestrial climate and rainfall. *Holocene* **5**: 304-312.

Connor DW, Gilliland PM, Golding N, Robinson P, Todd D, Verling E. 2006. *UKSeaMap: the mapping of seabed and water column features of UK seas*. Joint Nature Conservation Committee, Peterborough.

Coplen TB, Kendall C, Hopple J. 1983. Comparison of stable isotope reference samples, *Nature* **302**: 236-238.

Crisp DJ. 1965. Observations on the effect of climate and weather on marine communities. In *The Biological Significance of Climatic Changes in Britain*, Johnson CG, Smith LP (eds). Elsevier: New York; 63-77.

Elenga H, Maley J, Vincens A, Farrera I. 2004. Palaeoenvironments, palaeoclimates and landscape development in Atlantic Equatorial Africa: a review of key sites covering the last 25 kyrs. In *Past climate variability through Europe and Afrcia*, Battarbee, RW, Gasse F, Stickley CE (eds). Springer: Dordrecht; 181–198.

Ekaratne SUK, Crisp DJ. 1984. Seasonal growth studies of intertidal gastropods from shell micro-growth band measurements, including a comparison with alternative methods. *Journal of the Marine Biological Association of the United Kingdom* **64**: 13-210.

Fenger T, Surge D, Schone B, Milner N. 2007. Sclerochronology and geochemical variation in limpet shells (*Patella vulgata*): A new archive to reconstruct coastal sea surface temperature. *Geochemistry Geophysics Geosystems* **8**: Q07001, doi:10.1029/2006GC001488.

Friedman I, O'Neil JR. 1977. Compilation of stable isotope fractionation factors of geochemical interest. In Data of Geochemistry, Fleischer M (ed). U.S. Govt. Print. Office: Washington, D.C.; 1-12.

Goewert AE, Surge D. 2008. Seasonality and growth patterns using isotope sclerochronology in shells of the Pliocene scallop *Chesapecten madisonius*. *Geo-Marine Letters* **28**: 327-338.

Gonfiantini R, Stichler W, Rozanski K. 1995. Standards and intercomparison materials distributed by the International Atomic Energy Agency for stable isotope measurements. In References and Intercomparison Materials for Stable Isotopes of Light Elements, the Isotope Hydrology Section of the International Atomic Energy Agency (eds). IAEA: Vienna, Austria; 13-29.

Gunn JD. 2000. The years without summer: tracing A.D. 536 and its aftermath. *British Archaeological Reports International Series* **872**.

Hall IR, Bianchi GG, Evans JR. 2004. Centennial to millennial scale Holocene climate-deep water linkage in the North Atlantic. *Quaternary Science Reviews* **23**: 1529-1536.

Hallmann N, Burchell M, Schöne BR, Irvine GV, Maxwell D. 2009. High-resolution sclerochronological analysis of the bivalve mollusk *Saxidomus gigantea* from Alaska and British Columbia: Techniques for revealing environmental archives and archaeological seasonality. *Journal of Archaeological Science* **36**: 2353-2364.

Harkness DD. 1983. The extent of the natural ^{14}C deficiency in the coastal environment of the United Kingdom. *Journal of the European Study Group on Physical, Chemical and Mathematical Techniques Applied to Archaeology PACT 8 (IV.9)*: 351-364.

Hass HC. 1996. Northern Europe climate variations during late Holocene: evidence from marine Skagerrak. *Palaeogeography, Palaeoclimatology, Palaeoecology* **123**: 121-145.

Helama S, Hood BC. 2011. Stone Age midden deposition assessed by bivalve sclerochronology and radiocarbon wiggle-matching of *Arctica islandica* shell increments. *Journal of Archaeological Science* **38(2)**: 452-460.

Heusser CJ. 1995. Palaoecology of a Donatia-Astlia cushion bog, Magellanic Moorland-Subantarctic Evergreen Forest transition, southern Tierra del Fuego, Argentina. *Review of Paleobotany and Palynology* **89**: 429-40.

Holliday NP. 2003. Air-Sea interaction and circulation changes in the northeast Atlantic. *Journal of Geophysical Research* **108 (C8)**: 3259, doi:10.1029/2002JC001344.

Hufthammer AK, Høie H, Folkvord A, Geffen AJ, Andersson C, et al. 2010. Seasonality of human site occupation based on stable oxygen isotope ratios of cod otoliths. *Journal of Archaeological Science* **37**: 78-83.

Hughen K, Baille M, Bard E, Beck J, Bertrand C, Blackwell P, et al. 2004. Marine04 Marine radiocarbon age calibration, 26–0 ka BP. *Radiocarbon* **46**: 1059-1086.

Hurrell JW. 1995. Decadal trends in the North Atlantic Oscillation: regional temperatures and precipitation. *Science* **269**: 676-679.

Inall M, Gillibrand P, Griffiths C, MacDougal N, Blackwell K. 2009. On the oceanographic variability of the north-west European shelf to the west of Scotland. *Journal of Marine Systems* **77**: 210-226.

Jenkins SR, Hartnoll RG. 2001. Food supply, grazing activity and growth rate in the limpet *Patella vulgata* L.: A comparison between exposed and sheltered shores. *Journal of Experimental Marine Biology and Ecology* **258**: 123–139.

Ji J, Shen J, Balsam W, Chen J, Liu L, Liu X. 2005. Asian monsoon oscillations in the northeastern Qinghai-Tibet Plateau since the late glacial as interpreted from visible reflectance of Qinghai Lake sediments. *Earth and Planetary Science Letters* **233**: 61-70.

Jones D., Allmon WD. 1995. Records of upwelling, seasonality and growth in stable-isotope profiles of Pliocene mollusk shells from Florida. *LETHAIA* **28**: 61-74.

Jones KB, Hodgins GWL, Etayo-Cadavid MF, Andrus CFT, Sandweiss DH. 2010. Centuries of marine radiocarbon reservoir age variation within archaeological *Mesodesma donacium* shells from southern Peru. *Radiocarbon* **52(3)**: 1207-1214.

Kilian MR, van der Plicht J, van Geel B. 1995. Dating raised bogs: new aspects of AMS ^{14}C wiggle matching, a reservoir effect and climatic change. *Quaternary Science Reviews* **14**: 959-66.

Landscheidt T. 1987. Long-range forecasts of solar cycles and climate change. In *Climate History, Periodicity and Predictability*. Rampino MR, Sanders JE, Newman WS, Konigsson LK. (eds).Van Nostrand Reinhold: New York; 421–445.

Larsen G, Newton AJ, Dugmore AJ, Vilmundardóttir EG. 2001. Geochemistry, dispersal, volumes and chronology of Holocene silicic tephra layers from the Katla volcanic system, Iceland. *Journal of Quaternary Science* **16**: 119-132.

Larsen LB, Vinther BM, Briffa KR, Melvin TM, Clausen HB, Jones PD, et al. 2008. New ice core evidence for a volcanic cause of the A.D. 536 dust veil. *Geophysical Research Letters* **35**: L04708, doi:10.1029/2007GL032450.

Lee S, Kim H. 2003. The dynamical relationship between subtropical and eddy-driven jets. *Journal of the Atmospheric Sciences* **60**: 1490-1503.

LeGrande AN, Schmidt GA. 2006. Global gridded data set of the oxygen isotopic composition in seawater. *Geophysical Research Letters* **33**: L12604, doi:10.1029/2006GL026011.

Mann ME, Zhang Z, Rutherford S, Bradley RS, Hughes MK, et al. 2009. Global signatures and dynamical origins of the Little Ice Age and Medieval Climate Anomaly. *Science* **326**: 1256-1260.

Martín-Puertas C, Valero-Garcés BL, Brauer A, Mata MP, Delgado-Huertas A, Dulski P. 2009. The Iberian-Roman Humid Period (2600-1600 cal yr BP) in the Zoñar Lake varve record (Andalucía, southern Spain). *Quaternary Research* **71**: 108-120.

Matthews JA, Dresser PQ. 2008. Holocene glacier variation chronology of the Smørstabbtindan massif, Jotunheimen, southern Norway, and the recognition of century- to millennial-scale European Neoglacial events. *Holocene* **18**: 181-201.

Mauquoy D, van Geel B, Blaauw M, Speranza A, van der Plicht J. 2004. Changes in solar activity and Holocene climatic shifts derived from ^{14}C wiggle-match dated peat deposits. *Holocene* **14**: 45-52.

Oppo DW, McManus JF, Cullen JL. 2003. Deepwater variability in the Holocene epoch. *Nature* **422**: 277–278.

Patterson WP, Dietrich KA, Holmden C, Andrews JT. 2010. Two millennia of North Atlantic seasonality and implications for Norse colonies. *Proceedings of the National Academy of Sciences* **107 (12)**: 5306-5310.

Porter SC, Denton GH. 1967. Chronology of Neoglaciation in the North American Cordillera. *American Journal of Science* **265**: 177-210.

Rampino MR, Self S, Stothers RB. 1988. Volcanic winters. Annual Review of Earth and *Planetary Sciences* **16**: 73-99.

Renssen H, Goose H, Muscheler R. 2006. Coupled climate model simulation of Holocene cooling events: ocean feedback amplifies solar forcing. *Climate of the Past* **2**: 79-90.

Schifano G, Censi P. 1986. Oxygen and carbon isotope composition, magnesium and strontium contents of calcite from a subtidal *Patella coerulea* shell. *Chemical Geology* **58**: 325-331.

Schöne BR, Fiebig J, Pfeiffer M, Gleβ R, Hickson J, Johnson ALA, Dreyer W, Oschmann W. 2005. Climate records from a bivalved Methuselah (*Arctica islandica*, Mollusca; Iceland). *Palaeography, Palaeoclimatology, Palaeoecology* **228**: 130-148.

Schöne BR, Dunca E, Fiebig J, Pfeiffer M. 2005. Mutvei's solution: An ideal agent for resolving microgrowth structures of biogenic carbonates. Palaeogeography, Palaeoclimatology, Palaeoecology **228**: 149-166.

Seidenkrantz M.-S, Aagaard-Sørensen S, Sulsbrück H, Kuijpers A, Jensen KG, Kunzendorf H. 2007. Hydrography and climate of the last 4400 years in a SW Greenland fjord: implication for Labrador Sea palaeoceanography. *Holocene* **17**: 387-401.

Shackleton NJ. 1973. Oxygen isotope analysis as a means of determining season of occupation of prehistoric midden sites. *Archaeometry* **15**: 133-141.

Shindell DT, Schmidt GA, Mann ME, Rind D, Waple A. 2001. Solar forcing of regional climate change during the Maunder Minimum. *Science* **294**: 2149-2152.

Speranza A, van der Plicht J, van Geel B. 2000. Improving the time of control of the Subboreal/Subatlantic transition in a Czech peat sequence by ^{14}C wiggle-matching. *Quaternary Science Review* **19**: 1589-604.

Speranza A, van Geel B, van der Plicht J. 2002. Evidence for solar forcing of climate change at ca. 850 cal. BC from a Czech peat sequence. *Global and Planetary Change* **35**: 51-65.

Stothers RB, Rampino MR. 1983. Volcanic eruptions in the Mediterranean before A. D. 630 from written and archaeological sources. *Journal of Geophysical Research* **88**: 6357-6371.

Stuiver M, Reimer PJ, Reimer RW. 2005. CALIB Radiocarbon Calibration. http: // radiocarbon.pa.qub.ac.uk/calib.

Surge D, Walker K J. 2005. Oxygen isotope composition of modern and archaeological otoliths from the estuarine hardhead catfish (*Ariopsis felis*) and their potential to record low-latitude climate change. *Palaeogeography, Palaeoclimatology, Palaeoecology* **228**: 179-191.

Surge D, Walker KJ. 2006. Geochemical variation in microstructural shell layers of the southern quahog (*Mercenaria campechiensis*): Implications for reconstructing seasonality. *Palaeogeography, Palaeoclimatology, Palaeoecology* **237**: 182-190.

Swindles G, Plunkett G, Roe HM. 2007. A delayed climatic response to solar forcing at 2800 cal. BP: multiproxy evidence from three Irish peatlands. *Holocene* **17**: 177-182.

Tarutani T, Clayton RN, Mayeda TK. 1969. The effect of polymorphism and magnesium substitution on oxygen isotope fractionation between calcium carbonate and water. *Geochimica et Cosmochimica Acta* **33**: 987-996.

Tinner W, Lotter AF, Ammann B, Conedera M, Hubschmid P, van Leeuwen JFN, Wehrli M. 2003. Climatic change and contemporaneous land-use phases north and south of the Alps 2300 BC to 800 AD. *Quaternary Science Reviews* **22**: 1447-1460.

Tipping R, Davies A, McCulloch R, Tisdall E. 2008. Response to late Bronze Age climate change of farming communities in north east Scotland. *Journal of Archaeological Science* **35**: 2379-2386.

Trouet V, Esper J, Graham NE, Baker A, Scourse JD, Frank DC. 2009. Persistent positive North Atlantic Oscillation mode dominated the Medieval Climate Anomaly. *Science* **324**: 78-80.

van der Schrier G, Drijfhout SS, Hazeleger W, Noulin L. 2007. Increasing the Atlantic subtropical jet cools the circum-North Atlantic. *Meteorologische Zeitschrift* **16**: 1-8.

van Geel B, Bokovenko NA, Burova ND, Chugunov KV, Dergachev VA, et al. 2004. Climate change and the expansion of the Scythian culture after 850 BC, a hypothesis. *Journal of Archaeological Science* **31**: 1735-1742.

van Geel B, Heusser CJ, Renssen H, Schuurmans CJE. 2000. Climatic change in Chile at around 2700 BP and global evidence for solar forcing: a hypothesis. *Holocene* **10**: 659-664.

van Geel B, van der Plicht J, Kilian MR, Klaver ER, Kouwenberg JHM, Renssen H, Reynaud-Ferrera I, Waterbolk HT. 1998. The sharp rise of Δ^{14}C c. 800 cal BC: possible causes, related climatic teleconnections and the impact on human environments. *Radiocarbon* **40**: 535-550.

Walker KJ, Surge D. 2006. Developing oxygen isotope proxies from archaeological sources for the study of Late Holocene human–climate interactions in coastal southwest Florida. *Quaternary International* **150**: 3-11.

Wang T, Surge D, Walker KJ. (2011). Isotopic evidence for climate change during the Vandal Minimum from *Ariopsis felis* otoliths and *Mercenaria campechiensis* shells, southwest Florida, USA. *Holocene* **21(7)**: 1081-1091. doi:10.1177/0959683611400458.

Table 1.1. Time range of the archaeological limpets.

Specimen No.	BETA No.	Measured Age	$\delta^{13}C$ (‰)	Conventional Age (^{14}C yr BP)	2 Sigma Calibration
102b-43-1	252892	1930±40	+0.2	2340±40	cal. BP 2130-1930 (cal. BC 180-cal. AD 40)
103a-38-1	251118	1950±40	−0.1	2360±40	cal. BP 2150-1960 (cal. BC 200-10)
111-31-1	251120	2000±40	+0.5	2420±40	cal. BP 2280-2030 (cal. BC 330-80)
103a-39-1	252894	2030±40	+0.7	2450±40	cal. BP 2300-2080 (cal. BC 340-130)
103a-37-1	252893	2080±40	+1.3	2510±40	cal. BP 2330-2140 (cal. BC 380-190)
112-20-2	251121	2600±40	+1.0	3030±40	cal. BP 2950-2760 (cal. BC 1000-810)
109-33-1	252895	2910±40	+0.8	3330±40	cal. BP 3350-3160 (cal. BC 1400-1220)
110-32-1	252897	2940±40	+1.5	3370±40	cal. BP 3380-3220 (cal. BC 1430-1270)
109-23-1	251119	2960±40	+1.0	3390±40	cal. BP 3410-3240 (cal. BC 1460-1290)
110-30-1	252896	3100±40	+0.9	3520±40	cal. BP 3560-3380 (cal. BC 1620-1430)

Table 1.2. Summary statistics for temperature estimated from the Neoglacial limpets. For each specimen, distance between growth lines, coldest winter temperature and warmest summer temperature are all listed with the first year at bottom.

Specimen (cal. BP)	Distance between growth lines (mm)	Coldest winter temperature (^{o}C)	Average winter temperature with standard errors (^{o}C)	Warmest summer temperature (^{o}C)	Average summer temperature with standard errors (^{o}C)	Seasonal range (^{o}C)
112-20-2 (2950-2760)	2.52 2.51	6.0 6.6	6.3±0.3	13.6 15.2	14.4±0.8	8.1
109-33-1 (3350-3160)	4.19	6.0 6.1	6.0	14.9 14.9	14.9	8.9
110-32-1 (3380-3220)		6.1	6.1	15.5	15.5	9.4
109-23-1 (3410-3240)	2.46 2.08	7.1 7.5 7.0	7.2±0.2	12.6 14.0	13.3±0.7	6.1
110-30-1 (3560-3380)	1.61 2.16	7.8 7.1	7.5±0.4	15.7 15	15.4±0.4	7.9
Average in total			6.6±0.3		14.7±0.4	8.1±0.6

Table 1.3. Summary statistics for temperature estimated from the Roman Warm Period limpets. For each specimen, distance between growth lines, coldest winter temperature and warmest summer temperature are all listed with the first year at bottom.

Specimen (cal. BP)	Distance between growth lines (mm)	Coldest Winter Temperature (°C)	Average winter temperature with standard errors (°C)	Warmest summer temperature (°C)	Average summer temperature with standard errors (°C)	Seasonal range (°C)
	2.02	5.6		12.4		
102b-43-1	2.56	6.4		13.4		
(2130-1930)	2.20	5.8	5.9±0.2	13.1	13.0±0.3	7.1
		8.0		15.1		
	1.58	8.3		13.2		
	1.39	8.1		14.4		
103a-38-1	1.32	9.8		14.3		
(2150-1960)	1.04	7.5	8.3±0.4	14.5	14.3±0.3	6.0
				13.9		
		6.4		13.2		
	1.59	5.2		12.3		
	1.88	7.4		12.6		
111-31-1	2.13	6.2		12.8		
(2280-2030)	1.72	6.4	6.3±0.4	13.8	13.1±0.3	6.8
		6.6		13.3		
103a-39-1	1.66	5.9		12.8		
(2300-2080)	1.95	6.4	6.3±0.2	14.9	13.7±0.6	7.4
				13.4		
		6.0		11.6		
103a-37-1	2.20	7.0		12.3		
(2330-2140)	2.10	6.5	6.5±0.3	11.8	12.3±0.4	5.8
Average in total			6.3±0.1[1]		13.3±0.3	6.6±0.3

[1]6.3±0.1°C is calculated after excluding the outlier 103a-38-1.
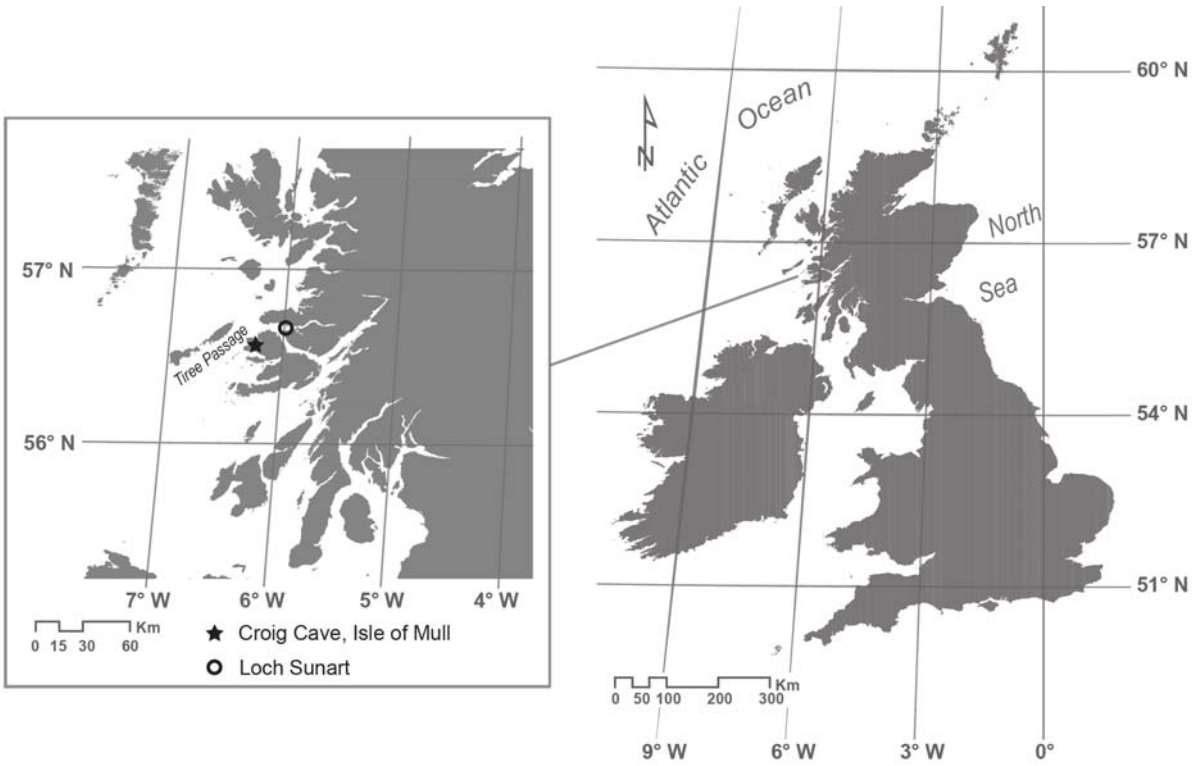
Figure 1.1. Map of Scotland and Isle of Mull. The star identifies the archaeological site Croig Cave, which is located on the northwestern shore of Mull. The circle indicates the position of Loch Sunart.
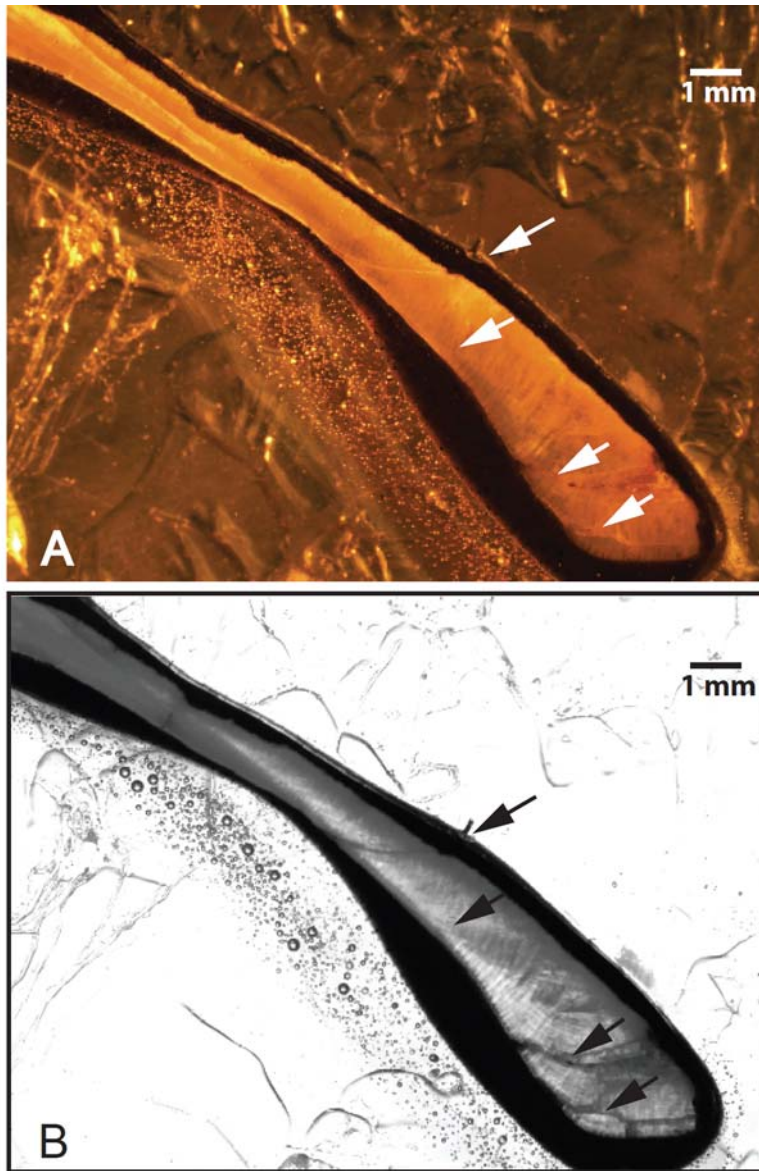
Figure 1.2. Cross-section along the axis of maximum growth of archaeological limpet 102b-43-1. Arrows identify prominent annual growth lines. (A) Cross-section observed under reflected light. (B) Cross-section observed under transmitted light.
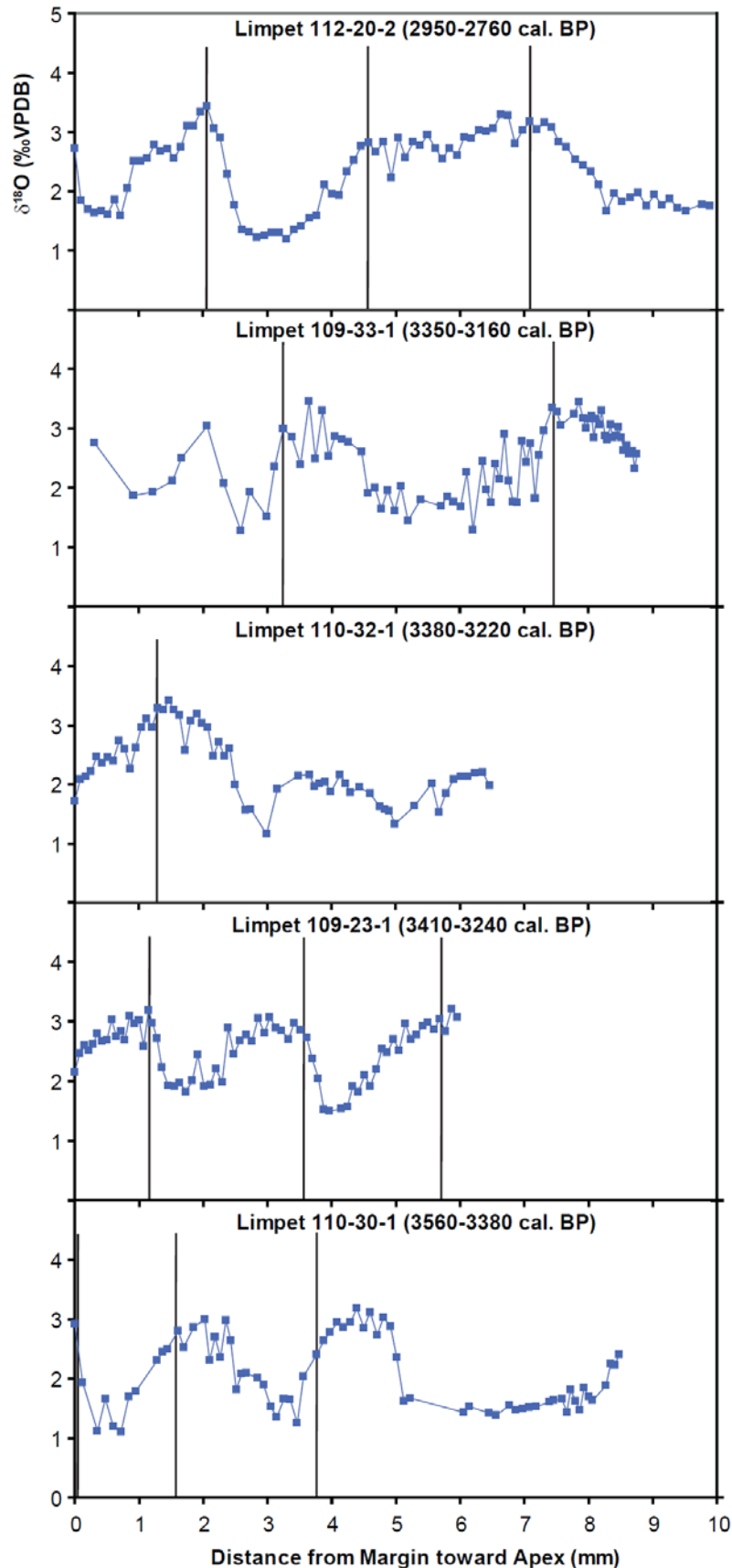
Figure 1.3. δ¹⁸O values of the Neoglacial limpets (110-30-1, 109-23-1, 110-32-1, 109-33-1, 112-20-2) versus distance from margin toward apex (growth direction is from right to left). The vertical lines represent the positions of annual growth lines.

34
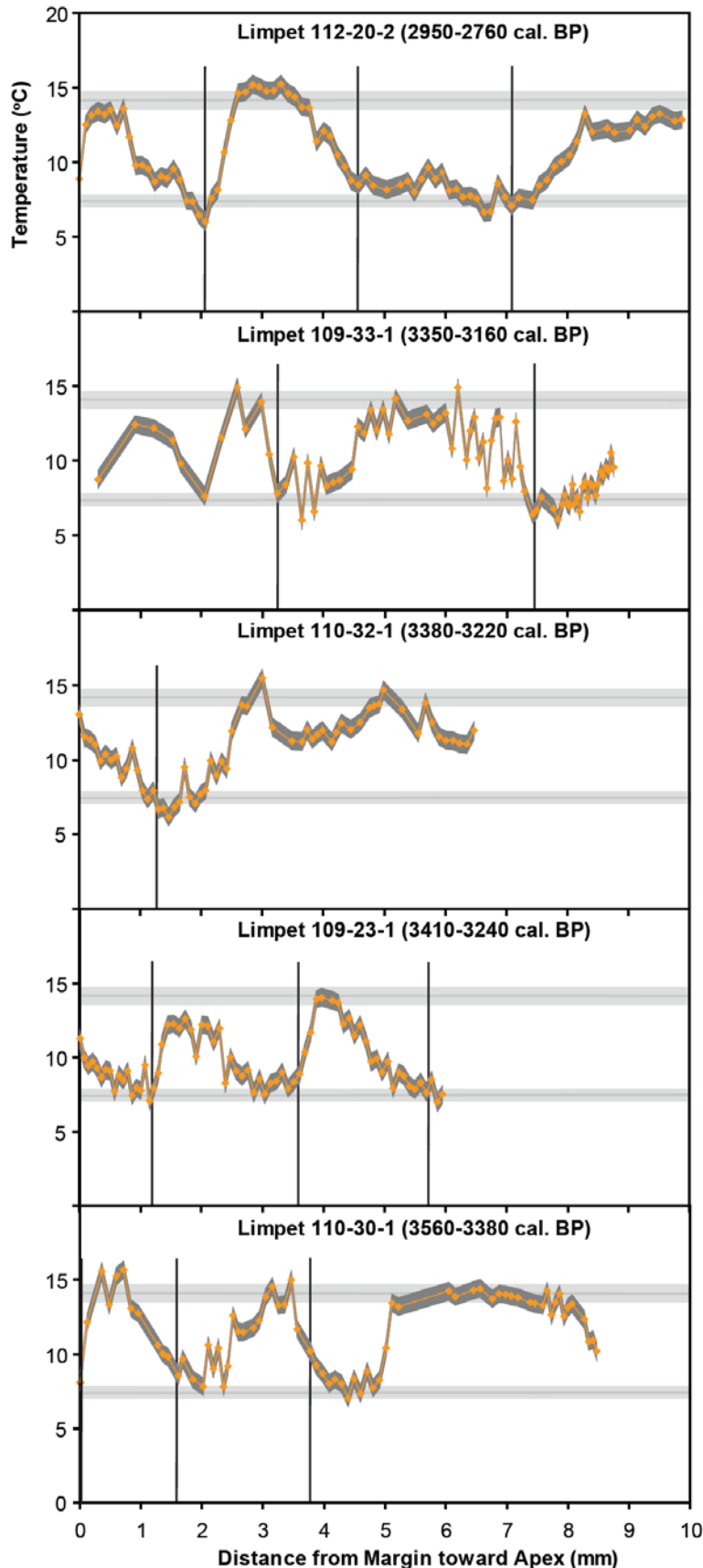
Figure 1.4. Estimated temperatures with errors from the Neoglacial limpets. The vertical lines represent the positions of annual growth lines. The horizontal bars indicate the average range of summer SST data (14.12±0.54°C) and winter SST data (7.40±0.35°C) from 1961-1990 around the grid (56°N, 6°W) provided by the National Oceanic and Atmospheric Administration (NOAA) Extended Reconstructed SST V2 database (http://www.cdc.noaa.gov).
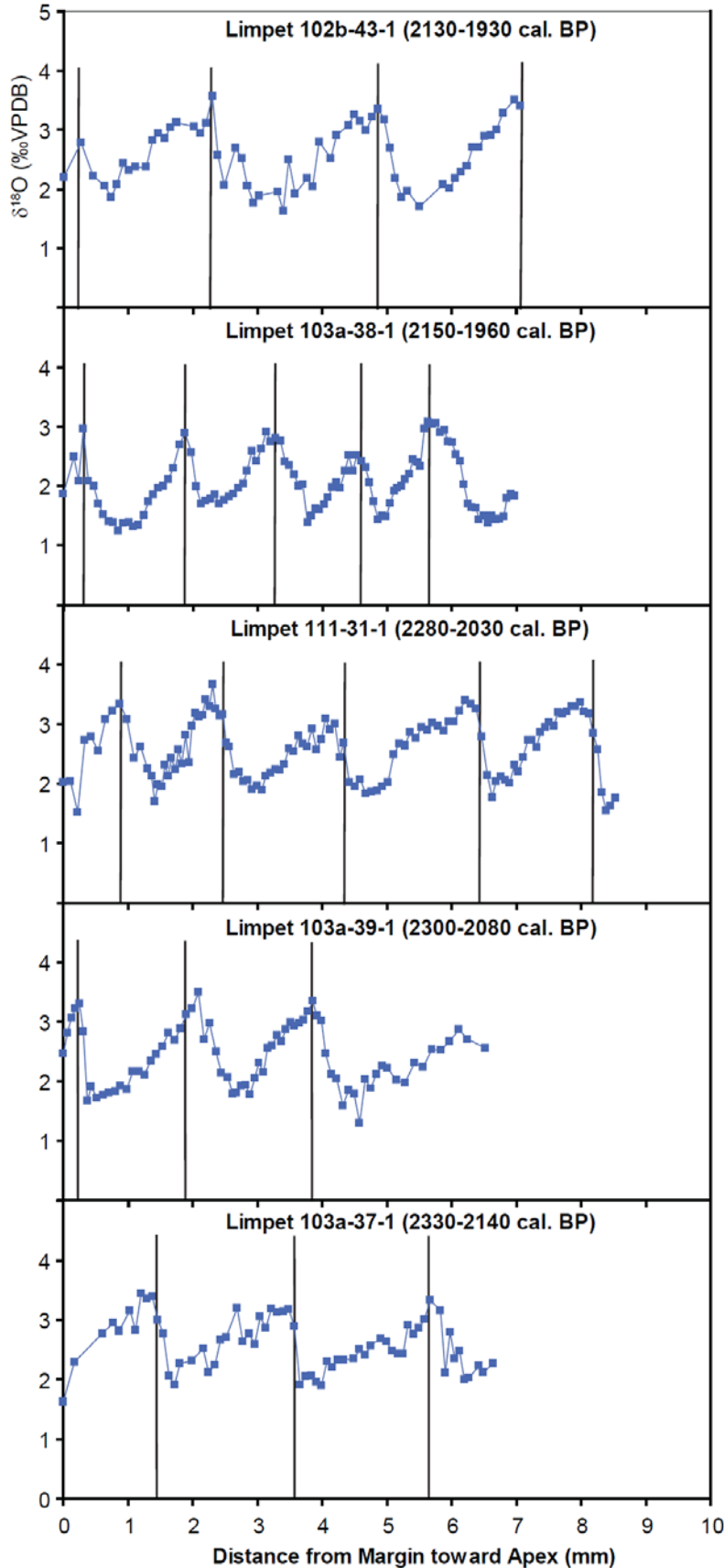
Figure 1.5. δ^{18}O values of the Roman Warm Period limpets (103a-37-1, 102b-41-1, 103a-39-1, 111-31-1, 103a-38-1, 102b-43-1) versus distance from margin toward apex (growth direction is from right to left). The vertical lines represent the positions of annual growth lines.
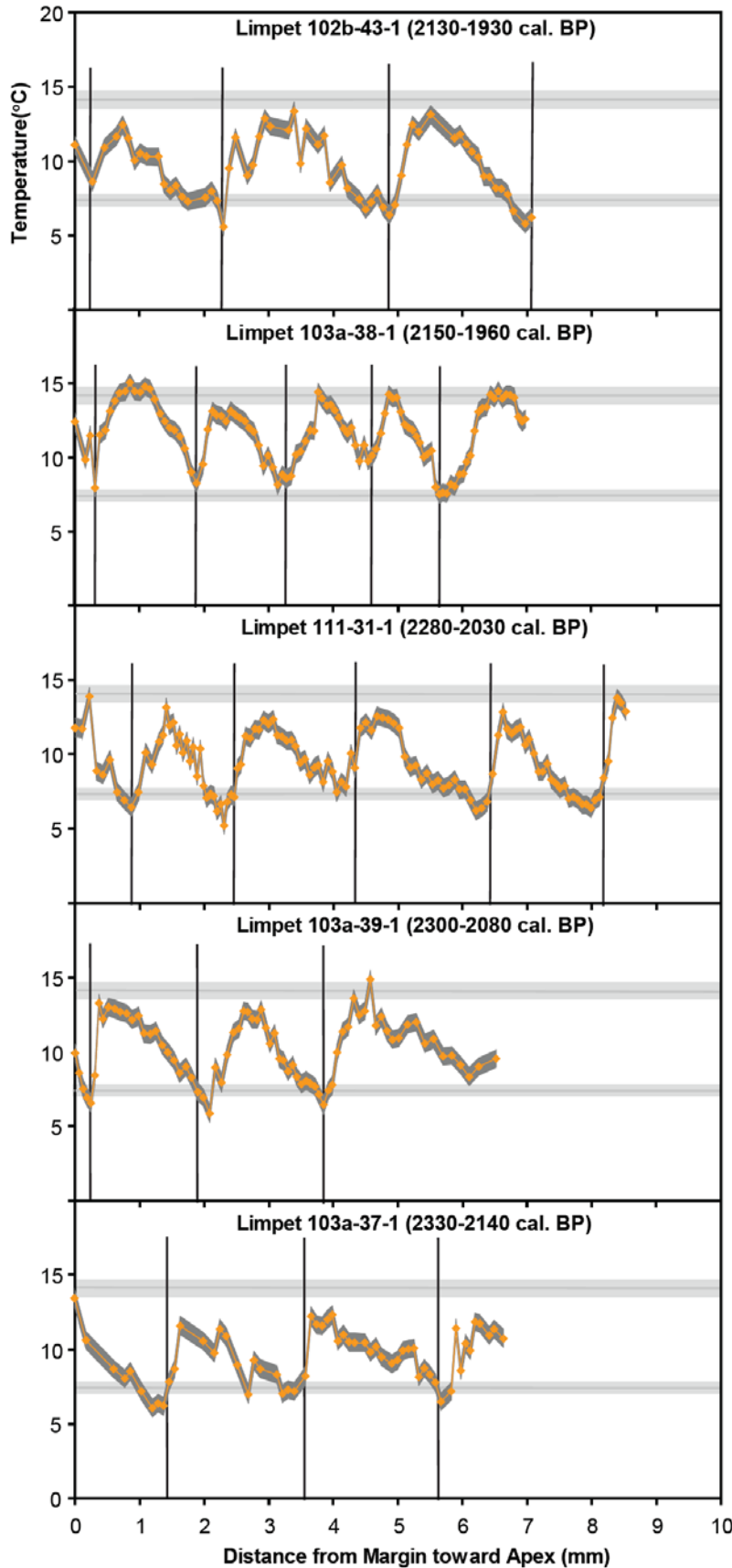
Figure 1.6. Estimated temperatures with errors from the Roman Warm Period limpets. The vertical lines represent the positions of annual growth lines. The horizontal bars indicate the average range of summer SST data (14.12 ± 0.54^{o}C) and winter SST data (7.40 ± 0.35^{o}C) around the grid (56°N, 6°W) from 1961-1990 provided by the National Oceanic and Atmospheric Administration (NOAA) Extended Reconstructed SST V2 database (http://www.cdc.noaa.gov).
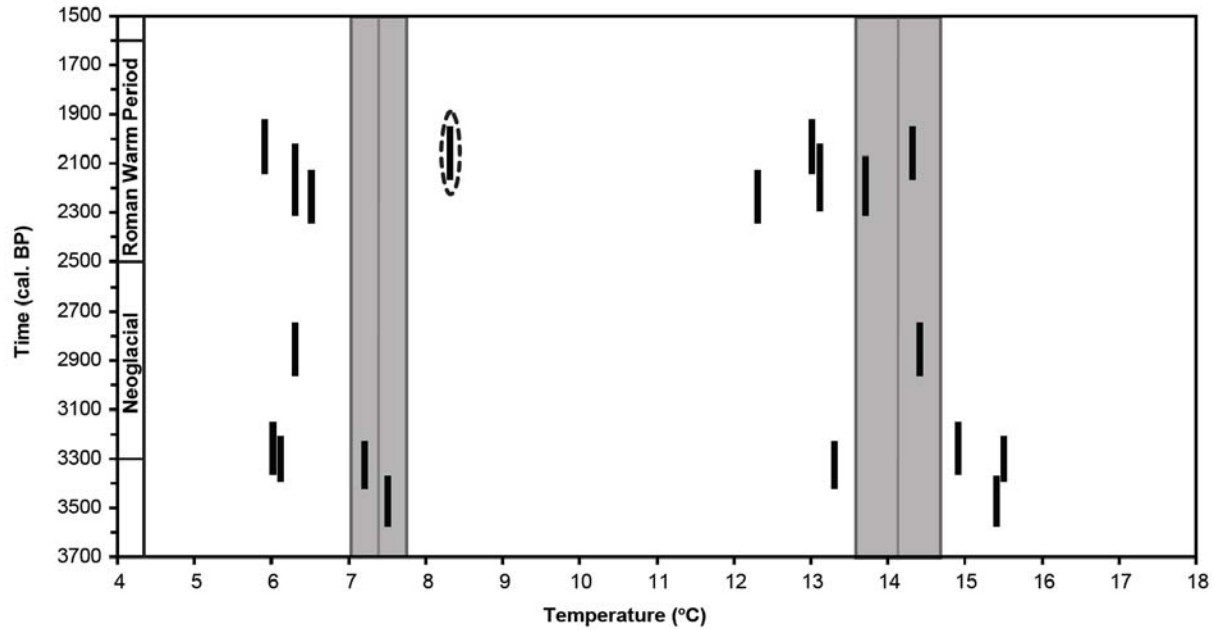
Figure 1.7. Temperature comparison between the Neoglacial and Roman Warm Period. The solid black lines refer to the age range of the limpets. The outlier 103a-38-1 is marked with dashed circle. The vertical bars indicate the average range of winter SST data ($7.40\pm0.35^{o}C$) and summer SST data ($14.12\pm0.54^{o}C$) around the grid ($56^{o}N$, $6^{o}W$) provided by the National Oceanic and Atmospheric Administration (NOAA) Extended Reconstructed SST V2 database (http://www.cdc.noaa.gov).

CHAPTER II

SEASONAL CLIMATE CHANGE ACROSS THE ROMAN WARM PERIOD/VANDAL MINIMUM TRANSITION USING ISOTOPE SCLEROCHRONOLOGY IN ARCHAEOLOGICAL SHELLS AND OTOLITHS, SOUTHWEST FLORIDA, USA

Abstract

Archaeological evidence suggests that southwest Florida experienced variably warmer and wetter climate during the Roman Warm Period (RWP; 300 BC-550 AD) relative to the Vandal Minimum (VM; 550-800 AD). To test this hypothesis, we reconstruct seasonal-scale climate conditions for the latter part of the RWP (1-550 AD) by using high-resolution oxygen isotope ratios ($\delta^{18}O$) of archaeological shells (*Mercenaria campechiensis*) and otoliths (*Ariopsis felis*). Eight shells radiocarbon-dated to 150-550 AD recorded RWP summers that were drier relative to today, which is represented by the average value of modern shell specimens. Eight otoliths indicate that RWP winters gradually increased in temperature from $18^{o}C$ (150-200 AD) to $23^{o}C$ (500-550 AD) punctuated by cold interruptions at 250-300 AD and 450-500 AD. Our climate reconstructions agree with archaeological observations and are partially coherent with the history of sea-level change. We observe a marked drying and cooling trend across the RWP/VM transition. The climate transition is not only consistent with falling sea level, but also coincident with reduced solar radiation. Reduced solar radiation might have triggered a change in atmospheric circulation patterns that precipitated the observed climate transition.

1. Introduction

The pre-European Calusa people in southwest Florida left behind abundant shell middens/mounds, artifacts, and other cultural remains (Marquardt 2004). Archaeological evidence from these deposits suggests that this region was impacted by abrupt climate change and sea-level fluctuation during two climate episodes in the first millennium: the Roman Warm Period (RWP; 300 BC-550 AD) and the Vandal Minimum (VM; 550-800 AD) (Marquardt and Walker, 2001). In an earlier study, we reconstructed seasonal climate change during the VM using oxygen isotope proxy data ($\delta^{18}O$) preserved in archaeological *Mercenaria campechiensis* shells and *Ariopsis felis* otoliths (fish "ear bones") from discrete chronostratigraphic layers within these Calusa middens and mounds (Wang et al., 2011). Following the earlier VM study, the primary intent of the present research is to reconstruct climate change in the RWP with oxygen isotope ratios of archaeological shell-otolith pairs and provide isotope evidence to test the archaeological findings across the RWP and VM climate episodes. Archaeological shell-otolith pairs are good study proxies for both paleoclimate reconstructions and human-climate relationships. The shell-otolith pairs provide high-resolution climate information on changes in summer wet season conditions and winter sea surface temperature (SST) (Walker and Surge, 2006). Because archaeological shells and otoliths were deposited during the RWP by the Calusa of southwest Florida, the climate proxies also reflect aspects of human behavior in the late Holocene.

40

Aside from providing isotope evidence for the archaeological findings, the climate reconstruction in this study should also be pivotal for studying the mechanism dominating late Holocene climate change. Accurate reconstruction of paleoclimate is essential to investigate the mechanism underlying the climate change. High-resolution climate proxies are able to help reduce uncertainties generated in the process of reconstruction. Oxygen isotope ratios of mollusc shells and fish otoliths have been widely used in high-resolution temperature or precipitation reconstructions, and are accepted as reliable and accurate climate proxies (Jones et al., 1989, 1990, 1996; Ivany et al., 2000; Wurster and Patterson, 2001; Surge and Walker, 2005, 2006; Wang et al., 2011). Moreover, there is increasing paleoclimate evidence that tropical/subtropical climate is actually more variable and dynamic than previously thought (Winter et al., 2000; Haug et al., 2001; Hodell et al., 2001; Black et al., 2007; Richey et al., 2009). The model simulation conducted by Barnett et al. (1992) identified the climate variability within the latitudes of 0°-30° as the primary contributor to global climate variability at multi-decadal to centennial timescales. Adjacent to our study area, the Gulf of Mexico, experienced a larger magnitude of cooling than the mean magnitude of northern hemisphere cooling during the Little Ice Age (Richey et al., 2009). Therefore, subtropical southwest Florida (26-27°N) is sensitive to climate change like other low-latitude regions and is appropriate for studying multi-decadal to centennial climate oscillations, such as the VM and RWP.

In this project, we present a multi-proxy record of $\delta^{18}O$ values that signal the variability of summer precipitation and winter temperature during the RWP in southwest

Florida. We further compare the RWP climate reconstruction with archaeological evidence to check if they are in agreement. Additionally, we integrate the climate records of RWP and VM with the history of sea level and solar activity to gain insights into the climate mechanism driving the late Holocene climate change in southwest Florida.

2. Study site

2.1. *Climatic context*

Coastal southwest Florida, and in particular the Charlotte Harbor-Pine Island Sound region (Fig. 2.1), is a low-lying, topographically flat estuarine environment, which makes it vulnerable to climate related disasters such as sea-level rise, floods, droughts, hurricanes and other storms, etc. (Beever III et al., 2009). Additionally, falls in sea level such as those indicated by regional beach-ridge research (Stapor et al. 1991) in a shallow-water bay such as Pine Island Sound (Fig. 1) would be or have been especially disastrous for a people dependent on the molluscan and fish populations of these inshore waters. In response to some of this variability, ancient Calusa people in this region may have shifted their residential locations several times during their long history there (Walker, 2000; Walker et al., 1995). Therefore, coastal southwest Florida is an ideal location for studying past human-climate interactions.

The climate of coastal southwest Florida is typically subtropical. The instrumental record of monthly average air temperature (from 1892-2007) at Fort Myers (Fig. 2.1B; www.ncdc.noaa.gov) shows that the coldest average monthly temperature is 17.4 ± 1.7^{o}C (n=116), whereas the warmest average monthly temperature is 28.1 ± 0.6^{o}C (n=116).

Therefore, the interannual temperature variability is larger in winter compared to summer months. The instrumental record for precipitation from 1931-2007 at Fort Myers (Fig. 2.1B; www.ncdc.noaa.gov) indicates that monthly accumulation of rainfall during the wet season (May-October) averages 181 mm/month, whereas the dry season (November-April) averages 50 mm/month. The rainfall during the wet season contributes approximately 78% of the annual rainfall, resulting in a seasonal pattern of warm/wet summers and cool/dry winters. The seasonal difference in wind conditions controls this pattern. In winter, continental cold fronts generate high-speed wind and carry cool and dry Arctic air from Canada to the study site, resulting in cooler and drier winters relative to summers (Bradley, 1972).

On the long-term basis of decades to centuries, the climate of southwest Florida is strongly influenced by atmospheric circulation patterns. Temperature change, especially winter temperature change, is mainly affected by a low-frequency circulation pattern resembling the North Atlantic Oscillation (NAO) (Marshall et al., 2001; Lund and Curry, 2004; Saenger et al., 2011). Precipitation change is largely influenced by the Atlantic Multidecadal Oscillation (AMO) which develops in high latitudes and secondarily from low-latitude climate patterns such as the El Niño-Southern Oscillation (ENSO) and Intertropical Convergence Zone (ITCZ) (Soto, 2005). Soto (2005) attributes increasing precipitation in Florida to an increase of warm, moist air delivered either from the tropical Pacific during El Niño years or from the Atlantic during warm AMO phases and northward migration of the ITCZ. Therefore, the long-term climate variability of southwest Florida is a combined reflection of high-latitude and low-latitude climate systems.

2.2. *Archaeological context*

In southwest Florida, Calusa people inhabited the highly productive Charlotte Harbor-Pine Island Sound region, which archaeologists refer to as the Caloosahatchee culture region (Fig. 2.1B; Walker, 1992). Although the Calusa people were culturally complex, their subsistence strategy was nonagricultural, and they relied heavily on aquatic foods (Widmer, 1988; Marquardt 2004). They regularly collected estuarine/marine fish, shellfish and other aquatic animals from the shallow-water zones close to their habitation sites (Walker, 1992). The skeletal remains of consumed aquatic animals were mostly deposited in sequence, so their accumulated middens and mounds are usually in stratigraphic succession (Walker, 1992; Walker et al., 1995; Walker 2000). Thus, these stratigraphic middens and mounds contain information about the temporal and spatial variation of animal diversity and abundance as well as settlement changes of the local people. Therefore, these stratigraphic middens and mounds represent an environmental archive that can be used to reconstruct the history of paleoenvironmental and paleoecological changes (Walker, 1992; Marquardt and Walker, 2001; Walker and Surge, 2006).

The archaeological specimens used in this study were collected from the shell middens and mounds at the Pineland Site Complex (see Marquardt and Walker, 2001; Marquardt and Walker, in press for detailed descriptions). The temporal focus of this study is the cultural period, Caloosahatchee I-late and the earliest part of the IIA-early period (1-550 AD), which correlates with the later part of the RWP (Walker and Surge, 2006). A schematic composite of the stratigraphy of the Pineland Site Complex for the cultural interval of Caloosahatchee I-late (Fig. 2.1A; Marquardt and Walker, in press) is characterized by beds of

44

sand and shell midden, sometimes with much intermixing. They variably contain hard-part remains of many fishes, mollusks, and echinoderms. Most remains were discarded by Pineland's human residents after consuming the fish and shellfish meats (e.g., of hardhead catfish and other fishes, and of oysters, surfclams, quahog clams, whelks, conchs, etc.). In other cases, remains such as small articulated marsh clam and ribbed mussel shells are in-situ specimens that died in life positions, indicating layers of natural sedimentation. One stratum, occurring at 300 AD and indicated by articulated surfclam shells and sea urchin remains is interpreted as a storm-surge deposit. Additionally, the remains of a dwelling floor located in one area of the site complex are indicated by a dark layer with an associated post mold.

3. Methods

3.1. *Dating*

Following the approach of Walker and Surge (2006) and Wang et al. (2011), we analyzed shell-otolith pairs dated to the Caloosahatchee I-late and the earliest part of the IIA-early period (1-550 AD). The archaeological pairs were chosen based on their chronostratigraphic context from multiple areas of the Pineland Site Complex (Walker et al., 1995; Walker, 2000; Marquardt and Walker, 2001). We selected eight shell-otolith pairs (CI-M6/CI-A6, CI-M7/CI-A7, CI-M8/CI-A8, CI-M3/CI-A3, CI-M5/CI-A5, CIIA-M6/CIIA-A6, CIIA-M7/CIIA-A7, and CIIA-M9/CIIA-A9) and two additional shells (CI-M2 and CI-M4) from the Pineland collections housed at the Florida Museum of Natural History (FLMNH) (see Table 2.1 for corresponding FLMNH shell catalog numbers). However, shells CI-M7 and CI-M3 are too small in size and hence were not sampled. The selected shells and otoliths were dated using accelerator mass spectrometry (AMS) at the National Ocean Sciences

Accelerator Mass Spectrometry (NOSAMS) Facility, Woods Hole Oceanographic Institute. Measured AMS ^{14}C ages of the archaeological shells were calibrated using MARINE04 of CALIB 5.0.2 and corrected for the global ocean reservoir effect (408 years), local reservoir effect (−5±20 years), and ^{13}C fractionation (Hughen et al., 2004; Stuiver et al., 2005). By combining the stratigraphic order of archaeological proveniences and the calibrated AMS ^{14}C dates, the 50-year archaeological AD time ranges of the specimens were estimated (Table 2.1).

3.2. *Microstructure and microsampling*

The accretionary growth patterns in *M. campechiensis* shells and *A. felis* otoliths contain annual markers, which guided our sampling strategy. We cut shells and otoliths into cross-sections along the axis of maximum growth. The cross-sections were polished down to 1μm diamond suspension grit until the internal growth increments were clearly visible. Shell cross-sections showed alternating dark slow growth increments (or translucent under transmitted light; Jones and Quitmyer, 1996) and light fast growth increments under reflected light (Fig. 2.2A). The surrounding environmental conditions dominate the growth rate of *Mercenaria* shells. When water temperature and salinity exceed the limits of shell growth, i.e., below 9°C or above 31°C or below 17 psu (practical salinity units), growth rate slows (Ansell, 1968; Kraeuter and Castagna, 2001). Therefore, dark increments in *Mercenaria* shells under reflected light form in summer for the southern hard clam *M. campechiensis* (Arnold, et al., 1991). The cross-sections of *A. felis* otoliths exhibited fast growth increments separated by prominent growth lines of slow growth rate (Fig. 2.2B; Wurster and Patterson, 2001). Because *A. felis* prefer living in warm water (25°C-36°C), the growth rate of *A. felis*

otoliths in our study area decreases in winter and forms growth lines (Jones et al., 1978). In addition, the microstructure of archaeological shells and otoliths displays that annual growth rate slows with ontogeny after 5 to 6 years of age.

Cross-sections of all archaeological shells and otoliths were examined using an Olympus stereomicroscope with a 12.5 megapixel DP71 digital camera to evaluate preservation of original aragonite. We only use specimens with preserved original aragonite and that were not diagenetically altered. Shells were microsampled at 24 to 26 samples per year during the first 5 years of growth and otoliths were microsampled at 15 to 20 samples per year across the second to sixth years of growth. Microsampling was performed using a Merchantek micromill fitted with a Brasseler carbide dental scriber (Fig. 2.2C). Each digitized drilling path produced approximately 40 to 60 μg of carbonate powder for isotopic analysis. Oxygen isotope ratios were measured using an automated carbonate preparation device (Kiel-III) coupled to a gas-ratio mass spectrometer (Finnigan MAT 252). Powdered samples were reacted with dehydrated phosphoric acid under vacuum at 70°C for one hour. The isotope ratio measurement was calibrated based on repeated measurements of NBS-19 and NBS-18. The precision of the measurements was ±0.1 ‰ for $\delta^{18}O$ (1σ). The results were reported in per mil units (‰) relative to the VPDB (Vienna Pee Dee Belemnite) standard.

3.3. *Estimated precipitation and temperature*

Mixing relations between oxygen isotope ratios and salinity in Charlotte Harbor exhibit a relatively steep gradient during the summer wet season compared to the winter dry season (Walker and Surge, 2006). However, the estuarine waters in Pine Island Sound have a

much more complex seasonal behavior. Pine Island Sound may behave like a restricted lagoon having limited communication with Charlotte Harbor. Moreover, near-surface aquifer systems may produce freshwater seeps in the shallow basin of Pine Island Sound further complicating the seasonal relationship between $\delta^{18}O_{water}$ and salinity. Therefore, although *M. campechiensis* shells and *A. felis* otoliths precipitate in oxygen isotope equilibrium with ambient water (Kalish, 1991; Iacumin et al., 1992; Patterson et al., 1993; Thorrold et al., 1997; Elliot et al., 2003), the complication of $\delta^{18}O_{water}$ making it difficult to estimate temperature from $\delta^{18}O_{shell}$ and $\delta^{18}O_{otolith}$ values. To overcome this complication, we used a multi-taxa approach to evaluate summer precipitation and winter temperature during the RWP. This approach has been successfully applied in previous studies by Walker and Surge (2006) and Wang et al. (2011).

We first compared $\delta^{18}O_{shell}$ values between modern (05PI05 and 05PI17 from Wang et al., 2011) and archaeological (CI-M6, CI-M8, CI-M2, CI-M4, CI-M5, CIIA-M6, CIIA-M7, and CIIA-M9) shells to make inferences about summer precipitation in the RWP. More negative summer $\delta^{18}O_{shell}$ values refer to more negative $\delta^{18}O_w$ values that result from increased input of freshwater due to more precipitation. The influence of temperature on summer $\delta^{18}O_{shell}$ is negligible because of low inter-annual variability observed in summer temperature ($0.6^{o}C$) between 1892 and 2007. The variability of $0.6^{o}C$ can only result in approximately 0.1‰ differences in $\delta^{18}O_{shell}$ values (Elliot et al., 2003). We assumed that the inter-annual variability of summer temperature during the RWP is similar to today because the low-frequency circulation pattern resembling NAO controls the long-term temperature change in southwest Florida and it mainly influences the winter temperature change.

Unlike *M. campechiensis* which are sessile, *A. felis* migrate between estuarine and marine environments seasonally. In winter and early spring, adults migrate from estuarine water into normal marine water in the Gulf of Mexico where $\delta^{18}O_w$ can be constrained to marine seawater values of ~+1‰VSMOW (Vienna Standard Mean Ocean Water) (Surge and Walker, 2005). In addition, *A. felis* live in water above the thermocline during winter, so $\delta^{18}O_{otolith}$ values record climatic temperature variability rather than depth-related temperature change (Muncy and Wingo, 1983). Therefore, the seasonal migration behavior of *A. felis* provides an opportunity to estimate winter temperature from winter $\delta^{18}O_{otolith}$ values. Following Surge and Walker (2005), we used the equilibrium fractionation equation reported by Patterson et al. (1993) to calculate temperature:

$$10^3 \ln\alpha = 18.56(10^3 T^{-1}) - 33.49$$
$$\alpha = (\delta^{18}O_{otolith} + 10^3)/(\delta^{18}O_w + 10^3)$$

where T is the temperature in Kelvin, and $\delta^{18}O_{otolith}$ and $\delta^{18}O_w$ are oxygen isotope ratios relative to the VSMOW scale. We converted $\delta^{18}O_{otolith}$ values from the VPDB scale to VSMOW following Gonfiantini, et al. (1995):

$$\delta^{18}O_{VSMOW} = 1.03091 \times \delta^{18}O_{VPDB} + 30.91.$$

4. Results

The temporal variations of $\delta^{18}O_{shell}$ values in all RWP shells (CI-M6, CI-M8, CI-M2, CI-M4, and CI-M5) followed a quasi-sinusoidal trend (Fig. 2.3). Dark increments (under reflected light) coincided at or near the most negative values in the $\delta^{18}O_{shell}$ time series (Fig. 2.3). The most negative $\delta^{18}O_{shell}$ values were selected for evaluation of summer precipitation (Fig. 2.3; Table 2.2). $\delta^{18}O$ values of RWP otoliths (CI-A6, CI-A7, CI-A8, CI-A3, and CI-A5) also varied sinusoidally (Fig. 2.4). The majority of prominent growth lines occurred at or near the most positive $\delta^{18}O_{otolith}$ values (Fig. 2.4). The coldest temperatures recorded in each otolith were selected to evaluate winter temperature change (Fig. 2.4; Table 2.2).

5. Discussion

5.1. *Oxygen isotope ratios of shells and otoliths*

Although varying $\delta^{18}O_w$ values of the estuarine water in our study area impedes the accurate estimation of temperature, variations in the $\delta^{18}O_{shell}$ values of archaeological shells can reflect the seasonal pattern that the most positive values represent cold winter temperatures and the most negative values represent warm summer temperatures (Fig. 2.3). In addition, combining the seasonal pattern of $\delta^{18}O_{shell}$ values with growth-increment analysis also reveals the relationship between temperature and growth rate. The increments of slow growth always coincide with the most negative $\delta^{18}O_{shell}$ values (i.e., warm summers), whereas the increments of fast growth rate are coeval with more positive $\delta^{18}O_{shell}$ values (i.e., colder temperatures) (Fig. 2.3). Therefore, the $\delta^{18}O_{shell}$ profile of archaeological shells exhibit relatively broad peaks and narrow valleys. The ontogenetic analysis is consistent with earlier studies in that *Mercenaria* shells from subtropical latitudes form slow growth increments in summer (Arnold et al., 1998; Surge and Walker, 2006; Surge et al., 2008).

50

Similar to the $\delta^{18}O_{shell}$ values of archaeological shells, the $\delta^{18}O_{otolith}$ values of archaeological otoliths exhibit a seasonal pattern with most positive values in winter and most negative values in summer (Fig. 2.4). Positions of most prominent growth lines are coincident with the most positive $\delta^{18}O_{otolith}$ values, suggesting that the growth rate decreased significantly in winter. However, there were one or two growth lines in otoliths CI-A3, CI-A8, and CI-A6 occurring at the negative $\delta^{18}O_{otolith}$ values instead of at the most positive $\delta^{18}O_{otolith}$ values. This indicates that the growth rate of otoliths is not only determined by temperature but also by biological factors, such as food and reproduction (Wang et al., 2011). Because a significantly slow growth rate can increase the time averaging during microsampling, the $\delta^{18}O_{otolith}$ profile potentially does not record the coldest winter temperature (Patterson et al., 1993). Wang et al. (2011) observed warmer winter temperature reconstructed from the modern otolith than that measured instrumentally. To reduce the biases of time averaging, we compared the winter temperatures of archaeological otoliths with the winter temperatures of modern otolith MOD2002 (from Wang et al., 2011), instead of with winter temperatures from the instrumental record.

5.2. *Reconstructed precipitation and temperature during the RWP*

Summer precipitation of the RWP was lower or similar to the late 20th century. The oldest shell (CI-M6; 150-200 AD) recorded more positive summer $\delta^{18}O_{shell}$ values in the first two years and similar values in the latter years compared to the average value of modern shell specimens measured by Wang et al. (2011) (Fig. 2.3). The average for the most negative $\delta^{18}O_{shell}$ values in the first, third, fourth and fifth summers was −1.9±0.3‰, slightly

51

higher than the average value of modern shell specimens (Table 2.2). Therefore, the summers over 150-200 AD were slightly drier than today, which is represented by the average value of modern shell specimens (Table 2.2). The second summer of CI-M6 was not included for average because we lost several samples for the second summer and risked not recording the most negative $\delta^{18}O_{shell}$ value. In 200-250 AD, shell CI-M8 recorded more positive $\delta^{18}O_{shell}$ values in the first and fourth summers and similar $\delta^{18}O_{shell}$ values in the second and third summers relative to modern specimens (Fig. 2.3). The average for the four summers was −2.1±0.2‰, which suggests slightly drier summers than today (Table 2.2). In 250-300 AD, shell CI-M2 recorded both summers drier than today (Fig. 2.3). In 300-350 AD, shell CI-M4 recorded similar a summer in the first year, then soon changed into drier summers relative to today (Fig. 2.3). The average for the most negative $\delta^{18}O_{shell}$ values of CI-M4 also suggests drier summer in 300-350 AD (Table 2.2). Shell CI-M5 also indicated four consistent drier summers than today in 300-350 AD although there appears to be a trend of increasing precipitation after the fourth summer. The average $\delta^{18}O_{shell}$ value for the four summers of CI-M5 was −1.6±0.1‰, similar to that of shell CI-M4 (−1.6±0.3‰). To summarize, the majority of RWP summers were drier than today with few summers similar to today.

Winter temperature of the RWP was colder or similar to today. In 150-200 AD, otolith CIA-6 recorded colder winters in the first and third winters and similar winter in the second winter compared to today, which is represented by the average winter temperature of modern otolith MOD2002 (Fig. 2.4). The average for the coldest temperatures of the three winters was 18.1±0.7°C, which was about 2°C colder than today (Table 2.2). In 200-250 AD, the winter temperatures of otoliths CI-A7 and CI-A8 were consistent and were similar or

52

slightly colder relative to today (Fig. 2.4). In 250-300 AD, all the three winters of otolith CI-A3 recorded colder winters than today and the coldest temperature (16.2°C) was almost 4°C colder than today (Fig. 2.4). In 300-350 AD, otolith CI-A5 recorded similar winter temperature in the first and third winters and warmer temperature in the second winter relative to today (Fig. 2.4). The average for the otolith CI-A5 was $20.6\pm0.5^{\circ}$C, which was similar to today (Table 2.2). Therefore, otoliths CI-A6 and CI-A3 recorded colder winters relative to today whereas otoliths CI-A7, CI-A8 and CI-A5 recorded similar winters to today.

Reconstructed summer precipitation and winter temperature are in agreement with the archaeological evidence for the RWP. In 150-200 AD, the shell/otolith pair CI-M/A6 suggests drier summers and colder winters relative to today (Fig. 2.5; Table 2.2). This was consistent with the early part of regression after a transgression peak at 150 AD in a sea level record reconstructed by Tanner (2000) (Fig. 2.5). The sand observed underlying the stratum of CI-M/A6 might have been deposited at the time of transgression peak (Marquardt and Walker, 2001). During 200-250 AD, shell CI-M8 recorded slightly drier summers and CI-A7&8 recorded slightly colder winters (Fig. 2.5; Table 2.2). Therefore, compared to the earlier deposited CI-M/A6, they suggest that both summer precipitation and winter temperature increased in 200-250 AD relative to 150-200 AD. This is in agreement with the dominance of eastern oyster shells, along with low numbers of the high-salinity associate, crested oysters in this time increment, which suggests relatively low-salinity water (Marquardt and Walker, in press). In 250-300 AD, summer precipitation decreased significantly as recorded by shell CI-M2 and winter temperature also decreased based on the winters of otolith CI-A3 (Fig. 2.5; Table 2.2). These results are plausible because these

specimens were both from the very bottom of Old Mound (OM)'s buried, waterlogged midden. The elevation of CI-M2/A3 was Level 102 (−0.46 m MSL), well below estimated MSL within Level 97. Therefore, the specimens represent the initiation of that midden which was deposited on a lowered shoreline and then accumulated up to a half-meter depth (Marquardt and Walker, in press). This is in agreement with the 250 AD sea-level low and subsequent abrupt reversal in 250-300 AD (Fig. 2.5). In 300-350 AD, shell CI-M4 also recorded dry summers, consistent with its high-salinity midden context and coincident with the beginning of a regression of sea level after a peak at 300 AD (Fig. 2.5; Tanner, 2000). After CI-M4, shell CI-M5 recorded dry summers, still relatively high water but consistent with falling sea level (Fig. 2.5; Tanner, 2000) and high abundance of crown conchs (Marquardt and Walker, in press), an opportunistic gastropod that flourishes in times of environmental stress (Walker 1992, 2000).

5.3. *Climate transition across the RWP and VM climate episodes*

We combined the RWP climate with VM climate (Table 2.3; Wang et al., 2011) together to investigate how the climate changed across the boundary of the two episodes (Fig. 2.5). During the 1-500 AD portion of RWP, summer precipitation was first lower than today in 150-200 AD, and then slightly increased in the interval of 200-250 AD, and later the precipitation decreased and summer became even drier in 250-500 AD. The winter temperature appeared to gradually increase from 18°C at 150-200 AD to 23°C at 500-550 AD, although there seemed having cold interruptions occurring at 250-300 AD and 450-500 AD. During the VM (500-800 AD), the summer precipitation was low at first and abruptly increased at 550-600AD. Then it began decreasing until 650-700 AD and slightly increased

in 700-750 AD. For the VM winters, a cooling trend was detected changing from 23°C at the end of RWP to 17°C at 700-750 AD. After the cooling, winter temperature increased again at 850-900 AD. Therefore, the climate change across the RWP and VM transition was characterized with a drying and cooling transition.

We also compared the RWP and VM climate change with a sea-level record from 1-900 AD (Fig. 2.5). Tanner (2000) reconstructed the Denmark sea level record for the past 2000 years based on the long, Jerup beach ridge sequence in northern Denmark. The 1-900 AD portion of this record is used here because its resolution (50.5 years on average) is higher than the existing sea level records for the Gulf of Mexico area (Marquardt and Walker, in press). Therefore, it provides more detailed sea-level fluctuations which are needed for comparison with the Pineland isotopic data. Moreover, Marquardt and Walker (in press) provide many lines of evidence justifying the Jerup Denmark record as appropriate in the study of southwest Florida, including its consistency with less detailed sea-level records around Florida and oceanic teleconnections throughout the North Atlantic region. To better visualize the comparison, we added the 1-900 AD portion of the Jerup record to the panels of reconstructed summer precipitation and winter temperatures, respectively (Fig. 2.5). The comparison shows that the RWP and VM climate data correlate with the sea-level record, although neither the RWP nor VM data were exactly synchronous with the sea-level oscillation. The dating errors (~50 years) of the sea level record and its lower resolution relative to the temperature and precipitation reconstructions might have contributed to the observed discrepancies. Nonetheless, despite the discrepancies, we observe a distinct match between a striking drying and cooling trend in 500-700 AD and a falling sea level (Fig. 2.5).

Solar radiation is a primary forcing factor in the Earth's climate change. In the late

Holocene, climate change often temporally coincides with solar activity. Examples are the

Subboreal/Subatlantic transition (2800-2700 cal a BP) with the Homeric Minimum, the

Medieval Warm Period (~1200-1400 AD) with the Medieval Maximum, and the Little Ice

Age (~1500-1700 AD) with the Maunder Minimum. Therefore, it is informative to assess the

temporal relationship between the climate of RWP or VM and solar activity. We compare the

reconstructed precipitation and temperature of the RWP and VM with variability of total

solar irradiance (TSI) over 1-900 AD (Fig. 2.6; Steinhilber, et al., 2009). Although the

comparison is rudimentary, the drying and cooling transition across the RWP and VM shows

substantial correlation with decreasing TSI (Fig. 2.6). Therefore, we infer that the RWP-VM

climate transition was likely driven by the change of solar forcing. As to how solar forcing

caused the RWP-VM drying and cooling transition, we refer to the explanation for the

drying/cooling of the Little Ice Age in the subtropical North Atlantic (Lund and Curry, 2004,

2006; Soto, 2005; Richey et al., 2009). The cooling in the Little Ice Age was explained by

positive NAO-like phases. When solar radiation decreased from the Medieval Maximum to

the Maunder Minimum, sea-surface temperatures of the North Atlantic became colder and

formed positive NAO-like phases. During the positive NAO-like phases, the north-south sea-

level pressure gradient increased and consequently oceanic meridional overturning increased,

which cooled the sea-surface temperatures of the subtropical North Atlantic (Marshall et al.,

2001). The proposed mechanism for the Little Ice Age drying involved multiple atmospheric

circulation patterns (Lund and Curry, 2004; Soto, 2005). Low sea-surface temperatures of the

North Atlantic caused a cold phase of AMO that is characterized by a small pressure

difference between the North Atlantic High and the Icelandic Low. The small pressure difference then produced weaker trade winds and hence decreased precipitation in Florida. The relative position of the ITCZ was forced to migrate southward by the Little Ice Age cooling which also decreased precipitation in subtropical Florida. Moreover, decreased solar radiation of the Little Ice Age might also trigger the cold phase of ENSO that would have further lowered rainfall in the study area. We hypothesize that the climate transition from RWP to VM experienced similar changes in atmospheric circulation patterns. However, this explanation is not conclusive and we do not exclude other possible mechanisms for the RWP-VM climate change.

6. Conclusions

Based on a multi-taxa approach, this study successfully reconstructed the seasonal paleoclimate in southwest Florida over the latter part of the RWP. The reconstruction indicates that the RWP summers were drier relative to today. The RWP winters gradually increased in temperatures from 18°C at 150-200 AD to 23°C at 500-550 AD with cold interruptions at 250-300 AD and 450-500 AD. Eight shells radiocarbon-dated to 150-550 AD recorded that RWP summers were drier relative to today, which is represented by the average value of modern shell specimens. The reconstructed variable RWP summer and winter climate agrees with the archaeological evidence observed during the cultural period Caloosahatchee I-late (1-500 AD).

Combining the RWP climate results with those of the previously estimated VM, we detect a cooling and drying climate transition across the RWP and VM climate episodes. The climate transition presented significant temporal coherence with falling sea level and decreasing solar radiation. Based on existing explanations for the Little Ice Age in the subtropical North Atlantic, we suggest that decreased solar radiation likely was a significant forcing factor for the cooling and drying RWP-VM climate transition in southwest Florida via modifying the atmospheric circulation patterns (NAO, AMO, ENSO, ITCZ).

Acknowledgements

References

Ansell AD. 1968. The rate of growth of the hard clam *Mercenaria mercenaria* (L.) throughout the geographic range. *Journal du Conseil* **31**: 364-409.

Arnold WS, Marelli DC, Bert TM, Jones DS, Quitmyer IR. 1991. Habitat-specific growth of hard clams *Mercenaria mercenaria* (L.) from the Indian River, Florida. *Journal of Experimental Marine Biology and Ecology* **147**: 245-265.

Arnold WS, Bert TM, Quitmyer IR, Jones DS. 1998. Contemporaneous deposition of annual growth bands in *Mercenaria mercenaria* (Linnaeus), *Mercenaria campechiensis* (Gmelin), and their natural hybrid forms. *Journal of Experimental Marine Biology and Ecology* **223**: 93-109.

Barnett TP, Del Genio AD, Ruedy R. 1992. Unforced decadal fluctuations in a coupled model of the atmosphere and ocean mixed layer. *Journal of Geophysical Research* **97**: 7341-7354.

Beever III JW, Gray W, Trescott D, Cobb D, Utley J, Beever LB. 2009. *Comprehensive Southwest Florida/Charlotte Harbor climate change vulnerability assessment*. Southwest Florida Regional Planning Council Charlotte Harbor National Estuary Program Technical Report 09-3.

Black DE, Abahazi MA, Thunell RC, Kaplan A, Tappa EJ, Peterson LC. 2007. An 8-century tropical Atlantic SST record from the Cariaco Basin: Baseline variability, twentieth-century warming, and Atlantic hurricane frequency. *Paleoceanography* **22**: 1-10.

Bradley JT. 1972. *Climate of Florida*. Asheville. NC: U .S. Department of Commerce. National Climatic Data Center. Climatography of the United States No. 60-8.

Elliot M, deMenocal PB, Braddock KL,Howe SS. 2003. Environmental controls on the stable isotopic composition of *Mercenaria mercenaria*: potential application to paleoenvironmental studies. *Geochemistry, Geophysics, Geosystems* **4**: 1056-1072.

Gonfiantini R, Stichler W, Rozanski K. 1995. Standards and intercomparison materials distributed by the International Atomic Energy Agency for Stable Isotopic Measurements. Reference and Intercomparison Materials for Stable Isotopes of Light elements. Techdoc-825, IAEA, Vienna, Austria; 13-29.

Haug GH, Hughen KA, Sigman DM, Peterson LC, Röhl U. 2001. Southward migration of the international convergence zone through the Holocene. *Science* **293**: 1304-1308.

Hodell DA, Brenner M, Curtis JH, Guilderson T. 2001. Solar forcing of drought frequency in the Maya lowlands. *Science* **292**: 1367-1370.

Hughen KA, Baillie MGL, Bard E, Bayliss A, Beck JW, Bertrand CJH, Balckwell PG, Buck CE, Burr GS, Cutler KB, Damon PE, Edwards RL, Fairbanks RG, Friedrich M, Guilderson TP, Kromer B, McCormac FG, Manning SW, Bronk Ramsey C, Reimer PJ, Reimer RW, Remmele S, Southon JR, Stuiver M, Talamo S, Taylor FW, van der Plicht J, Weyhenmeyer CE. 2004. Marine04 Marine radiocarbon age calibration, 26-0 ka BP. *Radiocarbon* **46**: 1059-1086.

Iacumin P, Bianucci G, Longinelli A. 1992. Oxygen and carbon isotopic composition of fish otoliths. *Marine Biology* **113**: 537-542.

Ivany LC, Patterson WP, Lohmann KC. 2000. Cooler winters as a possible cause of mass extinctions at the Eocene/Oligocene boundary. *Nature* **407**: 887-890.

Jones PW, Martin FD, Hardy JD Jr. 1978. *Development of fishes in the Mid-Atlantic Bight: an atlas of egg, larval, and juvenile stages*. Fish and Wildlife Service: U.S Department of Interior.

Jones DS, Arthur MA, Allard DJ. 1989. Sclerochronological records of temperature and growth from shells of *Mercenaria mercenaria* from Narragansett Bay, Rhode Island. *Marine Biology* **102**: 225-234.

Jones DS, Quitmyer IR, Arnold WS, Marelli DC. 1990. Annual shell banding, age, and growth rate of hard clams (*Mercenaria* spp.) from Florida. *Journal of Shellfish Research* **9**: 215-225.

Jones DS, Quitmyer IR. 1996. Marking time with bivalve shells: oxygen isotopes and season of annual increment formation. *Palaios* **11**: 340-346.

Kalish JM. 1991. ^{13}C and ^{18}O isotopic disequilibria in fish otoliths: metabolic and kinetic effects. *Marine Ecology Progress Series* **75**: 191-203.

Kraeuter JN, Castagna M. 2001. *Biology of the Hard Clam*. Elsevier.

Lund DC, Curry WB. 2004. Late Holocene variability in Florida Current surface density: Patterns and possible causes. *Paleoceanography* **19**: 1-17.

Lund DC, Curry WB. 2006. Florida Current surface temperature and salinity variability during the last millennium. *Paleoceanography* **21**: 1-15.

Marquardt WH. 2004. Calusa. In *Handbook of North American Indians, volume 14: Southeast*, Fogelson RD (ed). Smithsonian Institution: Washington, DC; 204-212.

Marquardt WH, Walker KJ. 2001. Pineland: a coastal wet site in southwest Florida. In *Enduring Records: The Environmental and Cultural Heritage of Wetlands*, Purdy BA (ed). Oxbow Books, Oxford and David Brown Book Company: Oakville; 48-60.

Marquardt WH, Walker KJ. in press. *The Archaeology of Pineland: A Coastal Southwest Florida Site Complex, A.D. 50 – 1710*. Institute of Archaeology and Paleoenvironmental Studies, Monograph 4. University of Florida, Gainesville.

Marshall J, Kushnir Y, Battisti DS, Chang P, Czaja A, Dickson R, Hurrell J, McCartney M, Saravanan R, Visbeck M. 2001. North Atlantic climate variability: Phenomena impacts and mechanisms. *International Journal of Climatology* **21**: 1863-1898.

Muncy RJ, Wingo WM. 1983. *Species profiles: life histories and environmental requirements of coastal vertebrates (Gulf of Mexico): sea catfish and gafftopsail catfish.* Washington, DC: National Coastal Ecosystems Team, Division of Biological Services, Fish and Wildlife Services, U.S. Department of the Interior.

Patterson WP, Smith GR, Lohmann KC. 1993. Continental paleothermometry and seasonality using the isotopic composition of aragonitic otoliths of freshwater fishes. In *Climate Change in Continental Isotopic Records*, Swart PK, Lohmann KC, McKenzie J, Savin, S (eds). American Geophysical Union: Washington DC; 191-202.

Richey JN, Poore RZ, Flower BP, Quinn TM, Hollander DJ. 2009. Regionally coherent Little Ice Age cooling in the Atlantic Warm Pool. *Geophysical Research Letters* **36**: 1-5.

Saenger C, Came RE, Oppo DW, Keigwin LD, Cohen AL. 2011. Regional climate variability in the western subtropical North Atlantic during the past two millennia. *Paleoceanography* **26**: 1-12.

Soto LR. 2005. Reconstruction of late Holocene precipitation for central Florida as derived from isotopes in speleothems. Unpublished Masters Thesis, Department of Geology, University of South Florida, Tampa, Florida.

Steinhilber F, Beer J, Fröhlich C. 2009. Total solar irradiance during the Holocene. *Geophysical Research Letters* **36**: 1-5.

Stuiver M, Reimer PJ, Reimer RW. 2005. CALIB5.0 radiocarbon calibration. http://radiocarbon.pa.qub.ac.uk/calib

Surge DM, Walker KJ. 2005. Oxygen isotope composition of modern and archaeological otoliths from the estuarine hardhead catfish (*Ariopsis felis*) and their potential to record low-latitude climate change. *Palaeogeography, Palaeoclimatology, Palaeoecology* **228**: 179-191.

Surge D, Walker KJ. 2006. Geochemical variation in microstructural shell layers of the southern quahog (*Mercenaria campechiensis*): Implications for reconstructing seasonality. *Palaeogeography, Palaeoclimatology, Palaeoecology* **237**: 182-190.

Surge D, Kelly G, Arnold WS, Geiger SP, Goewert AE, Walker KJ. 2008. Isotope sclerochronology of *Mercenaria Mercenaria*, *M. Campechiensis*, and their natural hybrid form: does genotype matter? *Palaios* **23**: 559-565.

Tanner WF. 2000. Beach ridge history, sea level change, and the A.D. 536 event. In *The Years without Summer: Tracing A.D. 536 and its aftermath*, Gunn JD (ed). Archaeopress: Oxford; 89-97.

Thorrold SR, Campana SE, Jones CM, Swart PK. 1997. Factors determining $\delta^{13}C$ and $\delta^{18}O$ fractionation in aragonitic otoliths of marine fish. *Geochimica et Cosmochimica Acta* **61**: 2909-2919.

Walker KJ. 1992. The zooarchaeology of Charlotte Harbor's prehistoric maritime adaptation: spatial and temporal perspectives. In *Culture and Environment in the Domain of the Calusa*, Marquardt WH (ed). University of Florida: Gainesville; 265-366.

Walker KJ, Stapor FW, Marquardt WH. 1995. Archaeological evidence for a 1750-1450 BP higher-than-present sea level along Florida's Gulf coast. *Journal of Coastal Research Special Issue No. 17: Holocene Cyclic Pulses and Sedimentation*: 205-218.

Walker KJ. 2000. A cooling episode in southwest Florida during the sixth and seventh centuries A.D. In *The Years without Summer: Tracing A.D. 536 and its aftermath*, Gunn JD (ed). Archaeopress: Oxford; 119-127.

Walker KJ, Surge D. 2006. Developing oxygen isotope proxies from archaeological sources for the study of Late Holocene human-climate interactions in coastal southwest Florida. *Quaternary International* **150**: 3-11.

Wang T, Surge D, Walker KJ. (2011). Isotopic evidence for climate change during the Vandal Minimum from *Ariopsis felis* otoliths and *Mercenaria campechiensis* shells, southwest Florida, USA. *Holocene* **21(7)**: 1081-1091. doi:10.1177/0959683611400458.

Widmer RJ. 1988. *The Evolution of the Calusa: A nonagricultural chiefdom on the Southwest Florida Coast*. University of Alabama Press: Tuscaloosa and London.

Winter A, Ishioroshi H, Watanabe T, Oba T, Christy J. 2000. Caribbean Sea surface temperatures: Two-to-three degrees cooler than present during the Little Ice Age. *Geophysical Research Letters* **27**: 3365-3368.

Wurster CM, Patterson WP. 2001. Late Holocene climatic change for the eastern interior United States: evidence from high-resolution $\delta^{18}O$ values of sagittal otoliths. *Palaeogeography, Palaeoclimatology, Palaeoecology* **170**: 81-100.

Table 2.1. Time range of the archaeological shells in the Roman Warm Period.

Specimen	FLMNH-ANT Catalog No.	NOSAMS No.	AMS radiocarbon age (^{14}C yrs BP)	δ^{13}C (VPDB ‰)	cal yr AD range (1 sigma)	Chronostratigraphic Range (AD)
CIIA-M9[1]	2003-38-8/2/5	OS-54183	1890±30	0.93	460-560	500-550
CIIA-M7[1]	95-3-31/5	OS-54181	1970±35	0.67	350-470	450-500
CIIA-M6[1]	92-24-2	OS-54180	1930±40	0.83	420-540	450-500
CI-M5	90-19-3	OS-54447	2050±35	0.95	270-380	300-350
CI-M4	92-11-66	N/A	N/A	N/A	N/A	300-350
CI-M3	92-18-18	OS-54185	2070±35	1.21	250-360	250-300
CI-M2	92-24-21	N/A	N/A	N/A	N/A	250-300
CI-M8	92-11-65	OS-54294	2120±40	−1.03	160-300	200-250
CI-M7	2001-128-15	OS-54293	2140±50	0.91	140-280	200-250
CI-M6	90-8-15/1	OS-54292	2130±30	0.73	160-270	150-200

[1]Data for the specimens CIIA-M/A9, CIIA-M/A7, and CIIA-M/A6 were published by Wang et al. (2011) as Vandal Minimum specimens. Marquardt and Walker (in press) update the chronostratigraphic range of the three specimens and add them to the Roman Warm Period specimens.
.

Table 2.2. Summary statistics for the modern and Roman Warm Period shells and otoliths. For each specimen, most negative summer $\delta^{18}O$ values or coldest winter temperatures are all listed with the first year at bottom.

Shell specimen (AD)	Most negative summer $\delta^{18}O$ values (VPDB ‰)	Average summer $\delta^{18}O$ values with standard error (VPDB ‰)	Otolith specimen (AD)	Coldest winter temperatures (°C)	Average winter temperature with standard error (°C)
05PI05[1]	−2.64 −2.07	−2.4±0.3		22.7 21.4 19.1 19.1	
05PI17[1]	−2.27 −2.70	−2.5±0.2	MOD2002[1]	21.2 20.9 20.7 19.2	20.5±0.5
CIIA-M9[2] (500-550)	−2.02 −1.72 −1.29 −1.45	−1.6±0.2	CIIA-A9[2] (500-550)	22.2 21.9 23.6 22.4	22.5±0.4
CIIA-M7[2] (450-500)	−1.79 −2.13 −1.62	−1.8±0.2	CIIA-A7[2] (450-500)	19.8 19.8 15.1	18.2±1.6
CIIA-M6[2] (450-500)	−1.73 −1.34 −1.36 −2.07	−1.6±0.2	CIIA-A6[2] (450-500)	21.6 21.5 20.1 19.5	20.7±0.5
CI-M5 (300-350)	−1.72 −1.85 −1.35 −1.41	−1.6±0.1	CI-A5 (300-350)	20.7 21.4 19.6	20.6±0.5
CI-M4 (300-350)	−1.20 −1.28 −1.29 −2.47	−1.6±0.3			

CI-M2 (250-300)	−1.28 −1.69	−1.5±0.2	CI-A3 (250-300)	17.6 18.3 16.2	17.4±0.6
			CI-A7 (200-250)	19.7 20.0 19.7 18.9	19.6±0.2
CI-M8 (200-250)	−1.82 −2.58 −2.33 −1.71	−2.1±0.2	CI-A8 (200-250)	19.3 20.0 20.8 19.5	19.9±0.3
CI-M6 (150-200)	−1.89 −2.34 −2.32 −1.14	−1.9±0.3	CI-A6 (150-200)	17.0 19.5 17.9	18.1±0.7

[1]Data for the modern shells (05PI05 and 05PI17) and otolith (MOD2002) and the archaeological specimens (CIIA-M/A9, CIIA-M/A7 and CIIA-M/A6) were published by Wang et al. (2011).
[2]Data for the specimens CIIA-M/A9, CIIA-M/A7, and CIIA-M/A6 were published by Wang et al. (2011) as Vandal Minimum specimens. Marquardt and Walker (in press) update the chronostratigraphic range of the three specimens and add them to the Roman Warm Period specimens.

Table 2.3. Summary statistics for the VM shells and otoliths. For each specimen, most negative summer $\delta^{18}O$ values or coldest winter temperatures are all listed with the first year at bottom. Most data have been published by Wang et al. (2011), except the data of CIIB-M/A4, CIIA-A5, CIIA-A1, and CIIA-A4, which were measured but unpublished by Wang et al. (2011).

Shell specimen (AD)	Most negative summer $\delta^{18}O$ values (VPDB ‰)	Average summer $\delta^{18}O$ values with standard error (VPDB ‰)	Otolith specimen (AD)	Coldest winter temperatures (^{o}C)	Average winter temperature with standard error (^{o}C)
CIIB-M4 (750-850)	−1.98 −1.58 −1.27 −1.54	−1.6±0.1	CIIB-A4 (750-850)	20.3 23.4 21.1 20.1	21.2±0.8
CIIA-M5 (700-750)	−1.29 −1.83 −1.68 −1.28	−1.5±0.1	CIIA-A5 (700-750)	17.9 16.4 17.0 17.4	17.2±0.3
CIIA-M2 (650-700)	−2.22 −2.36 −1.62 −1.88	−2.0±0.2	CIIA-A2 (650-750)	17.0 17.6 18.3 18.5	17.8±0.3
CIIA-M1 (650-700)	−1.34 −1.06 −1.67 −0.92	−1.3±0.2	CIIA-A1 (650-700)	21.7 21.2 18.0 17.4	19.6±1.1
CIIA-M8 (600-650)	−1.51 −1.84 −1.76 −3.02	−2.0±0.3	CIIA-A8 (600-650)	20.5 23.0 18.4 19.4	20.3±1.0
CIIA-M4 (550-600)	−2.99 −2.97 −2.11 −2.05	−2.5±0.3	CIIA-A4 (550-600)	21.6 21.1 20.8 20.5	21.0±0.2

Figure 2.1. Map and stratigraphy of the study area. (A) Synthetic stratigraphy of Pineland Site Complex (northwestern shore of Pine Island) for the cultural intervals of Caloosahatchee I-late and Caloosahatchee IIA-early (Marquardt and Walker, in press). Archaeological proveniences for the specimens are presented at the right of the stratigraphy. The abbreviations CR, SP, NWP, OM, SCR, LM, Lv and St represent Citrus Ridge, South Pasture, Northwest Pasture, Old Mound, Surf Clam Ridge, Low Mound, Level, and Stratum respectively. (B) Map of southwest Florida, United States, showing geographical features and sites discussed in the text.
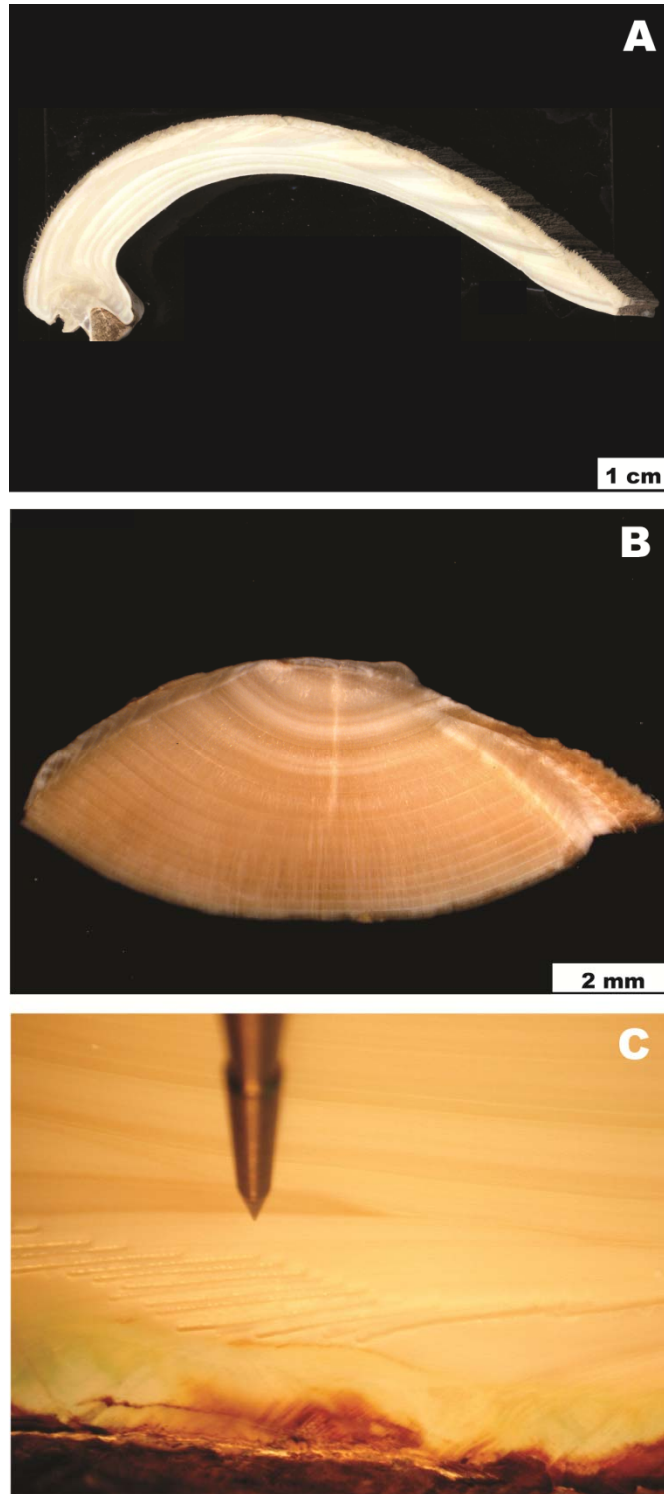
Figure 2.2. Microstructure and microsampling of archaeological specimens. (A) Cross-section of archaeological shell along the axis of maximum growth observed under reflected light. (B) Cross-section of archaeological otolith along the axis of maximum growth observed under reflected light. (C) Microsampling performed by a Merchantek micromill.
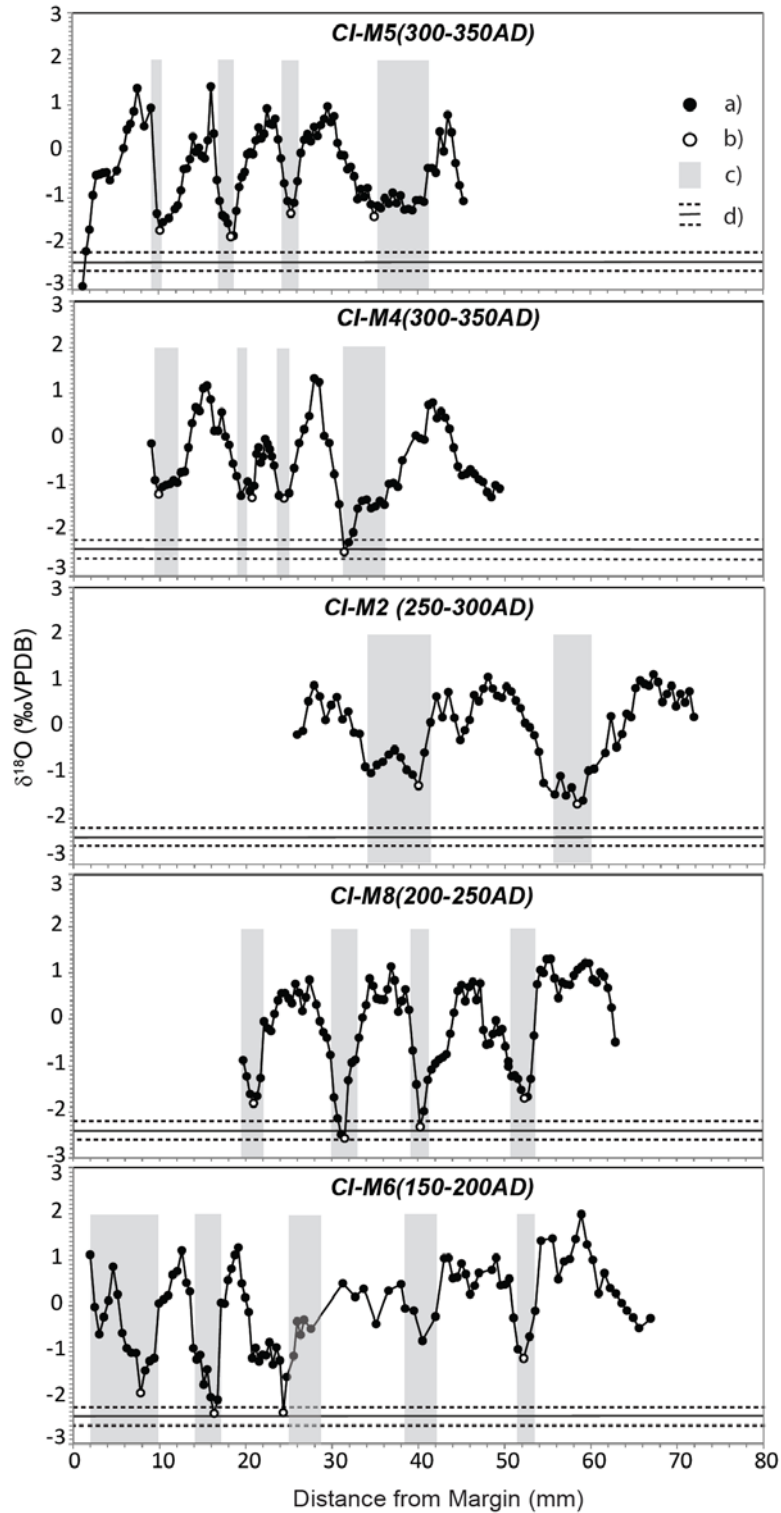
Figure 2.3. $\delta^{18}O$ values of archaeological shells versus distance from growth margin (growth direction is from right to left). (a) $\delta^{18}O$ values; (b) most negative $\delta^{18}O$ values selected for summer precipitation evaluation; (c) increments with slow growth rate; (d) average summer $\delta^{18}O$ value of modern shells 05PI05 and 05PI17 (from Wang et al., 2011).
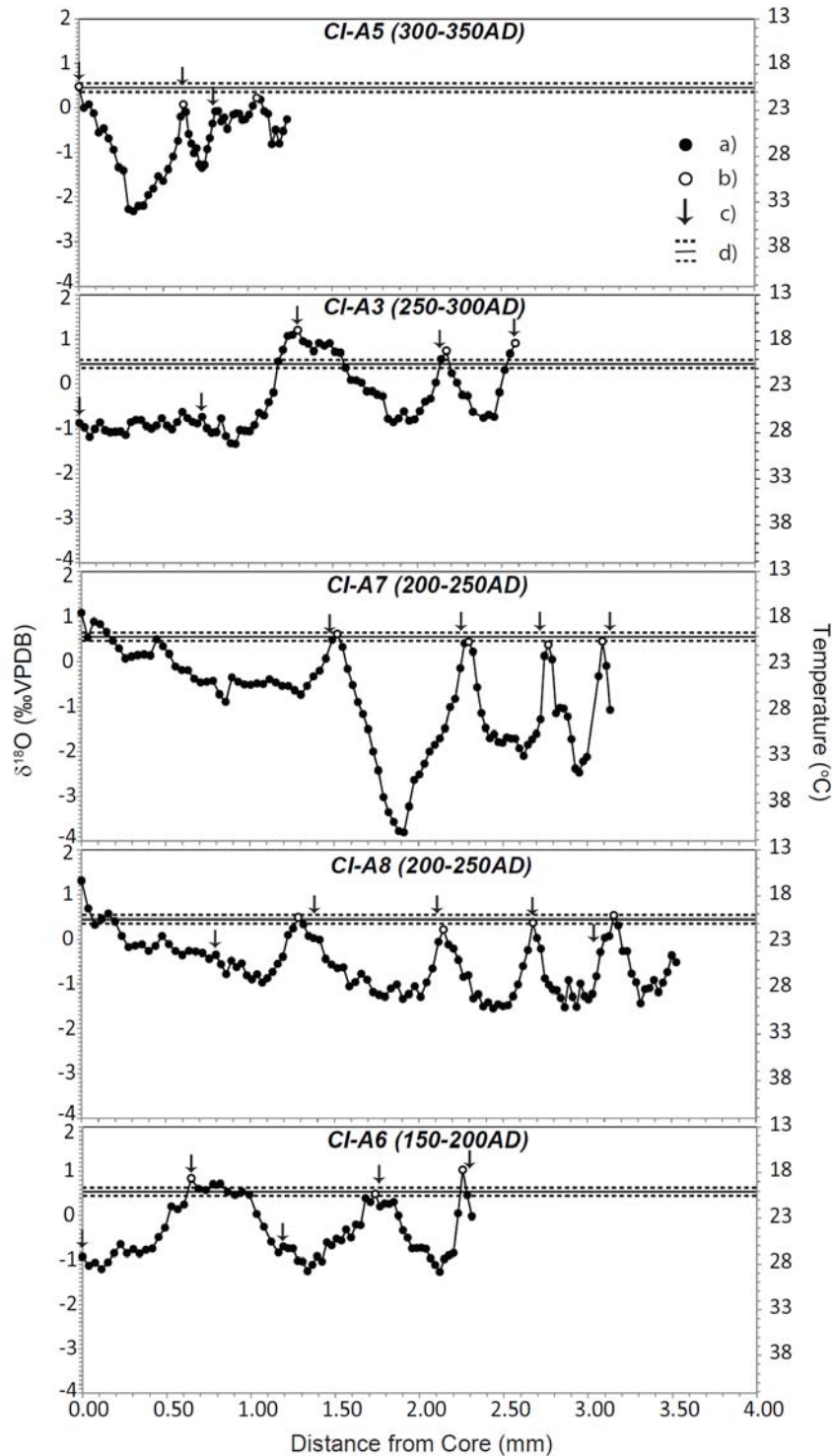
Figure 2.4. δ¹⁸O values and estimated temperatures of archaeological otoliths versus distance from the inner core toward the growth margin (growth direction is from left to right). The ordinate of temperature is decreasing upward to coincide with the temperature scale. (a) δ¹⁸O values and estimated temperatures; (b) coldest temperatures selected for winter temperature evaluation; (c) positions of primary growth lines; (d) average winter temperature of modern otolith MOD2002 (from Wang et al., 2011).
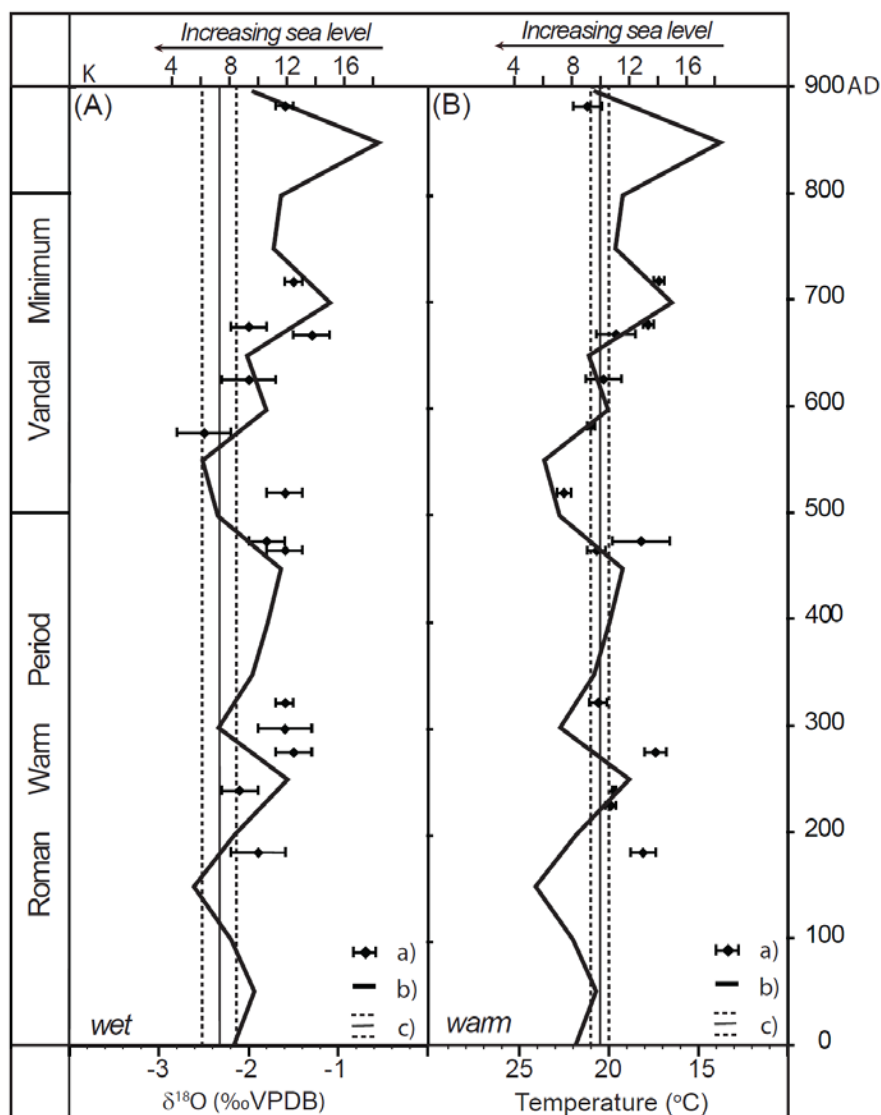
Figure 2.5. Reconstructed Roman Warm Period and Vandal Minimum summers and winters in comparison with sea-level change. (A) Summer precipitation represented by shell $\delta^{18}O$ values and sea-level positions based on kurtosis (K) values; (a) average summer $\delta^{18}O$ value of each archaeological shell; (b) the Denmark sea-level record (from Tanner, 2000); (c) average summer $\delta^{18}O$ value of modern shells 05PI05 and 05PI17 (from Wang et al., 2011). (B) Winter temperatures estimated from otolith $\delta^{18}O$ values and sea-level positions based on kurtosis (K) values; (a) average winter temperature of each archaeological otolith; (b) the Denmark sea-level record (from Tanner, 2000); (c) average winter temperature of modern otolith MOD2002 (from Wang et al., 2011).
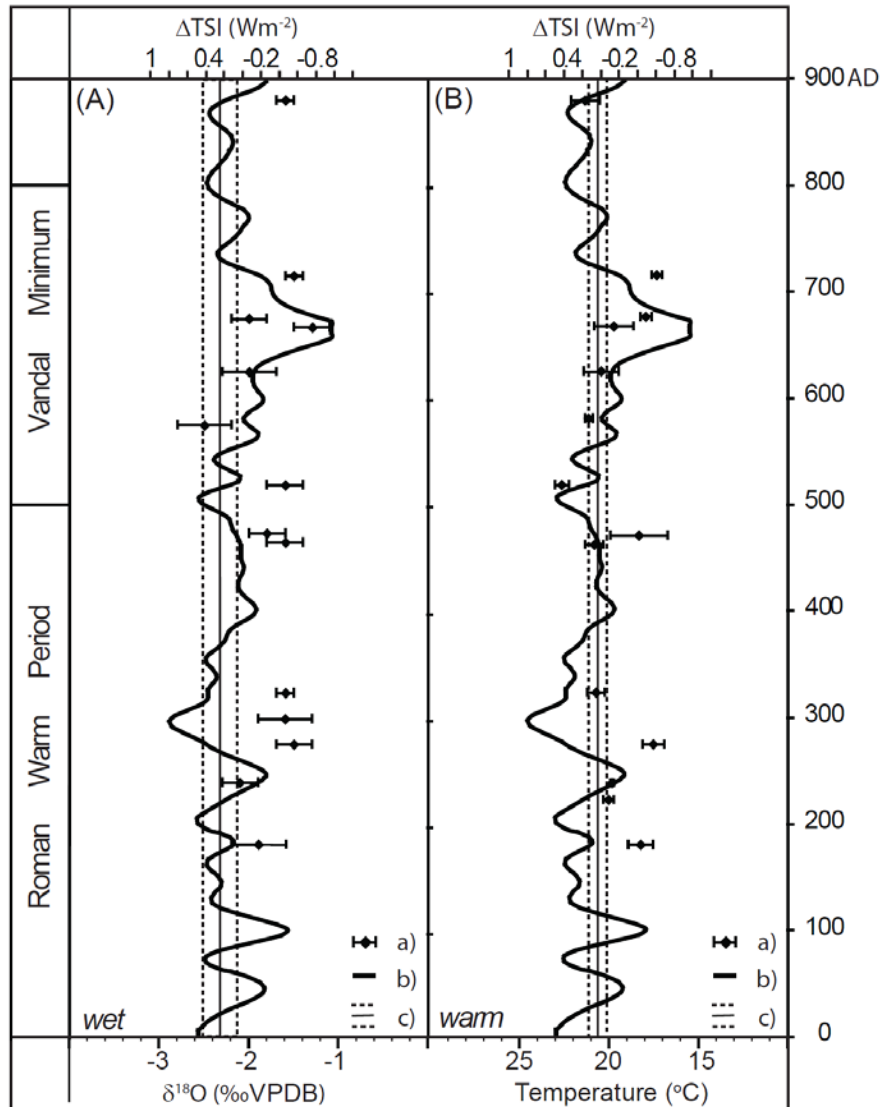
Figure 2.6. Reconstructed Roman Warm Period and Vandal Minimum summers and winters in comparison with solar irradiance change. (A) Summer precipitation represented by shell $\delta^{18}O$ values and the variation of total solar irradiance (ΔTSI); (a) average summer $\delta^{18}O$ value of each archaeological shell; (b) TSI value relative to the solar minimum in 1986 (1365.57 Wm^{-2}) (from Steinhilber et al., 2009); (c) average summer $\delta^{18}O$ value of modern shells 05PI05 and 05PI17 (from Wang et al., 2011). (B) Winter temperatures estimated from otolith $\delta^{18}O$ values and the variation of total solar irradiance (ΔTSI); (a) average winter temperature of each archaeological otolith; (b) relative value of TSI to the TSI in 1986 (1365.57 Wm^{-2}) (from Steinhilber et al., 2009); (c) average winter temperature of modern otolith MOD2002 (from Wang et al., 2011).

CHAPTER III

STOCHASTIC EVALUATION OF CLIMATE CHANGE OVER THE PAST 1000 YEARS

Abstract

Previous studies of climate change over the past millennium suggest that natural processes within the climate system (internal climate mechanism) are associated with stochastic processes intrinsic to the nonlinear climate system. To examine the extent to which the internal climate mechanism is stochastic, we used a conceptual linear stochastic climate model to simulate the temperature variations of Northern Hemisphere (NH) over the past millennium. The simulated temperature variations reproduced key features of the power spectrum and autocorrelation of the reconstructed temperature record. Using a conceptual model and replacing the Gaussian weather forcing with the reconstructed solar fluctuation we obtained improved simulation results, suggesting that solar power played a role in the forcing of climate change over the past millennium. We developed a new method of randomness evaluation for stochastic time series (RESTS) to quantitatively investigate not only the stochastic extent of internal climate mechanism but also the temporal evolution of the stochastic process in climate time series analysis. We applied this method to the temperature variations of NH over the past millennium, the climate change record of Greenland Ice Sheet Project 2 (GISP2), and the tree ring records from France and northern Sweden. The results

indicate that the stochastic extent generally decreased during the intervals of climate transition. The implication being that the natural processes within the climate system changed during the intervals of climate transition and as a result the internal climate mechanism might become more deterministic during climate transitions.

1. Introduction

The climate in the late Holocene (0-3000 BP) includes several climate change episodes, such as the Subboreal/Subatlantic transition (2800-2700 cal. BP), Roman Warm Period (RWP;~2500-1600 cal. BP), Vandal Minimum (VM;~400-800 AD), Medieval Warm Period (MWP; ~1200-1400 AD) and Little Ice Age (LIA; ~1500-1700 AD). These climate events have been detected in abundant historical records or paleoclimate proxy records (Lamb, 1995; Keigwin, 1996; Crowley and Lowery, 2000; Hodell et al., 2001; McDermott, et al., 2001; Jones and Mann, 2004 and many others). Although changes in solar radiation have been generally accepted as the driver of climate change in the late Holocene, there is no consensus on the mechanism responsible for these changes.

Different mechanisms have been proposed to explain climate variability in the late Holocene, especially the climate over the past millennium. Crowley (2000) modeled the temperature change over the last millennium with a linear upwelling/diffusion energy balance model. The modeled results suggest that external natural climate forcings (e.g., solar variability, greenhouse gas, volcanism and tropospheric aerosols) are able to explain part (41-64%) of the pre-anthropogenic low-frequency temperature variance. Therefore, internal

forcing processes such as the ocean's thermohaline circulation played a secondary role in the climate change over the past millennium. To examine the climate response to solar irradiance change, Shindell et al (2001) used the Goddard Institute for Space Studies general circulation model (GISS GCM) to simulate the climate change during the Maunder Minimum from the mid-1600s to the early 1700s. Their results suggested that relatively small change in solar irradiance will trigger shifts on the Arctic Oscillation (AO)/North Atlantic Oscillation (NAO) pattern and cause the century-scale Northern Hemisphere (NH) winter climate changes in the MWP and LIA. In addition, Hunt (2006) used a coupled general circulation model with no external forcings to simulate the low-frequency climate fluctuations of the Holocene to examine the internal mechanism of the climate system. The simulation results suggested that internal forcings in the climate system were capable to generate the basic features of MWP and LIA, such as spatial extent, surface temperature anomalies. However, the amplitude and duration of the simulated temperature anomalies were smaller relative to the observed temperature anomalies of MWP and LIA, and external forcings had to be included to sustain these centennial climate fluctuations. Moreover, the simulation did not support that the climate fluctuations of MWP and LIA were caused by the internal mechanisms such as the NAO and El Nino-Southern Oscillation (ENSO). Therefore, Hunt's study proposed that the stochastic process intrinsic to the nonlinear climate system partially caused the climate fluctuations of MWP and LIA, and mechanisms such as NAO and ENSO were probably just the spatial manifestation of naturally occurring climatic variability.

Stochastic climate model has been widely used to investigate climate fluctuations at different temporal and spatial scales (Majda et al., 1999; Dobrovalski, 2000; Ditlevsen, 2001;

Király and Jánosi, 2002; Roe and Steig, 2004 and many others). It was first developed by Hasselmann (1976) as a possible mechanism for generating the climate variations on time scales of months, years, decades or even longer. The theory of stochastic climate model postulated that the coupled ocean-atmosphere-cryosphere-land system of the earth can be divided into slowly responding climate components (the oceans, ice sheets, vegetation) and rapidly responding weather components (the atmosphere). Therefore, the stochastic climate model realizes statistical reduction of the complex climate system by separating the time-scale between climate and weather. According to this theory, the variability of climate components can be attributed to continuous random forcing by the short period weather components. The theory of stochastic climate model is primarily used to help understand the fundamental dynamics of climate system that govern the more complicated general circulation models. Except the general assumption that high-frequency weather components are a significant source of low-frequency climate variability, the stochastic model does not make any assumptions about the character or nature of feedback mechanisms. It simulates the low-frequency climate component from a zero-order approximation; therefore, it can not reproduce the mechanism of climate system in detail. Nevertheless, since climate system is a nonlinear system (Rial et al., 2004) and the climatic variable might be treated as a random variable (Dobrovalski, 2000), probabilistic approach is its primary study method and the statistical properties instead of details should be our major concerns (Vallis, 2010).

The objective of this study is to examine the extent to which the climate change in the late Holocene is stochastic, to enhance our insights into the internal climate mechanism responsible for the late Holocene climate changes, such as the RWP, MWP, LIA and etc. In

order to realize this goal, we first simulated the average temperature variations in NH over

the last millennium with a simple conceptual stochastic climate model and estimated the

extent of stochasticity by comparing the simulation results with the reconstructed record. We

also developed an analytical method to analyze how the randomness of climate time series

evolved temporally over the past millennium.

2. Methods

2.1. *Stochastic climate model*

　　According to the stochastic model, climate variability is explained as the integral

response of the climate to continuous random excitation by short time-scale disturbances

(Hasselmann, 1976), an approach analogous to the statistical treatment of the Brownian

motion. The evolution of the climate state in a stochastic climate model can be described by a

Langevin-type equation (Ruiz De Elvira et al., 1982),

$$\frac{dy(t)}{dt} = -v(t)y(t) + \omega(t)\,; \tag{1}$$

where $\dfrac{dy(t)}{dt}$ denotes the time evolution of climate variable $y(t)$. The variable $y(t)$ maybe

associated with sea surface temperature, ice coverage and other climate variables which

typically have time scales in the orders of several months, years or longer. The variable $v(t)$

works as the stabilizing internal feedback and maybe associated with the mean atmosphere-

ice-ocean interactions. The minus sign on the left-hand side of $v(t)$ turns the stabilizing

feedback $v(t)$ into negative feedback and hence prevents the value of $y(t)$ from growing

indefinitely. The variable $\omega(t)$ is used to describe the weather forcing in the time order of a few days and is normally approximated by white noise.

In this study, we use the linear stochastic climate model developed by Ditlevsen (2001). Therefore, we assume $\nu(t)$ to be a constant α, and use the product $\sigma x(t)$ to represent $\omega(t)$ where $x(t)$ is uncorrelated white noise with unit variance. Therefore, the Langevin-type equation is reduced to

$$\frac{dy(t)}{dt} = -\alpha y(t) + \sigma x(t).$$

(2)

The discrete version of equation (2) is a first-order auto-regressive process, AR(1) process, which conventionally generates weakly stationary time series. Therefore, this model is restricted to simulate stationary or weakly stationary time series. However, it is hard to verify if a climate process is stationary or not, earlier studies generally assume climate processes to be weakly stationary (von Storch and Zwiers, 1999). In the stochastic model, the constant α can be predicted from the time series by calculating its autocorrelation. Autocorrelation is the cross-correlation of a signal with itself and is usually used to analyze the repeat pattern in the time domain. The autocorrelation function is expressed as a function of the time lag τ (Ditlevsen, 2001),

$$c_y(\tau) = < y(t)y(t+\tau) >= \lim_{T\to\infty}\frac{1}{T}\int_{-T/2}^{T/2} y(t)y(t+\tau)dt$$

(3)

Combining with equation (2), we can obtain the derivative of autocorrelation function $c_y(\tau)$

(Ditlevsen, 2001),

$$\frac{d}{d\tau}c_y(\tau) = \frac{d}{d\tau}\int y(t)y(t+\tau)dt = -\alpha c_y(\tau) \qquad (4)$$

$$c_y(\tau) = c_0 \exp(-\alpha\,|\,\tau\,|) \qquad (5)$$

Therefore, the value of α^{-1} is the time lag it takes for the autocorrelation to drop its value

by a factor of e. We define this critical time lag as τ_c, which represents the memory of inertia

that characterizes the signal. Therefore, the critical time lag τ_c can also be treated as a

characteristic time scale associated with the physical process that restores the system to

equilibrium. The constant c_0 can be derived when τ is zero. With c_0 and α, we may derive

the constant σ from equation (6), which is based on the fluctuation-dissipation theorem,

$$c_0 = \frac{\sigma^2}{2\alpha} \qquad (6)$$

Therefore, the feedback coefficient α and the forcing variance σ can both be determined

from the analysis of time series.

2.2. *Randomness evaluation for stochastic time series (RESTS)*

Temperatures at the different time intervals of stochastic climate series may have

different degrees of randomness. At some time points, it is possible to predict the temperature

based on previous temperature record, such as the time points in correlated noise. At other

time points, these predictions based on historic data fail, such as the time points in white

noise. Therefore, it is noteworthy to evaluate the degree of randomness at each individual time point of the whole stochastic time series. To realize this, we developed an analytical method we call randomness evaluation for stochastic time series (RESTS). The method evaluates at each year of the time series how well it can predict the future temperature given the historic record before that year. For simplicity of the first approach we applied least square linear fitting (Mathews and Fink, 2004) to the past n years temperature records for a specified year and checked how well the prediction agreed with its future n years records. The coefficients of the linear fitting for a specified year i with window size w are given by equation (7) below.

$$ a = \frac{\begin{vmatrix} \sum\limits_{k=i-\lfloor\frac{w}{2}\rfloor}^{i} x_k y_k & \sum\limits_{k=i-\lfloor\frac{w}{2}\rfloor}^{i} x_k^2 \\ \sum\limits_{k=i-\lfloor\frac{w}{2}\rfloor}^{i} y_k & i \end{vmatrix}}{\begin{vmatrix} \sum\limits_{k=i-\lfloor\frac{w}{2}\rfloor}^{i} x_k^2 & \sum\limits_{k=i-\lfloor\frac{w}{2}\rfloor}^{i} x_k \\ \sum\limits_{k=i-\lfloor\frac{w}{2}\rfloor}^{i} x_k & i \end{vmatrix}}, \quad b = \frac{\begin{vmatrix} \sum\limits_{k=i-\lfloor\frac{w}{2}\rfloor}^{i} x_k^2 & \sum\limits_{k=i-\lfloor\frac{w}{2}\rfloor}^{i} x_k y_k \\ \sum\limits_{k=i-\lfloor\frac{w}{2}\rfloor}^{i} x_k & \sum\limits_{k=i-\lfloor\frac{w}{2}\rfloor}^{i} y_k \end{vmatrix}}{\begin{vmatrix} \sum\limits_{k=i-\lfloor\frac{w}{2}\rfloor}^{i} x_k^2 & \sum\limits_{k=i-\lfloor\frac{w}{2}\rfloor}^{i} x_k \\ \sum\limits_{k=i-\lfloor\frac{w}{2}\rfloor}^{i} x_k & i \end{vmatrix}} \tag{7} $$

We use the sum of square difference between the predicted temperatures and the real temperature records as described in equation (8) to quantitatively evaluate the disagreement.

$$ S[i] = \sum_{j=1}^{\lfloor\frac{w}{2}\rfloor} [Y(i+j) - (aX(i+j)+b)]^2 \tag{8} $$

The larger the disagreement the more randomness occurred at that year. We repeat this process for every year in the time series. The number of data points for fitting and the number of data points for disagreement evaluation sum together into the window size associated with a data point. If window size w is an odd number, the number of points for fitting is $(w+1)/2$ and number of points for prediction evaluation is $(w-1)/2$. Otherwise, if the window size w is an even number, the number of points for fitting is $w/2$ and the number of points for prediction evaluation is $w/2$. For completeness, we also vary the window size to evaluate how long the prediction in future temperature can be statistically meaningful. RESTS method takes a time series as input and outputs a matrix with columns representing data randomness along time and rows representing data randomness at different window sizes. The algorithm has been implemented as a matlab package named 'RESTS' which will be put up online for public use.

3. Results and discussion

3.1. *Evaluation of stochastic extent with linear stochastic climate model*

The simplified linear stochastic climate model has been applied in many climate studies, such as the daily average temperature data in Hungary (Király and Jánosi, 2002), and the oxygen isotope series from ice cores in central Greenland and West Antarctica (Roe and Steig, 2004). In this study, we aim to investigate the internal mechanism of climate changes in the late Holocene, which are basically at the centennial scale and are geographically widespread in the NH. Therefore, we simulated and evaluated the temperature fluctuation in the NH over the past millennium reconstructed by Crowley and Lowery (2000). This hemispherical reconstruction record is a composite of 15 NH climate records from different

sites and proxies. The proxies used in this reconstruction are more variable relative to other composite records. The proxies include ice core such as Greenland Ice Sheet Project 2 (GISP2), pollen from Michigan, tree ring from France and Sweden and etc. Therefore, this hemispherical reconstruction by Crowley and Lowery (2000) is heterogeneous in data source and preferred to use in this study.

To simulate the reconstructed temperature variations, quantitative analysis of the time series is essential to determine the coefficients in the stochastic climate model. The time series varied irregularly with a typical time scale of ~50-100 years in the time domain (Fig. 3.1a and b). The temperature was relatively warm during the MWP, and then gradually dropped approximately 0.2˚C during the LIA, and finally rapidly increased as much as 0.6˚C in the twentieth century (Fig. 3.1a). The power spectrum of the time series exhibits similar trend to the power spectrum of red noise that spectral power decreases with frequency (Fig. 3.1c). The weight of power spectrum concentrates at the low-frequency section ($\leq 10^{-2}$ years^{-1}) and therefore implies that most of the variance in the time series occurred at periods of longer than 100 years. The autocorrelation coefficients of the time series dropped rapidly to 0 when time lag τ changed from 0 to 241 years (Fig. 3.1d). The critical time lag τ_c is around 57 years, so the characteristic time scale of the natural processes working in the climate system should also be about 57 years. This time scale is much shorter than the time scale of thermohaline circulation, but is closer to the time scale of atmosphere circulation. This seems consistent with the simulation results by Shindell et al (2001) that the atmospheric circulation pattern AO/NAO acted as the primary internal mechanism in the centennial climate change of NH.

Through time series analysis, we obtained suitable coefficients for the stochastic climate model. The value of the feedback coefficient α equals to 1/57 and the value of c_0 equals to 0.0203, and hence the forcing variance σ can be calculated by $\sqrt{2 \times 0.0203/57}$. With the estimated α and σ, we simulated the temperature variations. We compared the ensemble average of 1000 runs of simulation with the reconstruction from frequency and time domain respectively (Fig. 3.2). In the frequency domain, the power spectrum of the simulation exhibits same decreasing trend as that of the reconstruction (Fig. 3.2a). In addition, the power spectrum of the simulation results is proportional to $f^{-0.89}$, similar to that of the reconstruction which is proportional to $f^{-0.94}$. The autocorrelation for the ensemble average of 1000 runs of simulation also presents similar trend to that generated from the reconstruction (Fig. 3.2b). Therefore, this simple stochastic climate model can explain the majority of the power spectrum and autocorrelation of the climate reconstruction.

In spite of the coherent trend of power spectrum and autocorrelation between the simulation and reconstruction, the deviation between the reconstruction and simulation is also visible. Király and Jánosi (2002) extended the white noise forcing in the stochastic climate model into power-law correlated (colored) noise forcing and well reproduced the linear correlation of the climate record with detrended fluctuation analysis. Therefore, we considered changing the white noise component in the stochastic climate model into other types of forcing. Because the Earth climate system can be thought as a closed system, the solar forcing will become the sole external forcing. We assume that the change of the solar forcing will quickly influence the weather and produce the change of the weather forcing

based on the close relationship observed between solar radiation change and weather (King, 1973). Therefore, under this assumption, we changed the white-noise weather forcing in the stochastic model into the reconstructed solar radiation variation (Steinhilber et al., 2009) over the past millennium. The simulated temperature fluctuation reproduced the warm MWP, however, it did not agree with the LIA (Fig 3.3a). The simulated temperature also underestimated the 20th century warming although it showed a gentle increasing trend from the beginning of 20th century. In addition, the simulated temperature did not generate the fine details in the reconstruction. There are many possible reasons for the observed deviation, such as the errors in the reconstruction of temperature or solar radiation, the absence of nonlinearity in the model, the direct use of solar forcing to take the place of weather forcing. Nevertheless, the power spectrum and autocorrelation both improved and reproduced more features relative to the earlier simulation forced by white noise (Fig. 3.3b and c). Therefore, this improvement supports the earlier studies that solar forcing has played a non-negligible role in the climate change over the past millennium. To summarize, although this heuristic stochastic climate model is very simple and cannot be treated as quantitatively accurate, it still repeated the principal features or trends of the reconstructed temperature change over the past millennium, which might work as evidence to support the stochastic nature of the internal climate mechanism.

3.2. *Temporal variations of stochastic extent over the past millennium*

Before applying the method RESTS to the climate record, we calibrated RESTS first with white noise and sinusoidal signal. The results indicate that white noise has very low predictability, and the scores representing disagreement between predicted data and actual

data increased very rapidly (Fig 3.4a). The sinusoidal signal presents good predictability when the window size is within 20 (Fig 3.4b). When the window size is between 20 and 40, the scores exhibit periodic change along the time scale. Because we use linear fitting in RESTS, when the window size is larger than 40, the scores all became very high that suggest no predictability. The score distribution of the combination of white noise and sinusoidal signal is intermediate between the white signal and the sinusoidal signal (Fig 3.4c). Therefore, this method should be able to measure the randomness inherent in the time series.

We applied the RESTS method to the time series of temperature variations in the NH over the past millennium. As we expected, when the window size increased, predictability decreased whereas randomness increased (Fig 3.5a). However, the changing rate of predictability (or randomness) exhibits variability with different time intervals. At some intervals, the color changed very rapidly from black to white, whereas at other intervals, the color slowly turned from black to white. On the century-scale, the most remarkable feature we observed is slow changing rate at the transition (~1300-1500 AD) from the MWP to the LIA. On the finer scale, we observed narrow black columns at every 40-50 years. In other words, the predictability at the time of black columns is always high and independent of window size change. The temperature fluctuation in the NH might have the risk of artificial change during incorporating different climate proxy records. Therefore, we also analyzed the climate change record of GISP2 (73^oN 38^oW) (Grootes et al., 1993; Meese et al., 1994; Steig et al., 1994; Stuiver et al., 1995; Grootes and Stuiver, 1997), tree ring records from France (44^oN 7^oE) (Mann et al., 1999) and northern Sweden (68^oN 19^oE) (Grudd, 2008). These records in the time domain all showed random pattern and no significant trend (Fig 3.5b, c

and d). However, their RESTS color maps exhibited similar features (blue dashed lines) to the color map of the NH temperature reconstruction. According to these features, the stochastic extent decreased and predictability increased during the intervals of directly before the MWP, the transition from the MWP to the LIA, after the LIA and the 20th century warming. However, these intervals are not equally obvious in these color maps. The intervals are generally more distinct in the color maps derived from the tree ring record in France and isotope record of GISP2 relative to that derived from the tree ring record in Sweden. We also observed that these intervals of relatively high predictability occurred at the frequency of 300-400 years before the 20th century warming.

Based on the features detected from the RESTS color maps, we infer that the internal climate mechanism might become more predictable and deterministic during climate transitions. According to the stochastic climate theory, the natural processes within the climate system can be treated as stochastic process. Therefore, the detected temporal variation of stochastic extent suggests that the natural processes involved in the climate system should change as well at different time intervals. In addition, the temporal variation that the stochastic extent decreased and predictability increased during the intervals of climate transitions may also indicate the changing relationship between noise component $\sigma x(t)$ and feedback component $-\alpha y(t)$ in the stochastic model. Noise component dominates the climate variation during the stable climate intervals and feedback component dominates the climate variation and increases the predictability during the unstable transition intervals. Therefore, the feedback coefficient α and the forcing variance σ in the stochastic climate model should change nonlinearly with time instead of being treated as fixed constants. As to

what forced the natural processes or the internal climate mechanism to change at different intervals, we infer the driver is external forcing based on the results of previous studies (Crowley, 2000; Shindell et al, 2001; Hunt, 2006) and the earlier stochastic climate model with solar forcing in this study. According to our conclusion, the solar variability should be responsible for driving the climate transitions in the pre-industrial period and the greenhouse gas for driving the 20th century warming.

4. Conclusions

In this study, we examined the extent to which the internal climate mechanism is stochastic as opposed to deterministic over the past millennium. To test this, we used a conceptual linear stochastic climate model to simulate temperature variations of NH over the past millennium. The model validation includes replicating the principal features and orders of magnitude of the power spectrum and autocorrelation of the reconstructed temperature variations. However, this only indicates that stochastic climate theory can explain the power spectrum and autocorrelation of the climate change over the past millennium, but is not enough to demonstrate that the internal climate mechanism is stochastic because power spectrum and autocorrelation cannot cover all the features of a time series. Therefore, this experiment is only a preliminary test of the relationship between stochastic processes and internal climate mechanism in the Holocene, and we will implement it with more evidence in future work. When we replaced the Gaussian weather forcing in the conceptual model with the solar forcing, we obtained an improved simulation result. This might reflect the forcing role of solar variability during the climate change over the past millennium. Additionally, we

87

developed a new method to quantitatively investigate the temporal evolution of the stochastic extent in climate analysis. Our results indicate that the stochastic extent generally decreased during the intervals of climate transition. The most distinct example is the transition (~1300-1500 AD) from the MWP to the LIA. We imply that external forcings such solar variability or greenhouse gas drive the internal climate mechanism to become more deterministic during climate transitions.

Acknowledgements

References

Crowley TJ. 2000. Causes of climate change over the past 1000 years. *Science* **289**: 270-277, doi: 10.1126/science.289.5477.270.

Crowley TJ, Lowery TS. 2000. How warm was the Medieval Warm Period. *Ambio: A Journal of the Human Environment* **29(1)**: 51-54, doi: 10.1579/0044-7447-29.1.51.

Ditlevsen PD. 2001. Stochastic climate dynamics observed in an ice-core record. *Proceedings ISSAOS 2001*, l'Aquilla.

Dobrovolski SG. 2000. *Stochastic climate theory: models and applications*. Springer-Verlag Berlin: Heidelberg New York.

Frankignoul C, Hasselmann K. 1977. Stochastic climate models, part II: application to sea-surface temperature anomalies and thermocline variability. *Tellus* **29**: 289-305.

Grootes PM, Stuiver M, White JWC, Johnsen SJ, Jouzel J. 1993. Comparison of oxygen isotope records from the GISP2 and GRIP Greenland ice cores. *Nature* **366**: 552-554, doi:10.1038/366552a0.

Grootes PM, Stuiver M. 1997. Oxygen 18/16 variability in Greenland snow and ice with 10^3 to 10^5-year time resolution. *Journal of Geophysical Research* **102**: 26455-26470, doi:10.1029/97JC00880.

Grudd H. 2008. Torneträsk tree-ring width and density AD 500-2004: a test of climatic sensitivity and a new 1500-year reconstruction of north Fennoscandian summers. *Climate Dynamics* **31**: 843-857, doi:10.1007/s00382-007-0358-2.

Hasselmann K. 1976. Stochastic climate models, Part I: theory. *Tellus* **28**: 473-485.

Hodell DA, Brenner M, Curtis J, Guilderson T. 2001. Solar forcing of drought frequency in the Maya lowlands. *Science* **292**: 1367-1370, doi: 10.1126/science.1057759.

Hunt BG. 2006. The Medieval Warm Period, the Little Ice Age and simulated climatic variability. *Climate Dynamics* **27**: 677-694, doi: 10.1007/s00382-006-0153-5.

Jones PD, Mann ME. 2004. Climate over past Millennia. *Reviews of Geophysics* **42**: 1-42, doi:10.1029/2003RG000143.

Keigwin LD. 1996. The Little Ice Age and Medieval Warm Period in the Sargasso Sea. *Science* **274**: 1504-1508, doi: 10.1126/science.274.5292.1504.

King JW. 1973. Solar radiation changes and the weather. *Nature* **245**: 443-446, doi:10.1038/245443a0.

Király A, Jánosi IM. 2002. Stochastic modeling of daily temperature fluctuations. *Physical Review* **65**: 051102, doi: 10.1103/PhysRevE.65.051102.

Lamb HH. 1995. *Climate, history and the modern world (second edition)*. Routledge: London and New York; 156-170.

Majda AJ, Timofeyev I, Eijnden EV. 1999. Models for stochastic climate prediction. *PNAS* **96**: 14687-14691, doi: 10.1073/pnas.96.26.14687.

Mann ME, Bradley RS, Hughes MK. 1999. Northern hemisphere temperatures during the past millennium. IGBP PAGES/World Data Center-A for Paleoclimatology, Data Contribution Series # 1999-014. NOAA/NGDC Paleoclimatology Program: Boulder CO, USA.

Mathews JH, Fink KD. 2004. *Numerical Methods Using MATLAB (fourth edition)*. Prentice Hall.

McDermott FD, Mattey P, Hawkesworth C. 2001. Centennial-scale Holocene climate variability revealed by a high-resolution speleothem $\delta^{18}O$ record from SW Ireland. *Science* **294**: 1328-1331, doi: 10.1126/science.1063678.

Meese DA, Alley RB, Fiacco RJ, Germani MS, Gow AJ, Grootes PM, et al. 1994. Preliminary depth-agescale of the GISP2 ice core. *Special CRREL Report 94-1*, US.

Rial JA, Pielke Sr. RA, Beniston M, Claussen M, Canadell J, Cox P, Held H, de Noblet-Ducudre N, Prinn R, Reynolds J, Salas JD. 2004. Nonlinearities, Feedbacks and Critical Thresholds Within the Earth's Climate System. *Climatic Change* **65(1-2)**: 11-38.

Roe GH, Steig EJ. 2004. On the characterization of millennial-scale climate variability. *J. Climate* **17**: 1929-1944.

Ruiz De Elvira A, Lemke P. 1982. A Langevin equation for stochastic climate models with periodic feedfack and forcing variance. *Tellus* **34**: 313-320.

Shindell DT, Schmidt GA, Mann ME, Rind D, Waple A. 2001. Solar forcing of regional climate change during the Maunder Minimum. *Science* **294**: 2149-2152, doi: 10.1126/science.1064363.

Steig EJ, Grootes PM, Stuiver M. 1994. Seasonal precipitation timing and ice core records. *Science* **266**: 1885-1886, doi: 10.1126/science.266.5192.1885.

Steinhilber F, Beer J, Fröhlich C. 2009. Total solar irradiance during the Holocene. *Geophysical Research Letters* **36**: L19704, doi:10.1029/2009GL040142.

Stuiver M, Grootes PM, Braziunas TF. 1995. The GISP2 ^{18}O climate record of the past 16,500 years and the role of the sun, ocean and volcanoes. *Quaternary Research* **44**: 341-354.

Vallis GK. 2010. Mechanisms of climate variability from years to decades. In *Stochastic Physics and Climate Modelling*, Palmer T, Williams P (eds). Cambridge University Press: Cambridge, UK; 1-34.

von Storch H., Zwiers FW. 1999. *Statistical analysis in climate research*. Cambridge University Press: Cambridge, UK.
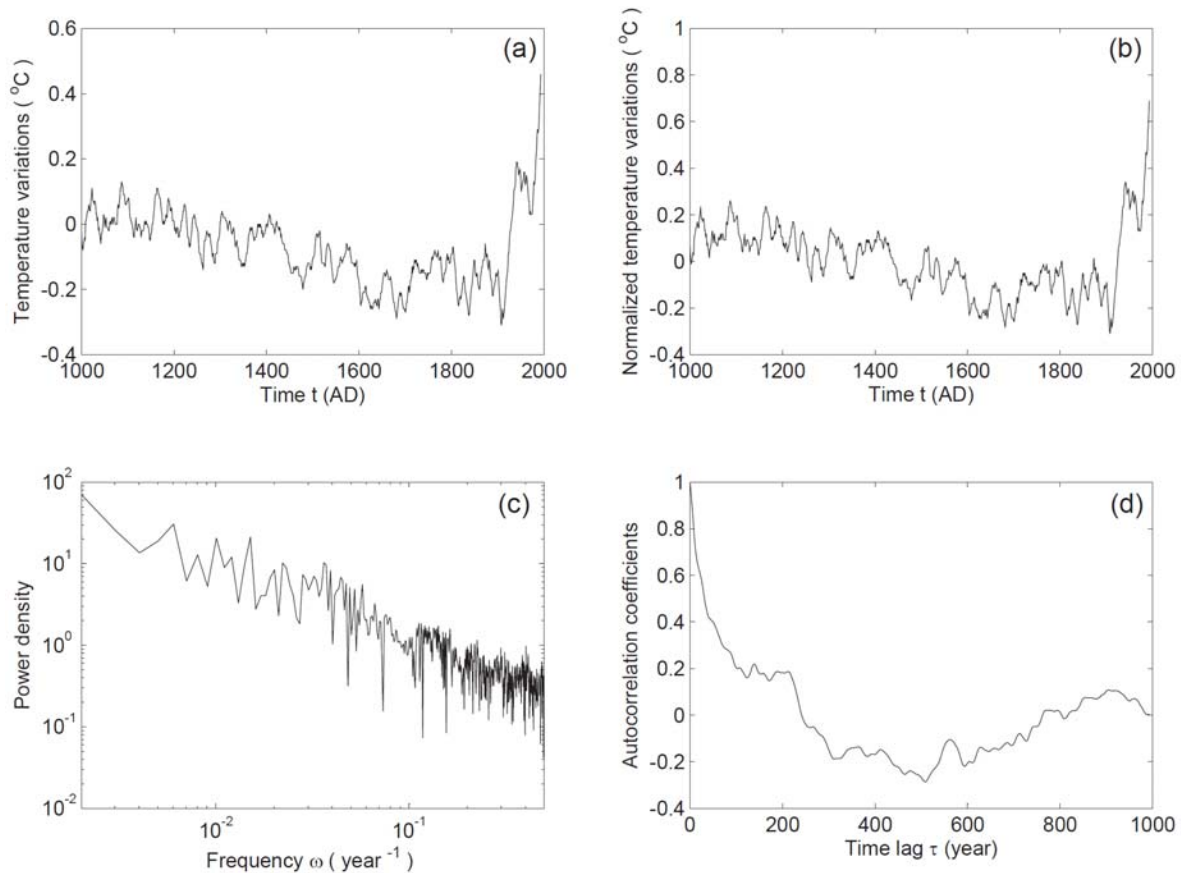
Figure 3.1. Temperature variations of Northern Hemisphere over the past millennium. (a) Time series of temperature variations from Crowley and Lowery (2000). (b) Normalized time series of temperature variations. (c) Power spectrum of the normalized temperature variations. (d) Autocorrelation of the normalized temperature variations.
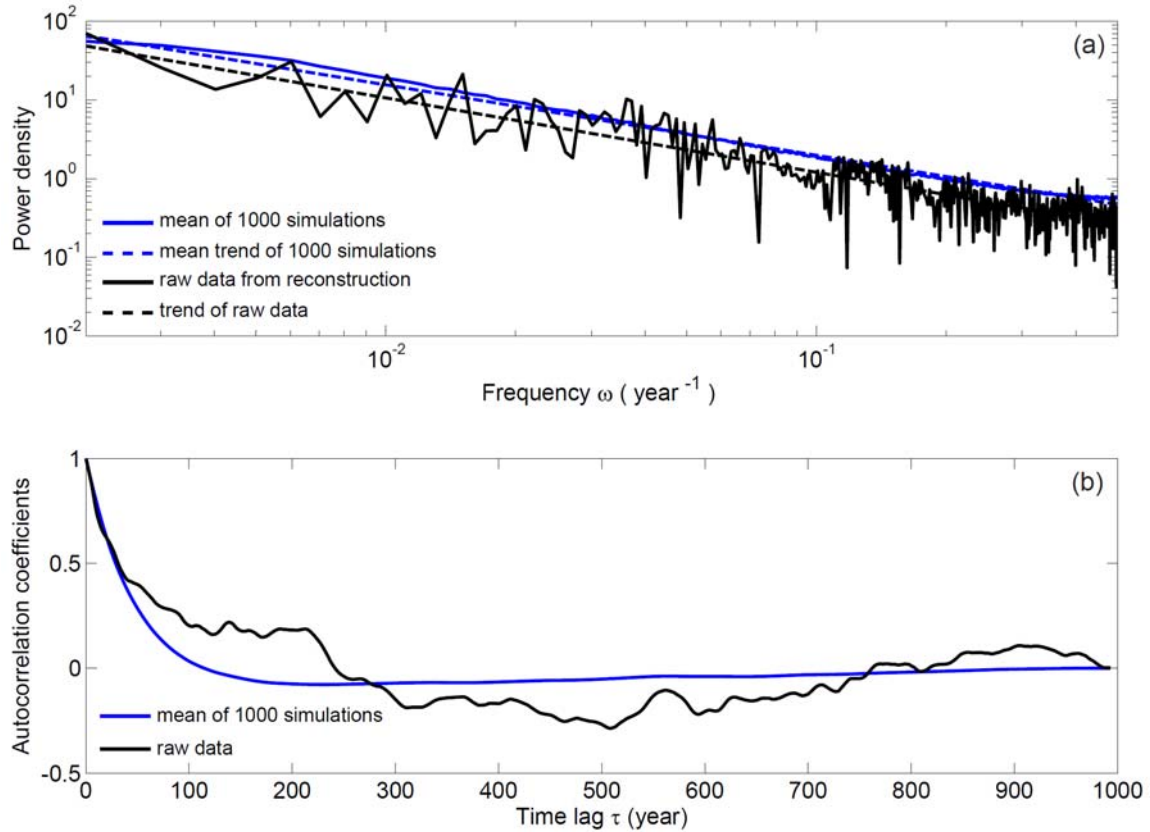
Figure 3.2. Comparison between the reconstruction and the ensemble average of 1000 runs of simulation. (a) Power spectrum of normalized temperature variations from simulation and reconstruction. The solid black (blue) line represents the power spectrum of the reconstruction (the ensemble average of 1000 simulations). The dashed black (blue) straight line represents the linear trend of the reconstruction (simulation) (b) Autocorrelation of normalized temperature variations from simulation and reconstruction. The solid black (blue) line represents the autocorrelation of the reconstruction (the ensemble average of 1000 simulations).
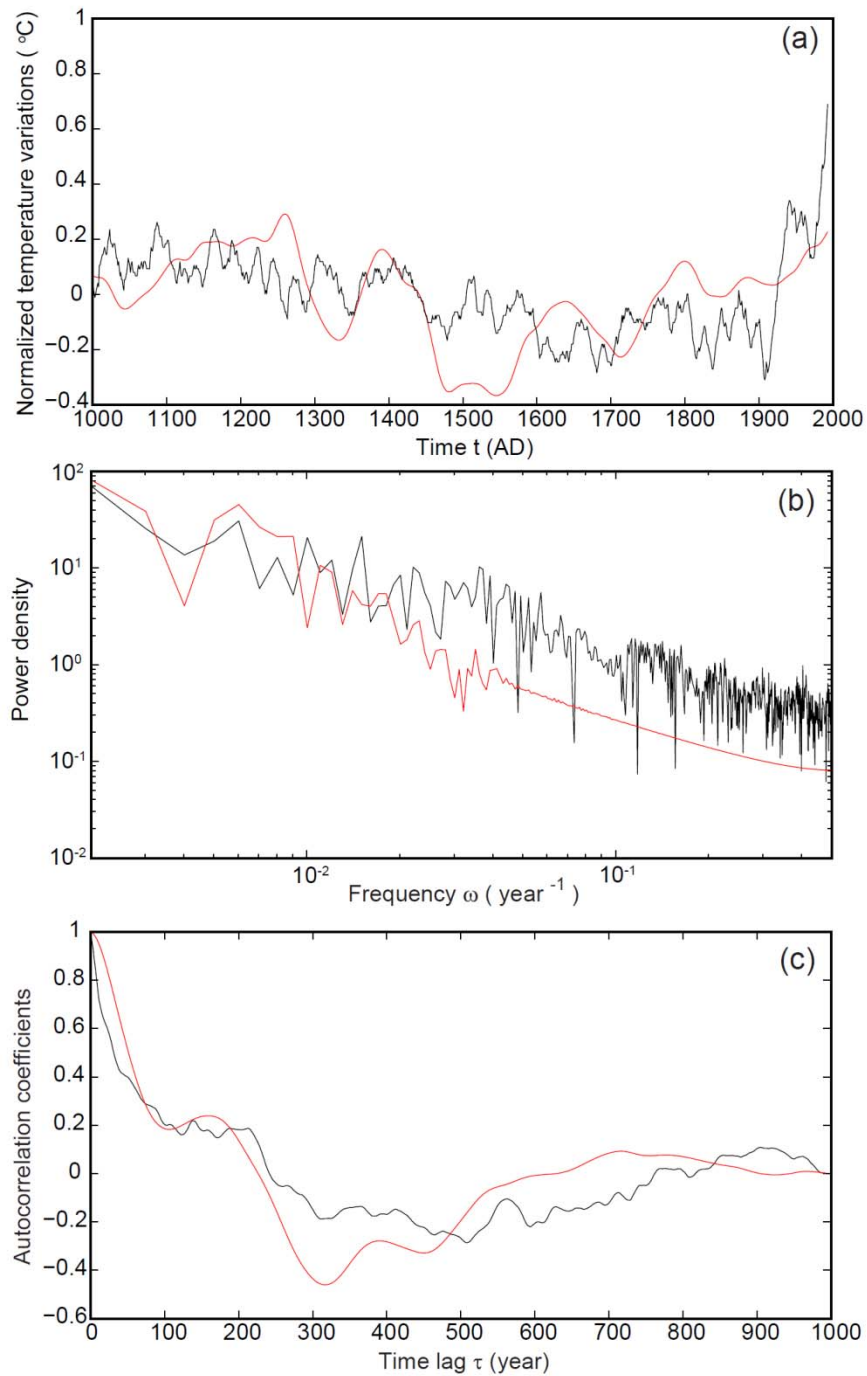
Figure 3.3. Comparison between the reconstruction and the simulation with solar forcing. (a) Normalized temperature variations of the reconstruction (black) and the simulation (red). (b) Power spectrum of normalized temperature variations from the reconstruction (black) and simulation (red). (b) Autocorrelation of normalized temperature variations from the reconstruction (black) and the simulation (red).
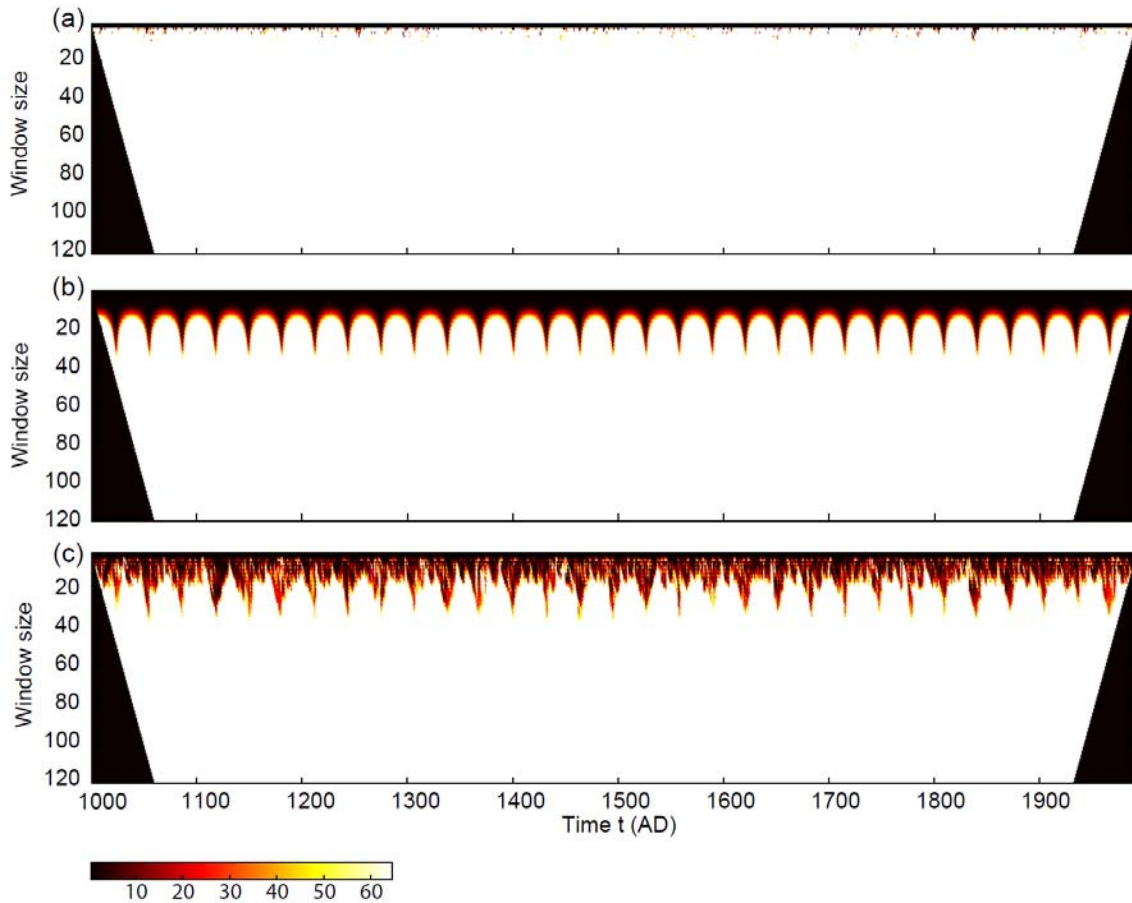
Figure 3.4. Calibration of the method RESTS. (a) Score distribution of white noise. (b) Score distribution of sinusoidal signal. (c) Score distribution of the combination of white noise and sinusoidal signal.
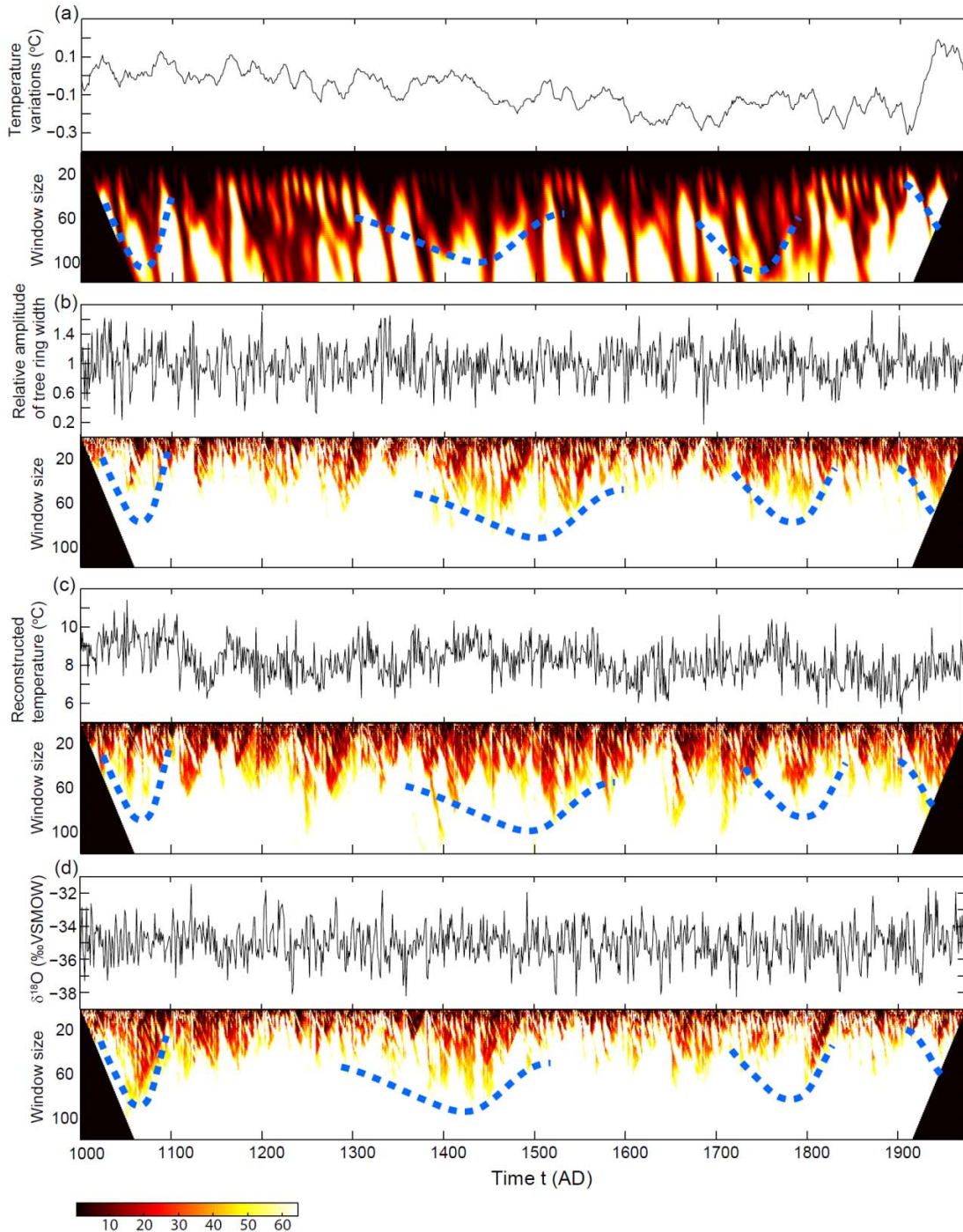
Figure 3.5. Different climate records and their score distribution with the method RESTS. (a) Time series of temperature variations from Crowley and Lowery (2000) and its score distribution. (b) Tree ring record from France (44°N 7°E) and its score distribution. (c) Temperature reconstructed from tree ring of northern Sweden (68°N 19°E) and its score distribution. (d) Time series of GISP2 $\delta^{18}O$ record and its score distribution. The blue dashed lines mark the intervals when the four different climate records shared similar score features.

BIBLIOGRAPHY

Ansell AD. 1968. The rate of growth of the hard clam *Mercenaria mercenaria* (L.) throughout the geographic range. *Journal du Conseil* **31**: 364-409.

Arnold WS, Marelli DC, Bert TM, Jones DS, Quitmyer IR. 1991. Habitat-specific growth of hard clams *Mercenaria mercenaria* (L.) from the Indian River, Florida. *Journal of Experimental Marine Biology and Ecology* **147**: 245-265.

Arnold WS, Bert TM, Quitmyer IR, Jones DS. 1998. Contemporaneous deposition of annual growth bands in *Mercenaria mercenaria* (Linnaeus), *Mercenaria campechiensis* (Gmelin), and their natural hybrid forms. *Journal of Experimental Marine Biology and Ecology* **223**: 93-109.

Austin WEN, Inall ME. 2002. Deep-water renewal in a Scottish fjord: temperature, salinity and oxygen isotopes. *Polar Research* **21**: 251-257.

Barnett TP, Del Genio AD, Ruedy R. 1992. Unforced decadal fluctuations in a coupled model of the atmosphere and ocean mixed layer. *Journal of Geophysical Research* **97**: 7341-7354.

Baxter JM, Boyd IL, Cox M, Cunningham L, Holmes P, Moffat CF. 2008. *Scotland's seas: towards understanding their state*. Fisheries Research Services, Aberdeen.

Beever III JW, Gray W, Trescott D, Cobb D, Utley J, Beever LB. 2009. *Comprehensive Southwest Florida/Charlotte Harbor climate change vulnerability assessment*. Southwest Florida Regional Planning Council Charlotte Harbor National Estuary Program Technical Report 09-3.

Bianchi GG, McCave IN. 1999. Holocene periodicity in North Atlantic climate and deep-ocean flow south of Iceland. *Nature* **397**: 515–517.

Blaauw M, van Geel B, van der Plicht J. 2004. Solar forcing of climatic change during the mid-Holocene: indications from raised bogs in the Netherlands. *Holocene* **14**: 1-35.

Black DE, Abahazi MA, Thunell RC, Kaplan A, Tappa EJ, Peterson LC. 2007. An 8-century tropical Atlantic SST record from the Cariaco Basin: Baseline variability, twentieth-century warming, and Atlantic hurricane frequency. *Paleoceanography* **22**: 1-10.

Blackmore DT. 1969. Studies of *Patella vulgata* L.I. Growth, reproduction, and zonal distribution. *Journal of Experimental Marine Biology and Ecology* **3**: 200–213.

Bond G, Kromer B, Beer J, Munscheler R, Evans MN, Showers W, Hoffmann S, Lotti R, Hajdas I, Bonani G. 2001. Persistent solar influence on North Atlantic climate during the Holocene. *Science* **294**: 2130–2136.

Booth RK, Jackson ST. 2003. A high-resolution record of late-Holocene moisture availability from a Michigan raised bog, USA. *Holocene* **13**: 863–876.

Bradley JT. 1972. *Climate of Florida*. Asheville. NC: U .S. Department of Commerce. National Climatic Data Center. Climatography of the United States No. 60-8.

Branch GM. 1981. The biology of limpets: Physical factors, energy flow, and ecological interactions. *Oceanography and Marine Biology: an annual review* **19**: 235-380.

Bridge MC, Haggart BA, Lowe JJ. 1990. The history and palaeoclimatic significance of subfossil remains of *Pinus sylvestris* in blanket peats from Scotland. *Journal of Ecology* **78**: 77-99.

Brown SL, Bierman PR, Lini A, Southon J. 2000. 10000 yr record of extreme hydrological events. *Geology* **28**: 335–338.

Cohen AL, Tyson PD. 1995. Sea-surface temperature fluctuations during the Holocene off the south coast of Africa: Implications for terrestrial climate and rainfall. *Holocene* **5**: 304-312.

Connor DW, Gilliland PM, Golding N, Robinson P, Todd D, Verling E. 2006. *UKSeaMap: the mapping of seabed and water column features of UK seas*. Joint Nature Conservation Committee, Peterborough.

Coplen TB, Kendall C, Hopple J. 1983. Comparison of stable isotope reference samples, *Nature* **302**: 236-238.

Crisp DJ. 1965. Observations on the effect of climate and weather on marine communities. In *The Biological Significance of Climatic Changes in Britain*, Johnson CG, Smith LP (eds). Elsevier: New York; 63-77.

Crowley TJ. 2000. Causes of climate change over the past 1000 years. *Science* **289**: 270-277, doi: 10.1126/science.289.5477.270.

Crowley TJ, Lowery TS. 2000. How warm was the Medieval Warm Period. *Ambio: A Journal of the Human Environment* **29(1)**: 51-54, doi: 10.1579/0044-7447-29.1.51.

Ditlevsen PD. 2001. Stochastic climate dynamics observed in an ice-core record. *Proceedings ISSAOS 2001*, l'Aquilla.

Dobrovolski SG. 2000. *Stochastic climate theory: models and applications*. Springer-Verlag Berlin: Heidelberg New York.

Ekaratne SUK, Crisp DJ. 1984. Seasonal growth studies of intertidal gastropods from shell micro-growth band measurements, including a comparison with alternative methods. *Journal of the Marine Biological Association of the United Kingdom* **64**: 13-210.

Elenga H, Maley J, Vincens A, Farrera I. 2004. Palaeoenvironments, palaeoclimates and landscape development in Atlantic Equatorial Africa: a review of key sites covering the last 25 kyrs. In *Past climate variability through Europe and Afrcia*, Battarbee, RW, Gasse F, Stickley CE (eds). Springer: Dordrecht; 181–198.

Elliot M, deMenocal PB, Braddock KL,Howe SS. 2003. Environmental controls on the stable isotopic composition of *Mercenaria mercenaria*: potential application to paleoenvironmental studies. *Geochemistry, Geophysics, Geosystems* **4**: 1056-1072.

Fenger T, Surge D, Schone B, Milner N. 2007. Sclerochronology and geochemical variation in limpet shells (*Patella vulgata*): A new archive to reconstruct coastal sea surface temperature. *Geochemistry Geophysics Geosystems* **8**: Q07001, doi:10.1029/2006GC001488.

Frankignoul C, Hasselmann K. 1977. Stochastic climate models, part II: application to sea-surface temperature anomalies and thermocline variability. *Tellus* **29**: 289-305.

Friedman I, O'Neil JR. 1977. Compilation of stable isotope fractionation factors of geochemical interest. In Data of Geochemistry, Fleischer M (ed). U.S. Govt. Print. Office: Washington, D.C.; 1-12.

Goewert AE, Surge D. 2008. Seasonality and growth patterns using isotope sclerochronology in shells of the Pliocene scallop *Chesapecten madisonius*. *Geo-Marine Letters* **28**: 327-338.

Gonfiantini R, Stichler W, Rozanski K. 1995. Standards and intercomparison materials distributed by the International Atomic Energy Agency for stable isotope measurements. In References and Intercomparison Materials for Stable Isotopes of Light Elements, the Isotope Hydrology Section of the International Atomic Energy Agency (eds). IAEA: Vienna, Austria; 13-29.

Grootes PM, Stuiver M. 1997. Oxygen 18/16 variability in Greenland snow and ice with 10^3 to 10^5-year time resolution. *Journal of Geophysical Research* **102**: 26455-26470, doi:10.1029/97JC00880.

Grootes PM, Stuiver M, White JWC, Johnsen SJ, Jouzel J. 1993. Comparison of oxygen isotope records from the GISP2 and GRIP Greenland ice cores. *Nature* **366**: 552-554, doi:10.1038/366552a0.

Grudd H. 2008. Torneträsk tree-ring width and density AD 500-2004: a test of climatic sensitivity and a new 1500-year reconstruction of north Fennoscandian summers. *Climate Dynamics* **31**: 843-857, doi:10.1007/s00382-007-0358-2.

Gunn JD. 2000. The years without summer: tracing A.D. 536 and its aftermath. *British Archaeological Reports International Series* **872**.

Hall IR, Bianchi GG, Evans JR. 2004. Centennial to millennial scale Holocene climate-deep water linkage in the North Atlantic. *Quaternary Science Reviews* **23**: 1529-1536.

Hallmann N, Burchell M, Schöne BR, Irvine GV, Maxwell D. 2009. High-resolution sclerochronological analysis of the bivalve mollusk *Saxidomus gigantea* from Alaska and British Columbia: Techniques for revealing environmental archives and archaeological seasonality. *Journal of Archaeological Science* **36**: 2353-2364.

Harkness DD. 1983. The extent of the natural ^{14}C deficiency in the coastal environment of the United Kingdom. *Journal of the European Study Group on Physical, Chemical and Mathematical Techniques Applied to Archaeology PACT 8 (IV.9)*: 351-364.

Hass HC. 1996. Northern Europe climate variations during late Holocene: evidence from marine Skagerrak. *Palaeogeography, Palaeoclimatology, Palaeoecology* **123**: 121-145.

Hasselmann K. 1976. Stochastic climate models, Part I: theory. *Tellus* **28**: 473-485.

Haug GH, Hughen KA, Sigman DM, Peterson LC, Röhl U. 2001. Southward migration of the international convergence zone through the Holocene. *Science* **293**: 1304-1308.

Helama S, Hood BC. 2011. Stone Age midden deposition assessed by bivalve sclerochronology and radiocarbon wiggle-matching of *Arctica islandica* shell increments. *Journal of Archaeological Science* **38(2)**: 452-460.

Heusser CJ. 1995. Palaoecology of a Donatia-Astlia cushion bog, Magellanic Moorland-Subantarctic Evergreen Forest transition, southern Tierra del Fuego, Argentina. *Review of Paleobotany and Palynology* **89**: 429-40.

Hodell DA, Brenner M, Curtis J, Guilderson T. 2001. Solar forcing of drought frequency in the Maya lowlands. *Science* **292**: 1367-1370, doi: 10.1126/science.1057759.

Holliday NP. 2003. Air-Sea interaction and circulation changes in the northeast Atlantic. *Journal of Geophysical Research* **108 (C8)**: 3259, doi:10.1029/2002JC001344.

Hufthammer AK, Høie H, Folkvord A, Geffen AJ, Andersson C, et al. 2010. Seasonality of human site occupation based on stable oxygen isotope ratios of cod otoliths. *Journal of Archaeological Science* **37**: 78-83.

Hughen K, Baille M, Bard E, Beck J, Bertrand C, Blackwell P, et al. 2004. Marine04 Marine radiocarbon age calibration, 26–0 ka BP. *Radiocarbon* **46**: 1059-1086.

Hunt BG. 2006. The Medieval Warm Period, the Little Ice Age and simulated climatic variability. *Climate Dynamics* **27**: 677-694, doi: 10.1007/s00382-006-0153-5.

Hurrell JW. 1995. Decadal trends in the North Atlantic Oscillation: regional temperatures and precipitation. *Science* **269**: 676-679.

Iacumin P, Bianucci G, Longinelli A. 1992. Oxygen and carbon isotopic composition of fish otoliths. *Marine Biology* **113**: 537-542.

Inall M, Gillibrand P, Griffiths C, MacDougal N, Blackwell K. 2009. On the oceanographic variability of the north-west European shelf to the west of Scotland. *Journal of Marine Systems* **77**: 210-226.

Ivany LC, Patterson WP, Lohmann KC. 2000. Cooler winters as a possible cause of mass extinctions at the Eocene/Oligocene boundary. *Nature* **407**: 887-890.

Jenkins SR, Hartnoll RG. 2001. Food supply, grazing activity and growth rate in the limpet *Patella vulgata* L.: A comparison between exposed and sheltered shores. *Journal of Experimental Marine Biology and Ecology* **258**: 123–139.

Ji J, Shen J, Balsam W, Chen J, Liu L, Liu X. 2005. Asian monsoon oscillations in the northeastern Qinghai-Tibet Plateau since the late glacial as interpreted from visible reflectance of Qinghai Lake sediments. *Earth and Planetary Science Letters* **233**: 61-70.

Jones D., Allmon WD. 1995. Records of upwelling, seasonality and growth in stable-isotope profiles of Pliocene mollusk shells from Florida. *LETHAIA* **28**: 61-74.

Jones DS, Arthur MA, Allard DJ. 1989. Sclerochronological records of temperature and growth from shells of *Mercenaria mercenaria* from Narragansett Bay, Rhode Island. *Marine Biology* **102**: 225-234.

Jones DS, Quitmyer IR, Arnold WS, Marelli DC. 1990. Annual shell banding, age, and growth rate of hard clams (*Mercenaria* spp.) from Florida. *Journal of Shellfish Research* **9**: 215-225.

Jones DS, Quitmyer IR. 1996. Marking time with bivalve shells: oxygen isotopes and season of annual increment formation. *Palaios* **11**: 340-346.

Jones KB, Hodgins GWL, Etayo-Cadavid MF, Andrus CFT, Sandweiss DH. 2010. Centuries of marine radiocarbon reservoir age variation within archaeological *Mesodesma donacium* shells from southern Peru. *Radiocarbon* **52(3)**: 1207-1214.

Jones PD, Mann ME. 2004. Climate over past Millennia. *Reviews of Geophysics* **42**: 1-42, doi:10.1029/2003RG000143.

Jones PW, Martin FD, Hardy JD Jr. 1978. *Development of fishes in the Mid-Atlantic Bight: an atlas of egg, larval, and juvenile stages*. Fish and Wildlife Service: U.S Department of Interior.

Kalish JM. 1991. ^{13}C and ^{18}O isotopic disequilibria in fish otoliths: metabolic and kinetic effects. *Marine Ecology Progress Series* **75**: 191-203.

Keigwin LD. 1996. The Little Ice Age and Medieval Warm Period in the Sargasso Sea. *Science* **274**: 1504-1508, doi: 10.1126/science.274.5292.1504.

Kilian MR, van der Plicht J, van Geel B. 1995. Dating raised bogs: new aspects of AMS ^{14}C wiggle matching, a reservoir effect and climatic change. *Quaternary Science Reviews* **14**: 959-66.

King JW. 1973. Solar radiation changes and the weather. *Nature* **245**: 443-446, doi:10.1038/245443a0.

Király A, Jánosi IM. 2002. Stochastic modeling of daily temperature fluctuations. *Physical Review* **65**: 051102, doi: 10.1103/PhysRevE.65.051102.

Kraeuter JN, Castagna M. 2001. *Biology of the Hard Clam*. Elsevier.

Lamb HH. 1995. *Climate, history and the modern world (second edition)*. Routledge: London and New York; 156-170.

Landscheidt T. 1987. Long-range forecasts of solar cycles and climate change. In *Climate History, Periodicity and Predictability*. Rampino MR, Sanders JE, Newman WS, Konigsson LK. (eds).Van Nostrand Reinhold: New York; 421–445.

Larsen G, Newton AJ, Dugmore AJ, Vilmundardóttir EG. 2001. Geochemistry, dispersal, volumes and chronology of Holocene silicic tephra layers from the Katla volcanic system, Iceland. *Journal of Quaternary Science* **16**: 119-132.

Larsen LB, Vinther BM, Briffa KR, Melvin TM, Clausen HB, Jones PD, et al. 2008. New ice core evidence for a volcanic cause of the A.D. 536 dust veil. *Geophysical Research Letters* **35**: L04708, doi:10.1029/2007GL032450.

Lee S, Kim H. 2003. The dynamical relationship between subtropical and eddy-driven jets. *Journal of the Atmospheric Sciences* **60**: 1490-1503.

LeGrande AN, Schmidt GA. 2006. Global gridded data set of the oxygen isotopic composition in seawater. *Geophysical Research Letters* **33**: L12604, doi:10.1029/2006GL026011.

Lund DC, Curry WB. 2004. Late Holocene variability in Florida Current surface density: Patterns and possible causes. *Paleoceanography* **19**: 1-17.

Lund DC, Curry WB. 2006. Florida Current surface temperature and salinity variability during the last millennium. *Paleoceanography* **21**: 1-15.

Majda AJ, Timofeyev I, Eijnden EV. 1999. Models for stochastic climate prediction. *PNAS* **96**: 14687-14691, doi: 10.1073/pnas.96.26.14687.

Mann ME, Bradley RS, Hughes MK. 1999. Northern hemisphere temperatures during the past millennium. IGBP PAGES/World Data Center-A for Paleoclimatology, Data Contribution Series # 1999-014. NOAA/NGDC Paleoclimatology Program: Boulder CO, USA.

Mann ME, Zhang Z, Rutherford S, Bradley RS, Hughes MK, et al. 2009. Global signatures and dynamical origins of the Little Ice Age and Medieval Climate Anomaly. *Science* **326**: 1256-1260.

Marquardt WH. 2004. Calusa. In *Handbook of North American Indians, volume 14: Southeast*, Fogelson RD (ed). Smithsonian Institution: Washington, DC; 204-212.

Marquardt WH, Walker KJ. 2001. Pineland: a coastal wet site in southwest Florida. In *Enduring Records: The Environmental and Cultural Heritage of Wetlands*, Purdy BA (ed). Oxbow Books, Oxford and David Brown Book Company: Oakville; 48-60.

Marquardt WH, Walker KJ. in press. *The Archaeology of Pineland: A Coastal Southwest Florida Site Complex, A.D. 50 – 1710*. Institute of Archaeology and Paleoenvironmental Studies, Monograph 4. University of Florida, Gainesville.

Marshall J, Kushnir Y, Battisti DS, Chang P, Czaja A, Dickson R, Hurrell J, McCartney M, Saravanan R, Visbeck M. 2001. North Atlantic climate variability: Phenomena impacts and mechanisms. *International Journal of Climatology* **21**: 1863-1898.

Martín-Puertas C, Valero-Garcés BL, Brauer A, Mata MP, Delgado-Huertas A, Dulski P. 2009. The Iberian-Roman Humid Period (2600-1600 cal yr BP) in the Zoñar Lake varve record (Andalucía, southern Spain). *Quaternary Research* **71**: 108-120.

Matthews JA, Dresser PQ. 2008. Holocene glacier variation chronology of the Smørstabbtindan massif, Jotunheimen, southern Norway, and the recognition of century- to millennial-scale European Neoglacial events. *Holocene* **18**: 181-201.

Matthews JH, Fink KD. 2004. *Numerical Methods Using MATLAB (fourth edition)*. Prentice Hall.

Mauquoy D, van Geel B, Blaauw M, Speranza A, van der Plicht J. 2004. Changes in solar activity and Holocene climatic shifts derived from ^{14}C wiggle-match dated peat deposits. *Holocene* **14**: 45-52.

McDermott FD, Mattey P, Hawkesworth C. 2001. Centennial-scale Holocene climate variability revealed by a high-resolution speleothem δ^{18}O record from SW Ireland. *Science* **294**: 1328-1331, doi: 10.1126/science.1063678.

Meese DA, Alley RB, Fiacco RJ, Germani MS, Gow AJ, Grootes PM, et al. 1994. Preliminary depth-agescale of the GISP2 ice core. *Special CRREL Report 94-1*, US.

Muncy RJ, Wingo WM. 1983. *Species profiles: life histories and environmental requirements of coastal vertebrates (Gulf of Mexico): sea catfish and gafftopsail catfish.* Washington, DC: National Coastal Ecosystems Team, Division of Biological Services, Fish and Wildlife Services, U.S. Department of the Interior.

Oppo DW, McManus JF, Cullen JL. 2003. Deepwater variability in the Holocene epoch. *Nature* **422**: 277–278.

Patterson WP, Dietrich KA, Holmden C, Andrews JT. 2010. Two millennia of North Atlantic seasonality and implications for Norse colonies. *Proceedings of the National Academy of Sciences* **107 (12)**: 5306-5310.

Patterson WP, Smith GR, Lohmann KC. 1993. Continental paleothermometry and seasonality using the isotopic composition of aragonitic otoliths of freshwater fishes. In *Climate Change in Continental Isotopic Records*, Swart PK, Lohmann KC, McKenzie J, Savin, S (eds). American Geophysical Union: Washington DC; 191-202.

Porter SC, Denton GH. 1967. Chronology of Neoglaciation in the North American Cordillera. *American Journal of Science* **265**: 177-210.

Rampino MR, Self S, Stothers RB. 1988. Volcanic winters. Annual Review of Earth and *Planetary Sciences* **16**: 73-99.

Renssen H, Goose H, Muscheler R. 2006. Coupled climate model simulation of Holocene cooling events: ocean feedback amplifies solar forcing. *Climate of the Past* **2**: 79-90.

Rial JA, Pielke Sr. RA, Beniston M, Claussen M, Canadell J, Cox P, Held H, de Noblet-Ducudre N, Prinn R, Reynolds J, Salas JD. 2004. Nonlinearities, Feedbacks and Critical Thresholds Within the Earth's Climate System. *Climatic Change* **65(1-2)**: 11-38.

Richey JN, Poore RZ, Flower BP, Quinn TM, Hollander DJ. 2009. Regionally coherent Little Ice Age cooling in the Atlantic Warm Pool. *Geophysical Research Letters* **36**: 1-5.

Roe GH, Steig EJ. 2004. On the characterization of millennial-scale climate variability. *J. Climate* **17**: 1929-1944.

Ruiz De Elvira A, Lemke P. 1982. A Langevin equation for stochastic climate models with periodic feedfack and forcing variance. *Tellus* **34**: 313-320.

Saenger C, Came RE, Oppo DW, Keigwin LD, Cohen AL. 2011. Regional climate variability in the western subtropical North Atlantic during the past two millennia. *Paleoceanography* **26**: 1-12.

Schifano G, Censi P. 1986. Oxygen and carbon isotope composition, magnesium and strontium contents of calcite from a subtidal *Patella coerulea* shell. *Chemical Geology* **58**: 325-331.

Schöne BR, Dunca E, Fiebig J, Pfeiffer M. 2005. Mutvei's solution: An ideal agent for resolving microgrowth structures of biogenic carbonates. Palaeogeography, Palaeoclimatology, Palaeoecology **228**: 149-166.

Schöne BR, Fiebig J, Pfeiffer M, Gleβ R, Hickson J, Johnson ALA, Dreyer W, Oschmann W. 2005. Climate records from a bivalved Methuselah (*Arctica islandica*, Mollusca; Iceland). *Palaeography, Palaeoclimatology, Palaeoecology* **228**: 130-148.

Seidenkrantz M.-S, Aagaard-Sørensen S, Sulsbrück H, Kuijpers A, Jensen KG, Kunzendorf H. 2007. Hydrography and climate of the last 4400 years in a SW Greenland fjord: implication for Labrador Sea palaeoceanography. *Holocene* **17**: 387-401.

Shackleton NJ. 1973. Oxygen isotope analysis as a means of determining season of occupation of prehistoric midden sites. *Archaeometry* **15**: 133-141.

Shindell DT, Schmidt GA, Mann ME, Rind D, Waple A. 2001. Solar forcing of regional climate change during the Maunder Minimum. *Science* **294**: 2149-2152.

Soto LR. 2005. Reconstruction of late Holocene precipitation for central Florida as derived from isotopes in speleothems. Unpublished Masters Thesis, Department of Geology, University of South Florida, Tampa, Florida.

Speranza A, van der Plicht J, van Geel B. 2000. Improving the time of control of the Subboreal/Subatlantic transition in a Czech peat sequence by ^{14}C wiggle-matching. *Quaternary Science Review* **19**: 1589-604.

Speranza A, van Geel B, van der Plicht J. 2002. Evidence for solar forcing of climate change at ca. 850 cal. BC from a Czech peat sequence. *Global and Planetary Change* **35**: 51-65.

Steig EJ, Grootes PM, Stuiver M. 1994. Seasonal precipitation timing and ice core records. *Science* **266**: 1885-1886, doi: 10.1126/science.266.5192.1885.

Steinhilber F, Beer J, Fröhlich C. 2009. Total solar irradiance during the Holocene. *Geophysical Research Letters* **36**: L19704, doi:10.1029/2009GL040142.

Stothers RB, Rampino MR. 1983. Volcanic eruptions in the Mediterranean before A. D. 630 from written and archaeological sources. *Journal of Geophysical Research* **88**: 6357-6371.

Stuiver M, Grootes PM, Braziunas TF. 1995. The GISP2 [18]O climate record of the past 16,500 years and the role of the sun, ocean and volcanoes. *Quaternary Research* **44**: 341-354.

Stuiver M, Reimer PJ, Reimer RW. 2005. CALIB Radiocarbon Calibration. http: // radiocarbon.pa.qub.ac.uk/calib.

Surge D, Kelly G, Arnold WS, Geiger SP, Goewert AE, Walker KJ. 2008. Isotope sclerochronology of *Mercenaria Mercenaria*, *M. Campechiensis*, and their natural hybrid form: does genotype matter? *Palaios* **23**: 559-565.

Surge DM, Walker KJ. 2005. Oxygen isotope composition of modern and archaeological otoliths from the estuarine hardhead catfish (*Ariopsis felis*) and their potential to record low-latitude climate change. *Palaeogeography, Palaeoclimatology, Palaeoecology* **228**: 179-191.

Surge D, Walker KJ. 2006. Geochemical variation in microstructural shell layers of the southern quahog (*Mercenaria campechiensis*): Implications for reconstructing seasonality. *Palaeogeography, Palaeoclimatology, Palaeoecology* **237**: 182-190.

Swindles G, Plunkett G, Roe HM. 2007. A delayed climatic response to solar forcing at 2800 cal. BP: multiproxy evidence from three Irish peatlands. *Holocene* **17**: 177-182.

Tanner WF. 2000. Beach ridge history, sea level change, and the A.D. 536 event. In *The Years without Summer: Tracing A.D. 536 and its aftermath*, Gunn JD (ed). Archaeopress: Oxford; 89-97.

Tarutani T, Clayton RN, Mayeda TK. 1969. The effect of polymorphism and magnesium substitution on oxygen isotope fractionation between calcium carbonate and water. *Geochimica et Cosmochimica Acta* **33**: 987-996.

Thorrold SR, Campana SE, Jones CM, Swart PK. 1997. Factors determining $\delta^{13}C$ and $\delta^{18}O$ fractionation in aragonitic otoliths of marine fish. *Geochimica et Cosmochimica Acta* **61**: 2909-2919.

Tinner W, Lotter AF, Ammann B, Conedera M, Hubschmid P, van Leeuwen JFN, Wehrli M. 2003. Climatic change and contemporaneous land-use phases north and south of the Alps 2300 BC to 800 AD. *Quaternary Science Reviews* **22**: 1447-1460.

Tipping R, Davies A, McCulloch R, Tisdall E. 2008. Response to late Bronze Age climate change of farming communities in north east Scotland. *Journal of Archaeological Science* **35**: 2379-2386.

Trouet V, Esper J, Graham NE, Baker A, Scourse JD, Frank DC. 2009. Persistent positive North Atlantic Oscillation mode dominated the Medieval Climate Anomaly. *Science* **324**: 78-80.

Vallis GK. 2010. Mechanisms of climate variability from years to decades. In *Stochastic Physics and Climate Modelling*, Palmer T, Williams P (eds). Cambridge University Press: Cambridge, UK; 1-34.

van der Schrier G, Drijfhout SS, Hazeleger W, Noulin L. 2007. Increasing the Atlantic subtropical jet cools the circum-North Atlantic. *Meteorologische Zeitschrift* **16**: 1-8.

van Geel B, Bokovenko NA, Burova ND, Chugunov KV, Dergachev VA, et al. 2004. Climate change and the expansion of the Scythian culture after 850 BC, a hypothesis. *Journal of Archaeological Science* **31**: 1735-1742.

van Geel B, Heusser CJ, Renssen H, Schuurmans CJE. 2000. Climatic change in Chile at around 2700 BP and global evidence for solar forcing: a hypothesis. *Holocene* **10**: 659-664.

van Geel B, van der Plicht J, Kilian MR, Klaver ER, Kouwenberg JHM, Renssen H, Reynaud-Ferrera I, Waterbolk HT. 1998. The sharp rise of Δ^{14}C c. 800 cal BC: possible causes, related climatic teleconnections and the impact on human environments. *Radiocarbon* **40**: 535-550.

von Storch H., Zwiers FW. 1999. *Statistical analysis in climate research*. Cambridge University Press: Cambridge, UK.

Walker KJ. 1992. The zooarchaeology of Charlotte Harbor's prehistoric maritime adaptation: spatial and temporal perspectives. In *Culture and Environment in the Domain of the Calusa*, Marquardt WH (ed). University of Florida: Gainesville; 265-366.

Walker KJ. 2000. A cooling episode in southwest Florida during the sixth and seventh centuries A.D. In *The Years without Summer: Tracing A.D. 536 and its aftermath*, Gunn JD (ed). Archaeopress: Oxford; 119-127.

Walker KJ, Stapor FW, Marquardt WH. 1995. Archaeological evidence for a 1750-1450 BP higher-than-present sea level along Florida's Gulf coast. *Journal of Coastal Research Special Issue No. 17: Holocene Cyclic Pulses and Sedimentation*: 205-218.

Walker KJ, Surge D. 2006. Developing oxygen isotope proxies from archaeological sources for the study of Late Holocene human–climate interactions in coastal southwest Florida. *Quaternary International* **150**: 3-11.

Wang T, Surge D, Walker KJ. (2011). Isotopic evidence for climate change during the Vandal Minimum from *Ariopsis felis* otoliths and *Mercenaria campechiensis* shells, southwest Florida, USA. *Holocene* **21(7)**: 1081-1091. doi:10.1177/0959683611400458.

Widmer RJ. 1988. *The Evolution of the Calusa: A nonagricultural chiefdom on the Southwest Florida Coast*. University of Alabama Press: Tuscaloosa and London.

Winter A, Ishioroshi H, Watanabe T, Oba T, Christy J. 2000. Caribbean Sea surface temperatures: Two-to-three degrees cooler than present during the Little Ice Age. *Geophysical Research Letters* **27**: 3365-3368.

Wurster CM, Patterson WP. 2001. Late Holocene climatic change for the eastern interior United States: evidence from high-resolution δ^{18}O values of sagittal otoliths. *Palaeogeography, Palaeoclimatology, Palaeoecology* **170**: 81-100.